SCALABLE MILLIMETER WAVE ANTENNA ARRAY DESIGN WITH BEAMFORMING CAPABILITIES FOR 5G APPLICATIONS

A THESIS
SUBMITTED TO THE COMMUNICATION TECHNIQUES
ENGINEERING DEPARTMENT
IN PARTIAL FULFILLMENT OF THE REQUIREMENTS FOR
THE TECHNICAL MASTER DEGREE
IN
COMMUNICATION ENGINEERING

By

Amjad Abdulsatar Maseer

Supervised by

Prof. Dr. Faris Mohammed Ali

July / 2021

Supervisor Certification

I certify that this thesis titled " Scalable Millimeter Wave Antenna Array Design with Beamforming Capabilities for 5G Applications" which is being submitted by Amjad Abdulsatar Maseer was prepared under my supervision at the Communication Techniques Engineering Department, Engineering Technical College-Najaf, AL-Furat Al-Awsat Technical University, as a partial fulfillment of the requirements for the degree of Master of Technical in Communication Engineering.

Signature :

Name : **Prof. Dr. Faris Mohammed Ali**

(Supervisor)

Date : / / 2021

In view of the available recommendation, I forward this thesis for debate by the examining committee.

Signature :

Name : **Prof. Dr. Ahmad T. Abdulsadda**

(Head of comm. Tech. Eng. Dept.)

Date : / / 2021

Committee Report

We certify that we have read this thesis titled **"Scalable Millimeter Wave Antenna Array Design with Beamforming Capabilities for 5G Applications"** which is being submitted by **Amjad Abdulsatar Maseer** and as Examining Committee, examined the student in its contents. I our opinion, the thesis is adequate for award of degree of Master.

Signature:
Name:**Prof.Dr. Faris Mohammed**
(Supervisor)
Date: / / 2021

Signature:
Name:**Asst.Prof.Dr. Asaad S. Daghal**
(Member)
Date: / / 2021

Signature:
Name:**Asst.Prof.Dr. Mohanad Hasan**
(Member)
Date: / / 2021

Signature:
Name: **Prof. Zaid Asaad**
(Chairman)
Date: / / 2021

Approval of the Technical Engineering Collage

Signature:
Name: **Asst. Prof. Dr. Hassanain Ghani**
Dean of Technical Engineering Collage
Date: / / 2021

Linguistic Certification

This is to certify that this thesis entitled **Scalable Millimeter Wave Antenna Array Design with Beamforming Capabilities for 5G Applications** was reviewed linguistically. Its language was amended to meet the style of the English language.

Signature :

Name :

Date : / / 2021

Abstract

In this thesis, two single elements and one a phased array antenna are designed and investigated by ANSYSEDT 2020R2 software. The first design a cylindrical Dielectric Resonator Antenna (CDRA) with a dual feeding line is designed at 28 GHz. The dual feeds line used to excite the CDRA with multi relative permittivity which contributes to a high impedance bandwidth (BW). A CDRA has been mounted on two substrates. The optimized element has been applied to improve the gain (G) and achieve the required G performance. The radiation pattern, BW and G are simulated. The antenna obtains a reflection coefficient response from 26.2 GHz to 30 GHz which cover the desired frequency band. This antenna achieved BW=4.7 GHz and G=7 dB.

The 2nd, a C-DRA loaded by a circular patch is presented for emerging wideband wireless communications. The proposed antenna is fed by two orthogonal aperture-coupled feeding slots in order to generate polarization diversity pattern. The shape and location of the slots were optimized to realize the highest operating BW and highest isolation between the two feeds. To achieve high polarization purity a crossed dumbbell-shaped slots were etched on the circular patch. Simulation results show that antenna realizes 2 GHz of impedance BW centred at 27.6 GHz with isolation between the two feeding ports better than 25 dB over the operating BW, which indicates a pure diverse polarization can be realized by such antenna.

A rectangular array of 64-element C-DRA loaded patch with beam steering capability was modelled in this thesis. The phase coupled to each array element is regulated by adjusting the phase excitation between array elements in order to achieve a precise progressive phase distribution. The feeding ports have achieved progressive phase shift between the elements without the use of a phase shifter, resulting in a simple and low-cost array design. Radar correspondence and other wideband remote applications operating at 28 GHz for forthcoming 5G applications for moving targets will benefit from the proposed proposal, which has BW=2 GHz and G=22.97dB.

Acknowledgements

I am pleased to extend my sincere thanks to my parents who helped me and watched my upbringing and education since childhood.I am also pleased to extend my thanks and appreciation to the professors and doctors who were credited with preparing this research, and I also extend my thanks and gratitude to the university administration, which had the greatest role in providing facilities and services to the students as a whole.I would like to express my thanks and gratitude to God Almighty first. I also thank Professor Faris Muhammad Ali for his supervision of this project. My special thanks and gratitude to Dr.Hussam Al-Saadi,for standing by me in the most difficult circumstances while doing this work.I do not forget my sincere thanks to Dr.Nasr Al-Khafaji for his assistance in the beginning of the launch of this project. I especially thank to those who stood beside me, to those who supported me, to those who shared the tiredness and trouble of this sun, my wife and sweetheart.

Declaration

I hereby declare that the work in this thesis my own except for quotations and summaries which have been duly acknowledged.

/ /2021 Amjad Abdulsatar Maseer

Contents

List of Tables

List of Figures

List of Symbols

Sample	Description
S_{11}	Reflection Coefficient
S_{21}	Transmission Coefficients
E	Electric Field
H	Magnetic Field
TE	Transverse Electric mode
TH	Transverse Magnetic mode
HE	Hybrid Electric Magnetic mode
G	Gain
BW	Impedance bandwidth
AR	Axial Ratio
CP	Circular Polarization
LP	Liner Polarization
DR	Dielectric Resonator
DRA	Dielectric Resonator Antenna
$C-DRA$	Cylindrical Dielectric Resonator Antenna
$CDR-P$	CDRA embedded antenna
$DRAA$	Dielectric Resonator Antenna Array
L_s	Substrate Length
W_s	Substrate Width
H_s	Substrate Height
PAA	Phased Array Antenna
$R-DRA$	Rectangular Dielectric Resonator Antenna

List of Greek symbol

Sample	Description
$k_o a$	Free-Space Wavenumber
$Q - factor$	Quality Factor
ε_r	Relative Permittivity
λ_o	Free Space Wavelength
λ_g	Guided Wavelength
$tan\delta$	Losses Tangent
θ	Electrical Length
α	Progressive phase
d	Distance between element array

CHAPTER ONE

Introduction

1.1 The fifth generation

Because of the problems faced by previous generations of communications : limited capacity (600 MHz), crowded band frequency (3 MHz to 3 GHz), speed of data rate, Coverage area, and number of users . scientists and researchers turned to the use of the fifth generation (5G) , since : large bandwidth ($\geq$ 10 GHz), high speed data rates, less latency ($\leq$ 1 ms), and use mm-waves (30 – 300) GHz [1].

In last few years, Advances in the field of mobile communication have a significant impact on economic and social growth. As a result, fifth generation (5G) technology has risen to the top of the priority list for the 2020 generation. 5G is a new technology that offers both evolutionary and revolutionary services. It is the next generation of technology that enables ultra-high data speeds, extremely low latency, increased capacity, and exceptional service quality. It's worth noting that 5G technology will open up new ways to overcome existing development restrictions [1],[2].

Because 5G technology enables Internet Of Thing (IoT), it has the potential to drive significant societal change in industries such as education, industry, medical, and other social areas. 5G technology is intended to enable a large IoT ecosystem in which many devices will be linked and a network will be able to

meet communication demands by maintaining a trade-off among latency, cost, and speed. The 3GPP standards are updated on a regular basis[27],[28].

The 3GPP (The 3rd Generation Partnership Project) studies a planned release of new functionality and is in charge of new standard releases according to schedule. The 3GPP has identified three possible 5G communication usage scenarios, that are as follows [30].

1. **Enhanced Mobile Broadband (eMBB)**: it connects you to the internet at ultra-high speeds both indoors and outdoors. It promotes consistent and high-quality service at the cell's edge, on roads, in planes, and on trains. In addition, it provides high data speeds of up to 20 Gbps indoors and 2 Gbps outside.

2. **Massive Machine Type Communications (mMTC)**: it helps to link a huge number of applications through IoT. A single base station may handle tens of thousands of devices for various applications such as smart power grids, intelligent buildings, and so on.

3. **Ultra-reliable and Low Latency Communications (uRLLC)** : it has strict requirements, such as low latency (less than 1 millisecond) and minimal packet loss (1 in 10,000 packets). Remote medical surgery, healthcare, and industrial process control are just a few examples.

5G networks can be speedier due to the usage of high frequencies (mmwaves between 30 GHz and 300 GHz) for 5G networks. It can operating in both lower and higher frequency bands (e.g., sub 6 GHz and mmWave). 5G is far faster than 4G, with peak transmission speeds of up to 20 Gbps and average data rates of +100 Mbps. An antenna is one of the most important components of a 5G applications, as it must perform at higher gain, bandwidth, and with lower radiation losses. As a result, antenna design for 5G applications becomes extremely important while keeping the above-mentioned 5G communication requirements in mind [1].

In this study, we attempted to investigate all 5G antennas presented in recent years in a holistic manner, taking into account their performance enhancing strategies. This chapter also intends to point researchers in the right direction for future advancements in 5G antenna design based on their use. Several 5G antenna designs have been proposed in recent years, each adopting a different performance increase methodology.

5G represented the future of mobile communication systems. The bandwidth, gain, number of uses, coverage area, data rate, and capacity, were being developed significantly with 5G. By depending on millimetre waves, more space was available to connect huge devices and new applications from IoT for example. New materials (dielectric resonator) will be alternative solutions for previous materials (such as metal), that will reduce cost and complexity for antenna manufactures. DR antenna may be good candidates for modern generations, with absences losses and propagation surfers wave very suitable for many types of array antenna due to reduction mutual coupling between elements array [2].

Varies geometry shapes from DRA made it integrated with the most integrated circuit easily, which used in phone devices and medical applications. The phased array antennas are the best option to overcome multipath losses with misalignment of the orientation between transmitter and receiver. Moreover, the multi-elements array provided high gain that means long-distance for coverage area. So, it is necessary to understand how DRAs can work with exciting suitable modes by choosing properly dimensions and the geometry shape of the radiator in the antenna design [28].

1.2 Classification of antennas based on input output ports

The simplest method of categorizing antennas, as illustrated in figure1.1, is based on input output ports. Antennas are classed as follows:

i . **Single Input Single Output (SISO)**: For 5G applications, several re-

searchers have constructed the SISO antenna, which may be used as a single or multi-element antenna. The SISO antenna is simple to build and install. It's also simple to include into 5G communication equipment. A single element antenna must be big to provide a high gain [31].Signals incur significant propagation losses and service quality declines in frequency ranges over 6 GHz. To obtain consistent and high performance, a multi-element antenna (array antenna) must be used instead of a single element antenna [32]. A multi-element antenna is primarily used to boost an antenna's gain at the expense of greater size and complexity of design [33].

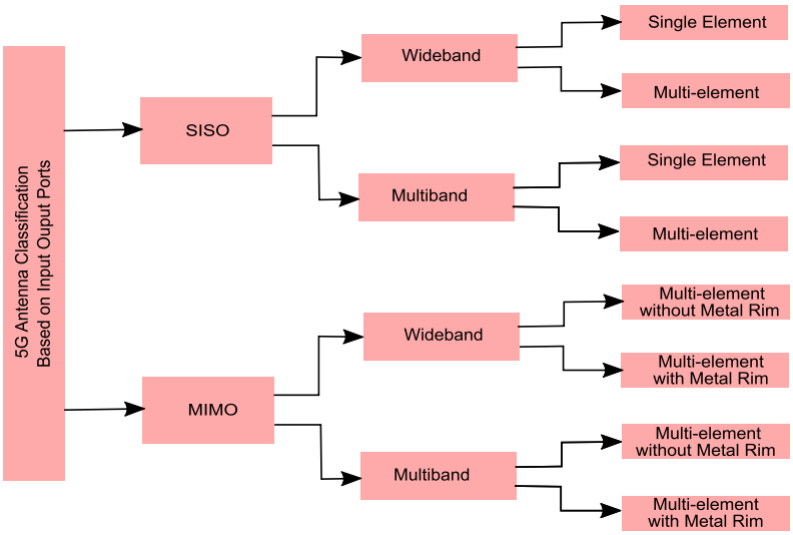

Figure 1.1: 5G Antenna grouping dependent on input output ports [1]

ii . **Multiple Input Multiple Output (MIMO)** Interference, multipath fading, and radiation losses are all problems with wireless communication. It also becomes worse at higher frequencies. Multiple input multiple output (MIMO) antennas become highly crucial to solve these challenges since increase the transmission range without raising the signal power.As a result, in 5G, MIMO architecture may be employed to achieve low latency, high throughput, and high efficiency. More signals can be broadcast intelligently utilizing several antennas in MIMO, considerably increasing channel capacity [1].

The technique used to diminish the quantity of an antenna in MIMO is to

utilize multiband antennas that give inclusion of various wireless applications. Further, the MIMO antennas can be ordered relying on their frequency band as wideband and multiband antennas. The wideband and multiband antennas can be additionally characterized into multi-element with a metal edge and multi-element without metal edge antennas. The metal edge antenna great mechanical strength as well as stylish appearance to cell phones [34].

1.3 Classification based in antenna types

As illustrated in figure1.2, another major way of categorization is based on antenna types. According to the literature, there are several types of antennas that are suited for 5G applications:

i . **Monopole Antenna**: It is made up of a straight microstrip line with a length of $\lambda/4$, where λ is the wavelength of the antenna's resonant working frequency. Several modifications have been presented in the literature that modify the fundamental structure into various forms such as conical, spiral, and others depending on the uses and needs [35], [36].

ii . **Dipole Antenna**: It comprises of two straight microstrip lines, each of $\lambda/4$ length, with feeding in the space between them. As a result, the dipole antenna's overall length is $\lambda/2$ [37],[38].

iii . **Magneto-Electric (ME) Dipole Antenna** : It comprises of a planar electric dipole and vertically shorted planar magnetic dipole. The feeding is given to the magnetic dipole from the base side of the substrate [39], [40].

iv . **Loop Antenna** : It is made up of a ring that is circular, rectangular, square, and any other form. The loop antenna's radius is lower than the wavelength [36], [41].

v . **Fractal Antenna** : It is made up of repeated repetitions of the same structure. It's made with the use of an iterative mathematical rule. The fractal antenna can take the form of a rectangle, circle, star, triangle, or other shape [42], [43].

vi . **Inverted F Antenna (IFA)** : It comprises of a microstrip line with one twist and feeding is given to the straight part of the microstrip line. The feed point is close to the twisted part and subsequently the general look of an antenna is of upset F type [44], [45].

vii . **Planar Inverted F Antenna (PIFA)** : It is made up of a patch antenna and a ground plane that are joined by a shorting pin, with feeding coming from the substrate's bottom side. It takes up less area since it resonates at a $\lambda/4$ [46], [47].

Most of the aforementioned antennas suffer from narrow bandwidth and lack of gain, in addition to the presence of metal losses in many of them, which affects the performance of the antenna and reduces the radiation efficiency. So, Many researchers have used a variety of performance enhancement strategies in antenna designs with the goal of improving one or more parameters such as bandwidth, gain, efficiency, mutual coupling mitigation, compact size, and more were mentioned in [1]:

1. Substrate Choice.
2. Corrugation.
3. Multi-element.
4. Dielectric Lens
5. Mutual Coupling Reduction Techniques
   (a) Neutralization Lines.
   (b) Decoupling Network.
   (c) Electromagnetic Bandgap (EBG) Structure.
   (d) Dielectric Resonator.
   (e) Defected ground structure (DGS).
   (f) Metamaterial.
   (g) Slot Elements.

(h) Complementary Split Ring Resonators (CSRR).

(i) Frequency Reconfigurable.

Dielectric resonator antennas are antennas that feature a dielectric resonator (DRA). DRA is a high-gain, high-radiation-efficiency, low-loss device. With its dual-band characteristic, DRA may also provide great isolation.

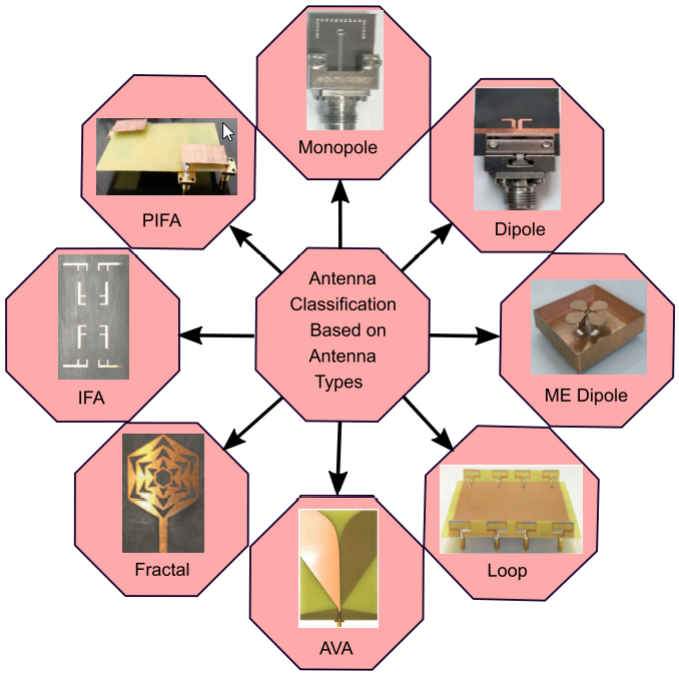

Figure 1.2: 5G Antenna classification based on antenna types [1]

1.4 Dielectric Resonator Antenna (DRA)

In the last several years, In microwave (MW) and MM-Wave engineering, the DRA has received a lot of attention. Some books and review articles [48, 27, 49] provide extensive coverage of cutting-edge developments. DRAs are intriguing candidates to replace traditional radiating components (as patch) at high frequencies, notably for mm-wave and beyond applications.

This is mostly due to the fact that DRAs do not suffer from conduction losses and have a high radiation efficiency when suitably stimulated. Radiating resonators are used in DRAs to convert directed waves into unguided waves (RF signals). In the earlier, these antennas were mostly made out of ceramic materials

with high permittivity and Q factor (between 20 and 2000). DRAs constructed of plastic (PolyVinyl Chloride (PVC)) are currently being developed . The following are the primary benefits of DRAs [2]:

1. Compared to traditional metallic antennas, DRAs have a smaller form factor, particularly when a material with a high dielectric constant (ε_r) is used in the architecture.

2. Because of the shortfall of conducting material, the DRAs are described by high radiation efficiency when a low-loss dielectric material is picked. This trademark makes them truly reasonable for applications at high frequencies, such as , the reach from 30 GHz to 300 GHz.

3. If the size of the resonator and the material ε_r are properly selected, DRAs can have a broad impedance bandwidth(BW).

4. Different ways may be used to excite DRAs, which is useful in a variety of systems and for array integration.

5. Different design strategies may be used to readily alter the gain, BW, and polarization properties of a DRA, easily controlled.

6. It can be designed in different geometry shapes, as shown in figure1.3.

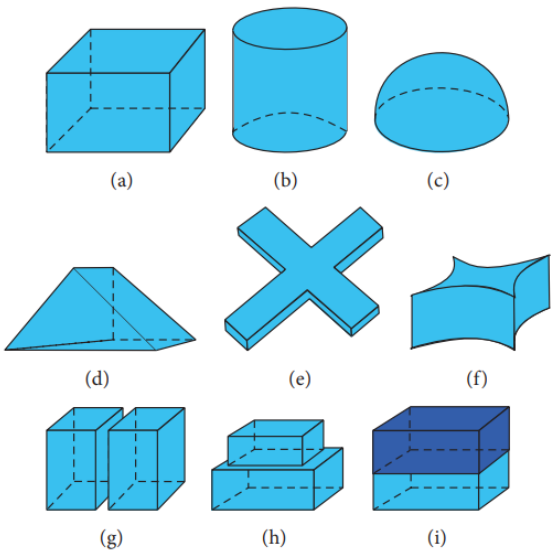

Figure 1.3: DRAs employ a variety of radiating structures [2]

According to all DRAs merits such as mentioned above and low loss mutual coupling and easily integrating with integrated circuits, these merits make it more suitable for structures array antenna, especially phased array antenna (PAA), which needs to stable radiation pattern during mechanical steering beam radiation operation to any direction in scanning range [50].

1.5 Beamforming technique

It is a technique used to focus the energy radiated by the antennas in a specific direction, and thus the energy for a specific user will increase and decrease in other directions, which leads to a reduction in interference.

The energy radiated by the antenna in previous generations of communication is in all directions, or the so-called omnidirectional, which is be formed such as concentric circles. Therefore, the energy or signal strength that the subscriber receives depends on the subscriber's position to the tower, and because the signal is distributed in all directions, the signal exchanged between the subscriber and the tower is subject to interference.

As for 5G, the energy will be focused in a specific direction or the so-called beam, where the width of that beam ranges from $1^o - 30^o$, and accordingly, the energy will be concentrated in a specific direction, which reduces interference and allows the signal to be sent to greater distances.

The process of forming the beam in the beamforming technique is done by generating a delay time between the antenna elements of the array by changing the phase difference in the antenna stimulation. The increase in the number of antennas in the array lead to narrow beam because mutual coupling phenomenon. figure1.4 explains the mechanism of beamforming in mobile communication system.

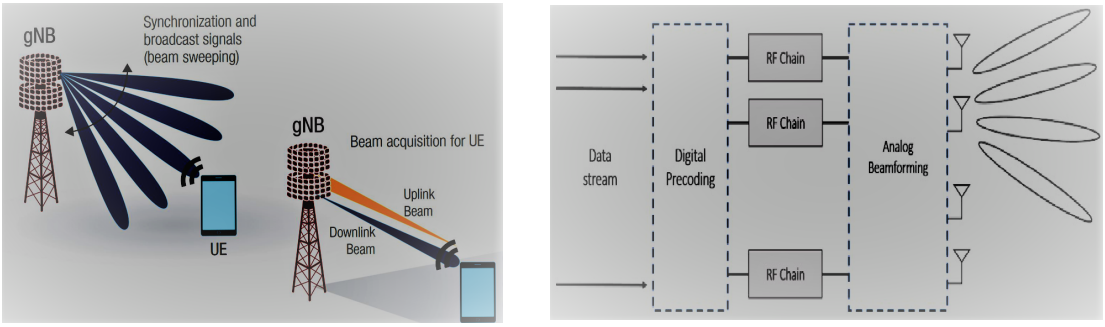

(a) (b)

Figure 1.4: (a)Illustration of the signal exchange process between the tower and the user by beamforming. (b) Schematic diagram of beamforming antennas . [source: Develop paper website]

1.6 Dielectric Resonator Array Antenna (DRAA)

When one or more antenna components are deliberately arranged near to one another, their separate radiation patterns can be combined to provide qualities that would otherwise only be possible with a much bigger antenna, such as narrower beamwidth and greater range. When one or more antenna components are carefully arranged adjacent to one another, their distinct radiation patterns can be merged to provide qualities that would otherwise only be possible with a much bigger antenna, such as narrower beamwidth and higher gain. The term "antenna array" refers to a grouping of two or more pieces. Antenna arrays are particularly effective in radar applications, which frequently demand a small, highly directional beam [51].

Another significant advantage of an array is the ability to modify the phase of each radiating member individually. Phased arrays are the name for these types of arrays. Mechanical electronic beam scanning is possible with phased arrays, which removes the requirement for mechanical antenna steering. In radar applications, electronic beam scanning also enables for the tracking of numerous targets [51].

Large value, a stable radiation pattern, and a larger frequency band are the most significant features of 5G antennas. Most researchers are designing multi-

element antennas for 5G applications since these criteria cannot be met by a individual element antenna (many previous works about array antenna description in Chapter two.

DRAA characterized by a lightweight, low loss manual coupling that mean the elements with bear from each one due to small size to array area , wide bandwidth, and high radiation efficiency, compared with a traditional antenna array. According to knowledge, the beam generated from any array must be fixed in the desired direction with average gain. Some times, the fixed beam will not be enough for most 5G applications special when the target is moving and which caused to more losses by multi-pass losses that may decrease the total efficiency of array. So that, The last array topic to be covered is that of phased arrays. As already mentioned, phased arrays allow for electronic beam steering by varying the phase or time delay to each element.

Phased array antenna had some benefits compared than the arrays with fixed beam [52]:

1. It has a higher degree of directivity. The directivity of an array increases as the number of items increases.

2. It has electronic steering, which eliminates the need for clumsy mechanical steering utilizing servo motors. As a result, the beam may be shifted in the indeed direction in milliseconds.

3. It can be utilized for surveillance and tracking in radar application .

4. It can radiate multiple beams simultaneously to achieved multifunction operations.

5. Mechanised beam steering is possible in both planes (XZ and YZ) using planar array structure

6. The components of a linear array must be arranged in a very simple way.

1.7 Problem statement

Most existing antenna arrays working with fixed one beams are not suitable for the 5G systems. Also, they support one polarization, so their spatial capabilities are limited. Furthermore, other limitations are the operating frequency bandwidth, beam steering coverage area, high mutual coupling, and large size. Some of these limitations belong to a type of the antenna utilized in the array design and some belong to the array structure. Here, our attention will be focused on some these limitations such as impedance bandwidth, gain, coverage beam steering, and size antenna to come up with new design that can mitigate them.

1.8 Thesis contribution

i . Create a single cylindrical dielectric resonator antenna by modifying the radiator part with stacked DRs to increase G and BW.

ii . Design other cylindrical dielectric resonator antenna and modified by using other technique which call DR embedded patch antenna to enhance the gain.

iii . Design and study dielectric resonator planar array antenna which performance on the individual antenna radiation pattern.

iv . Increasing scanning angle range of beam steering by selection 8x8 planar array geometry shape.

1.9 Layout of thesis

i . Chapter Two: deals with literature review of many of the antennas that relate to our work.

ii . Chapter Three: deals with antenna theory on single and multi elements.

iii . Chapter Four: covers the theory and design of the proposed dielectric resonator based on modified radiator method for individual element.

iv . Chapter Five: this chapter includes a design phased array planar.

v . Chapter Six: in this chapter includes the conclusions of proposed single C-DR antennas and C-DR array antenna.

CHAPTER TWO

Literature Review

Many antennas based on monopoles, dipoles, and microstrip patches for mm-wave applications have been proposed in the past. These suggested antennas are simple to build and construct on the chip, and they offer advantages such as low cost, compact size, and weight. However, in addition to these benefits, these antennas struggle from conduction losses narrow impedance BW and lower radiation efficiency due to the presence of lossy silicon substrate materials. This issue can be handled by employing a dielectric resonator, which can decrease loss even at mm- wave frequencies. DRA has been an appealing contender with the development of ceramic material with various desirable properties in the 1980s for use in 5G applications [53]. Broadband antennas with sufficient gain and excellent radiation efficiency with a small construction are required in current microwave systems, as with mobile and portable radio devices .

Different techniques to increasing bandwidth include combining two nearby resonators and adjusting the feed architecture [12].Various approaches for dielectric resonator antenna gain augmentation have been published, such as stacked multi layers DRAs [5], decreasing the Q-factor of the DR [54], modifying mechanism the feed antenna [55], combination two adjacent modes resonated [56]. However, many methods are represented to improve the gain such as the use of many DRAs configuration in an array can enhancement the gain in the boresigth direction [57], the utilized of electromagnetic band gap (EBG) designs [58],

And utilizing DRA in its higher order modes [54], DRA embedded patch

antenna [59]. Moreover, many researchers have used different performance enhancement strategies in antenna designs to improve one or more parameters such as BW, gain, efficiency, mutual coupling reduction, and compactness sizing.

So, according to the designs are represent in this thesis, the literature review chapter will be organized as follows: the geometrical designs and parameters of the stacked DRAs method are discussed in next Section , followed by DRA loaded patch antenna technique then array with beam steered (Phased array antenna) discussion in Section 3 .

2.1 Overview single Element.

In [3] a rectangular dielectric resonator (R-DRA) with a ground layer is under R-DRA made from material with relative permittivity of 10 and loss tangent of 0.002 A micro-strip line feed printed on a substrate (Rogers RT/Droid 5880 has a relative permittivity of 2.2 and thickness is 0.25mm) below the ground. R-DRA excited by aperture slot coupling etched under the radiator . As shown in figure2.1, the position slot under R-DRA directly, can generate higher order mode $TE^{x}_{\delta 15}$ that be make the maximum gain achieved is 9.2 dBi with narrow band width, so array cylindrical holes inserted in DR for improve BW = 17.3% (ranging from 23.8 GHz to 28.3 GHz) as in , which that caused a decrease in the value Q-factor ($BW \propto \frac{1}{Q}$).

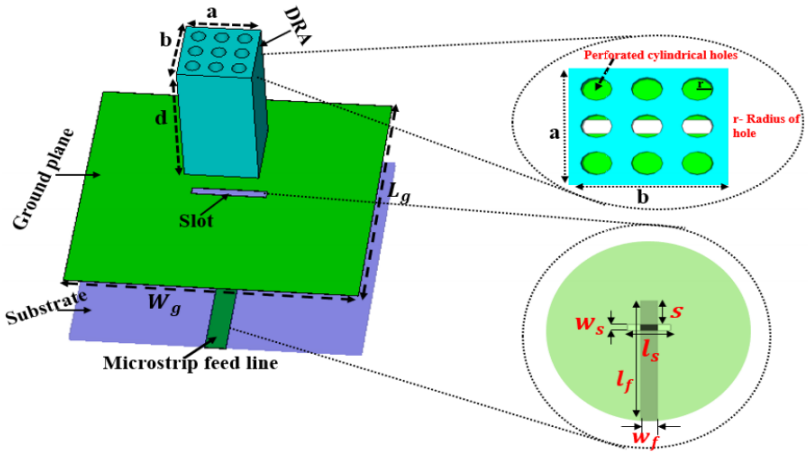

Figure 2.1: Geometry of the prototype R-DRA [3]

The antenna achieved symmetry radiation in both E-plane (XZ) and H-pane (YX), so that over the whole impedance bandwidth, the pattern exhibits a broadside radiation feature.

A dual polarizations dual ports stacked R-DRA were presented in [4], two DRs putting each one on other vertically with dimensions are Hb = 1000, Lb = 1400, Hd1 = Hd2 =525, Ld1 = 1000, Ld2 = 800, Lg = 6000, s = 300, and d = 500 where the unit is μm and excited by orthogonal wires for generated circular polarization suitable for mm-wave applications. The purpose of excited by dual wires to reduce effect interference caused by the reflection of the electromagnetic waves between DR layers. Therefore, double wire bended is added to the design to reduce this phenomenon, as shown in figure2.2 and 2.3.

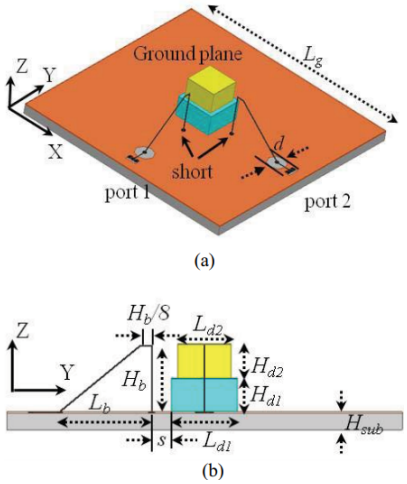

Figure 2.2: (a) 3D and (b) Cross-sec. views of stacked [4]

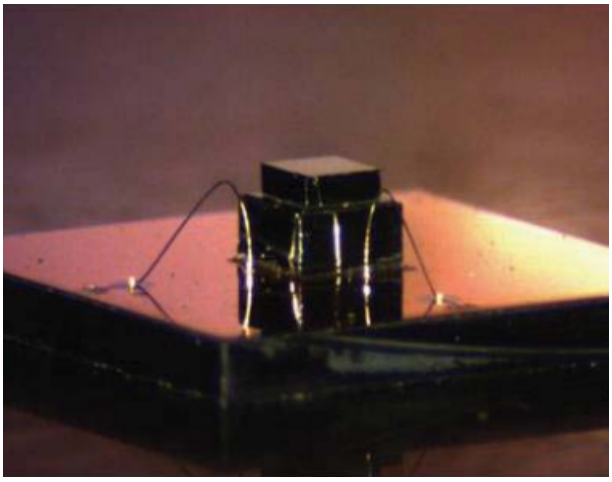

Figure 2.3: Photographs of implementation stacked DRA [4]

Meanwhile, the wires are contributed by other mode is (TE^x_{111}) shared with the original mode. The bandwidths applied to the dual band of V band and E band are from 53.5 to 65 GHz of 60 GHz and from 74.5 to 91 GHz with resonant frequency 81 GHz. Th antenna gains are 5.1 dBi at 60 GHz and 6.3 dBi at 81 GHz, respectively.

Three boxes DRs stacked with properly selection of dimensions to generated three resonant modes were represented in [5]. As shown in figure 2.4, the first box (L2=10mm, B2=20mm, and H2=5mm) is put over the substrate layer (designed by

Arlon DiClad 522(tm)) and excited $HEM_{11}\delta$ mode which is reduced by simulated by a coaxial probe inside the first box and extends to other boxes 2nd (L3=10mm, B3=10mm, and H3=6mm) and third (L4=10mm, B4=10mm, and H4=10mm) since 2nd with 3rd made by using Rogers TMM 6 (tm)with permittivity 6 and Taconic CER-10 (tm) with permittivity 10 respectively. Moreover, given the remaining modes $HEM_{21}\delta$ and $TM_{01}\delta$ respectively. The sizes of box 2nd and 3rd are different and installed above the first box; on the other hand, a metal layer as aground plan adjoining in lower side from the substrate. The results show BW=2.9 GHz product by combining three modes each with other and G=9.023 dB.

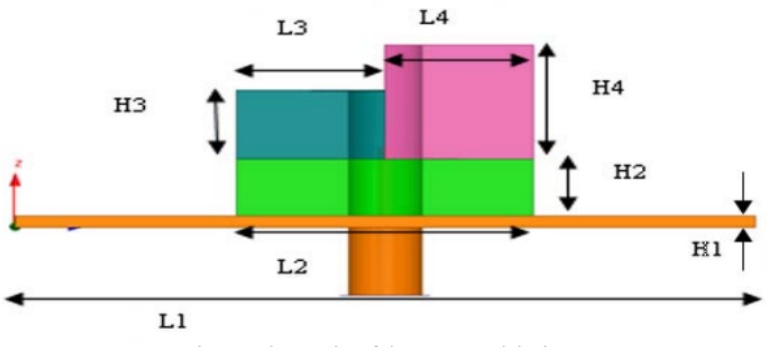

Figure 2.4: Structure of the design [5]

In [6] CDRs (height of dielectric sheets (d1 and d2) are 6.5 and 0.5 mm with $\varepsilon_1 = 2.2$ and $\varepsilon_2 = 23$ respectively) arranged vertically and installed on the upper side from the ground. By looking figure2.5 and figure2.6 , CDR is excited by the coaxial probe beside the stack and touch it through vertical metal propped at the radiator's wall, which controls the matching, if the metal dimensions choice properly. $HE_{11}\delta$ mode is generated to improve gain.

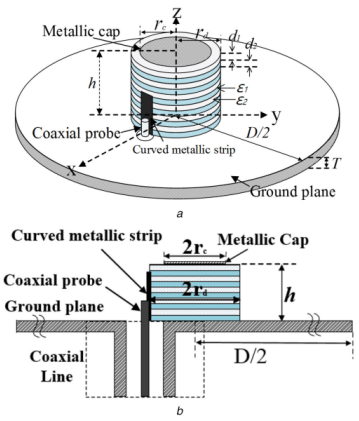

Figure 2.5: Geometry of prototype design (a) 3D view, (b) side view [6]

Figure 2.6: The fabricated antenna [6]

The electric distribution fields inside cylindrical DR guided by disk metal above stacked DRs. Since the disk's affection will be cancelled any component of the tangent electric field and concentrated inside the cylindrical, which increases gain virtually.

A wideband aligned DRs antenna suitable for 5G applications was represented in [7]. The proposed design about two DR sheets arrange over some with high dielectric constant ($\varepsilon_r \geqslant 36.5$) the air cap separated between both sheets and put above cavity substrate, finally, plan ground installed in the lower face of the substrate as shown in figure2.7 and figure2.8. The purpose of air caps (one between DRs stacked and one in the substrate) is to make the dual DRs sheet work such as magnetic wall and the ground as electric walls after excited the antenna with H-slot aperture coupling with microstrip beneath the slot.

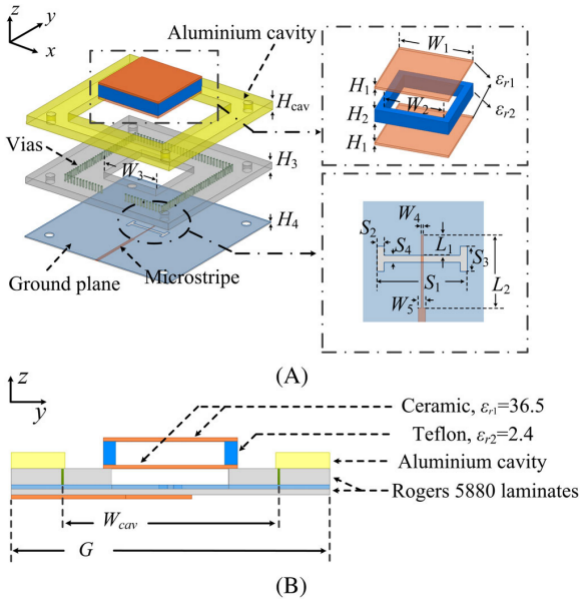

Figure 2.7: Geometry of prototype design (a) 3D view, (b) side view [7].

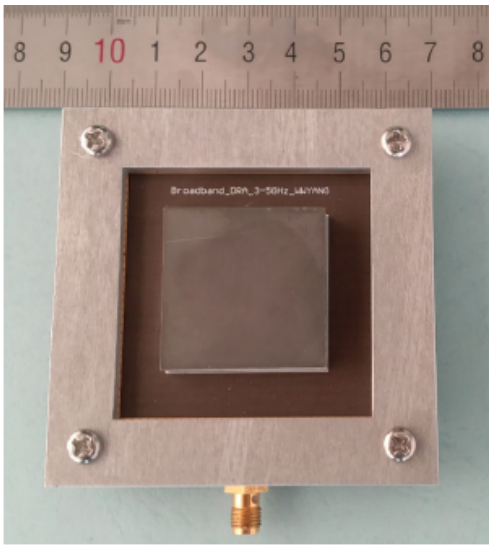

Figure 2.8: Photograph of the prototype stacked DRs antenna [7].

Four modes merged excited by mentioned design due to enhance bandwidth (54%), Q-factor decreases by tuning the distance among the magmatic (M) and electric (E) walls as follow: TE_{111} , TE_{131} modes excited from tunable M and E walls and the feeding slot generates other.

An annular conical-cylindrical DRs (CCDRs) design excited by a coax-fed cylindrical monopole (MP) was represented in [8]. On its top face, the substrate DR put the CCDRs, and the bottom face installed on the ground(see figure2.9). MP connected with the inner of coaxial to control the coupling. The antenna work at a wide range frequency (5 - 35)GHz with multi modes simulated to formed wide impedance bandwidth suitable for ultra-wideband wireless applications and as wideband electromagnetic interference (EMI) sensors. From figure2.9 , figure2.10, the coupling between two elements is managed from a distance among MP and CCDRs. Total gain is 7.14 dB, respectively centre frequency 27.5 GHz.

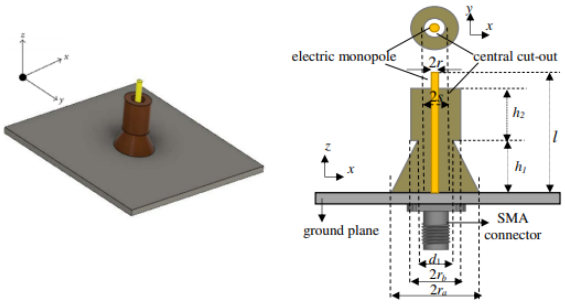

Figure 2.9: The structure prototype CCDRs [8]

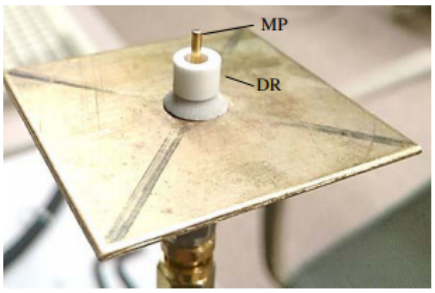

Figure 2.10: Photograph of total CCDRs [8]

In [9] two radiators R-DRA high dielectric constant ($\varepsilon_r = 9.8$) installed above a substrate made from Roger RT/Duroid 5880 ($\varepsilon_r = 2.2$), pair symmetry slots were cut in both left and right sides of the upper R-DRA as shown in figure2.11, figure2.12, to excite DRA, microstrip line put under the lower R-DRA directly on the top face of the substrate. To mitigation the back radiation, layer from metal adjoining of the bottom face of the substrate. The proposed antenna covered two 5G bands 28, 38 GHz , by three impedance bandwidths (7.34, 4.04 and 3.30 GHz) and maximum gain of 7.6 dBi.

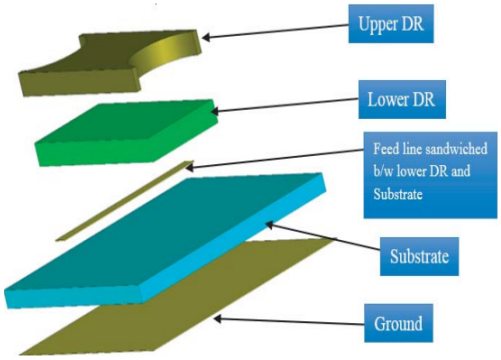

Figure 2.11: The geometry shape of total design. [9]

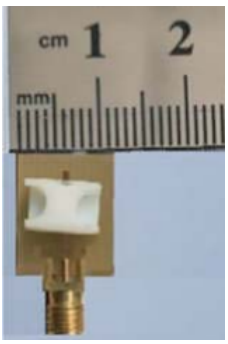

Figure 2.12: Photograph of prototype antenna . [9]

A CP C-DRA was presented in [10], which consists of FR4 and RogersRO6010 in stacked (two C-DRA above the substrate and excited by incorporate microstrip feed was printed on lower face in the substrate as illustrated in figure2.13. The antenna is suitable for 5G application at operating frequency 28 GHz with impedance BW 22.5 GHz from 24 to 30.3 GHz. The maximum gain of the radiation pattern is 10.93 dB at center frequency 28 GHz.

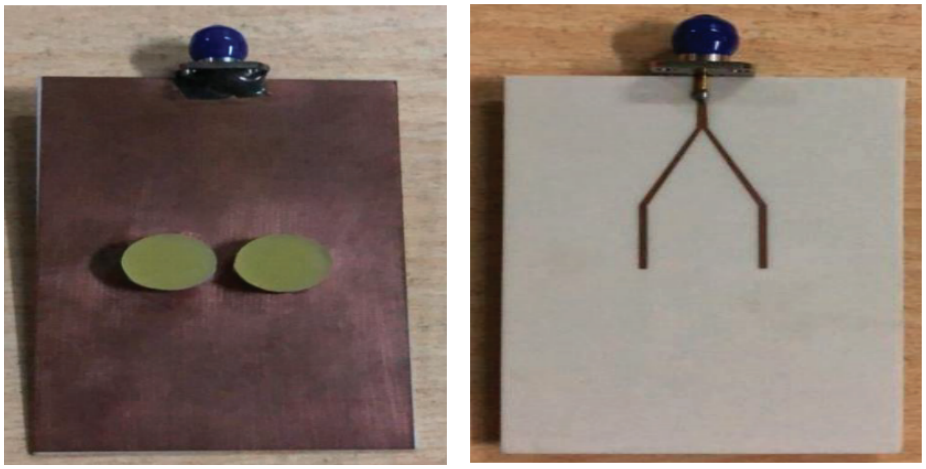

Figure 2.13: Top and bottom photo of the fabricated C-DRA [10]

After surveying many papers about stacked DR methods with different geometry shapes and explaining how to enhance bandwidth and gain with stacked DR. Now will start to present several articles to improve antenna parameters using the dielectric resonator loaded patch antenna technique. By review, previous researches can notice this method easy in fabrication compared to stacked DRs. An aperture-coupled cylindrical dielectric resonator antenna (C-DRA) was presented in [60].

In order to enhance the frequency bandwidth and miniaturize the antenna size, a multilayer structure with metallic posts was utilized. The presented antenna showed a wide-band operating frequency, as shown in figure2.14. $HE_{11}\delta$ excited inside C-DRA and combined with other two modes generated from the embedded patch and metallic posts loaded C-DRA to give wider bandwidth than traditional C-DRA. The proposed antenna offers a fractional BW of 16.5 at the center frequency of 9.27 GHz and a peak gain more than 4.56 dB in the matching band.

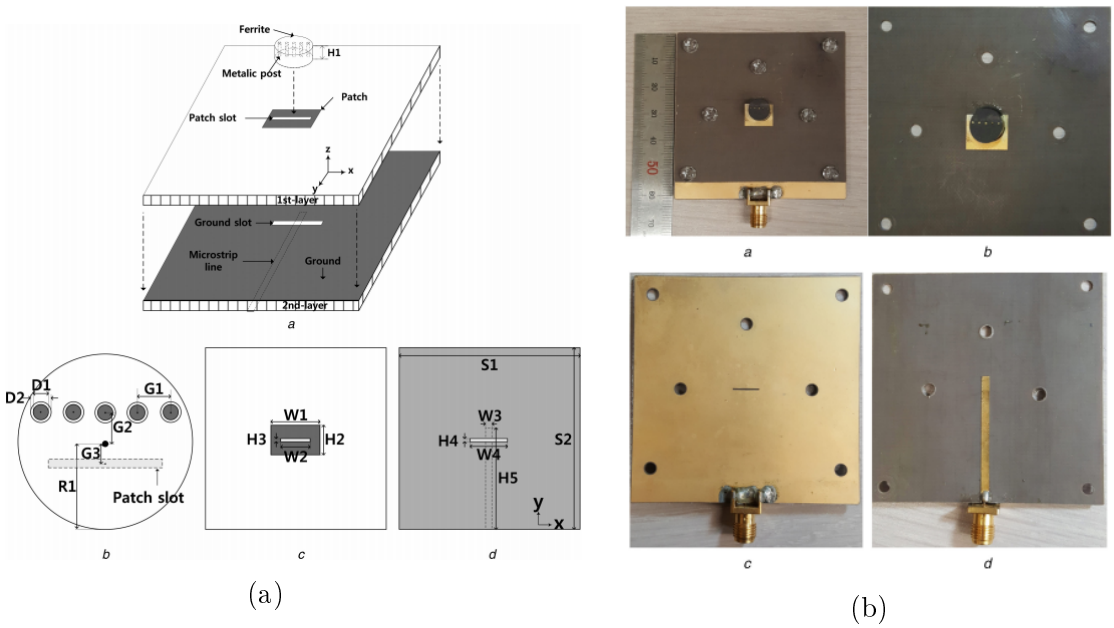

(a) (b)

Figure 2.14: (a), Geometry of the prototype antenna (b), Photograph of implementation the design. [60]

A wide-band dual fed C-DRA for 5G mm-wave application was introduced in [11]. The presented design showed a wide operating frequency band and high gain for both linear polarization patterns. In figure2.15, C-RDA (ε_r of 4.5 for the Preperm L450 resonator material) install above substrate which made from $\varepsilon_r = 3.38$ for the Rogers 4003 and thickness a 0.203 mm. CDRA is excited by a spatial feeding structure on metal pieces put under C-DRA. This helps produce many bands resonant frequency. The prototypes of a single element a maximal gain of 7.1 dBi with fractional BW 40% and 20%.

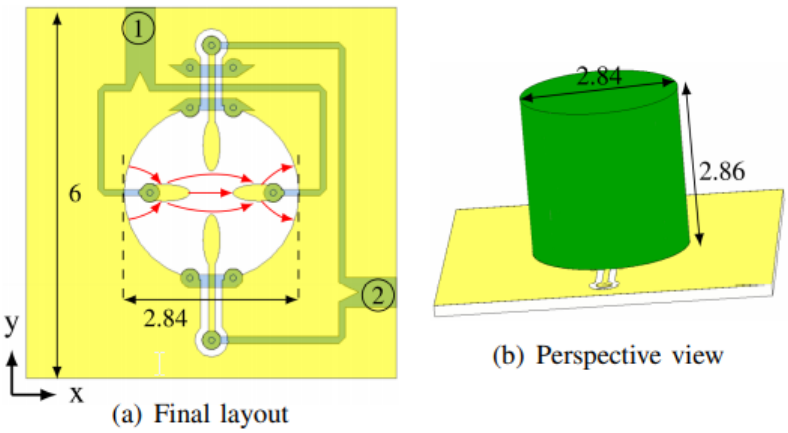

Figure 2.15: Geometry of the prototype antenna [11]

In [12] DR loaded patch antenna was represented. R-DRA over a substrate

and which be excited by coaxial feed beside the rectangular patch antenna is installed vertically above R-DRA as shown in figure 2.16. TE^{y}_{111} mode simulated by R-DRA and by choice properly, the patch TM^{z}_{100} mode was generated and merged with the previous mode to enhance band gain 11.5 dB with BW=52%.

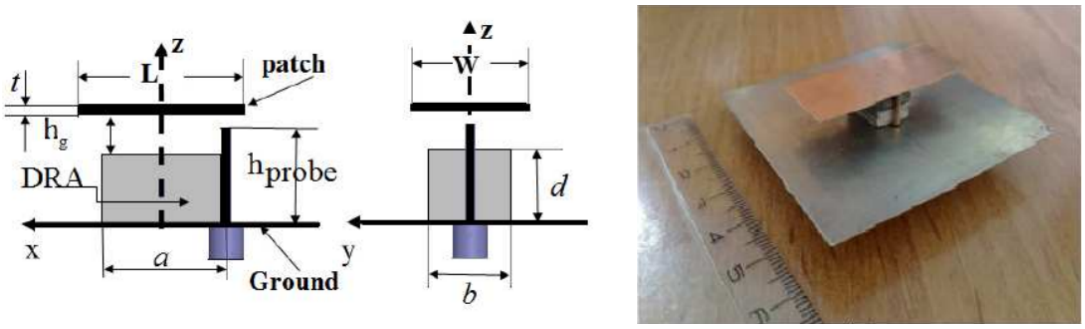

(a) (b)

Figure 2.16: (a), Geometry of total design (the left is XY side view, the right is YZ side view). (b), Photograph of implementation the design. [12]

The Air cap among R-DRA and patch was controlled to improve the gain and shifting TM^{z}_{100} mode to upper on lower frequencies, so it is selected carefully. The surfaces wave propagation decreases by increasing the air cap between R-DRA and patch.

A hybrid C-DRA and patch antenna design were studied in the paper [13]. A half-cylindrical DRs (HC-DRs) with varies $\varepsilon_r s$ have been aggregated on top of a substrate, under HC-DRAs printed slot-patch antenna to excited DR with the partial ground in the same location (see figure2.17). Patch antenna fed by microstrip line and divided into parts first is a rectangular patch to increase the gain and second was slot patch for achieving circular polarization (CP). The fraction impedance bandwidth enhanced by multi modes excited from dual HC-DRs, simulated by CPW.

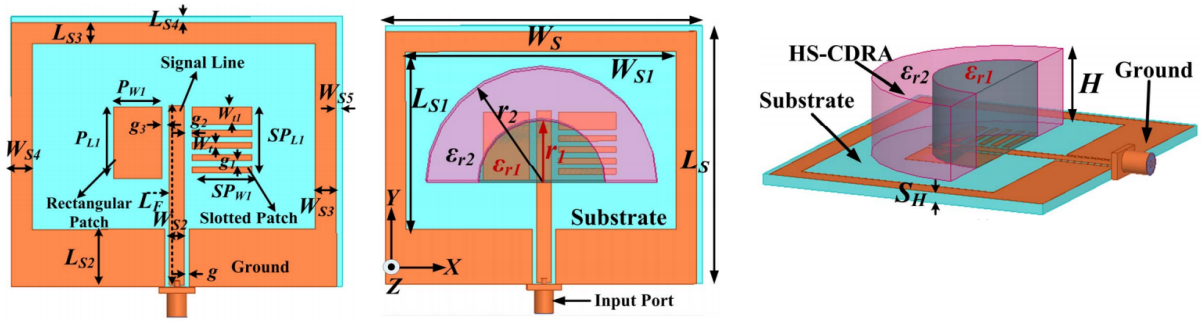

(a) (b) (c)

Figure 2.17: Geometry shape of prototype antenna (a) modified CPW-feed (b) HC-DRA (c) 3D [13].

Due to these benefits over linearly polarized (LP) antennas, circularly polarized (CP) antennas are utilized to transmit and receive antenna signal stability, weather penetration, and reduction of multipath interference. Therefore, the proposed design attained CP at some band resonant frequency in 5.2 GHz.

The geometry shape of the patch can help to enhance BW and gain or both. In [14] C-DRA loaded patch antenna with two different patch shapes (circular and crescent), which improved impedance bandwidth. The DRA was excited by a coplanar waveguide (CPW), which terminated by magnetic dipole mounted in the center of C-DRA underneath it, such as shown in figure2.18 (a) , (b).

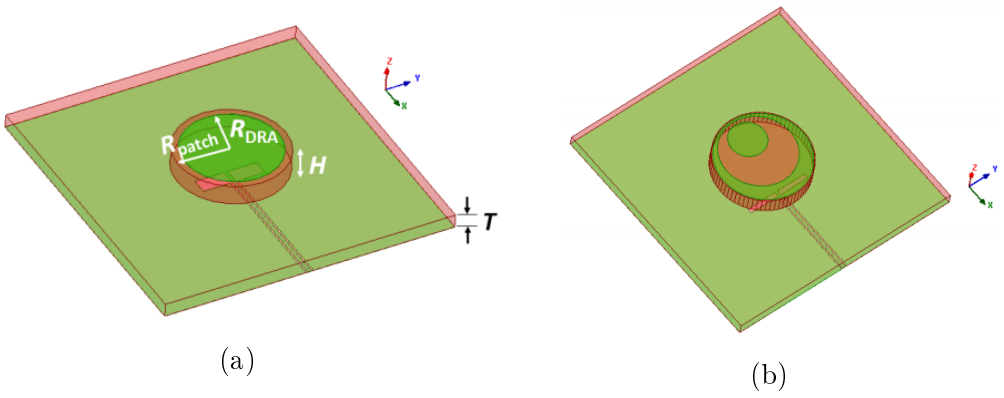

(a) (b)

Figure 2.18: Geometry shape of prototype antenna (a) circular patch (b) crescent patch . [14]

Figure 2.19 explain the electric field distribution along the top side of the DRA since the main field was created along the x-axis, which is matches that of DRA. Both patch antenna was generated in other mode merged with original mode,

which excited in DRA led to expanded bandwidth. Furthermore, the crescent shape provides wider BW compared to circular patch at operating frequency 60 GHz.

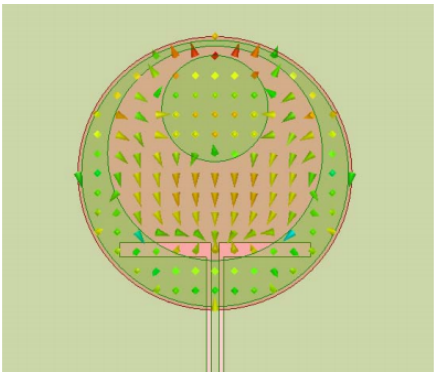

Figure 2.19: The virtually E-field distributions of the prototype design at 60 GHz

A Ultra Wide Band (UWB) hybrid DR and metal patch antenna was studied and implemented in [15].A rectangular planar monopole with CPW feed structure was installed on a substrate made from a dielectric constant is 3 and $tan\delta = 0.0013$, on the other hand, triangular-DR ($\varepsilon = 20$, $tan\delta = 0.002$) stacked on top of the patch monopole as shown figure2.20 (a). The prototype radiator (equilateral triangular and patch monopole) was provide from total radiation and alleviate the cross-polarization. The proposed design attained 112% impedance bandwidth from 3.2 to 11.35 GHz and gain is 3.3 dB for omnidirectional applications.

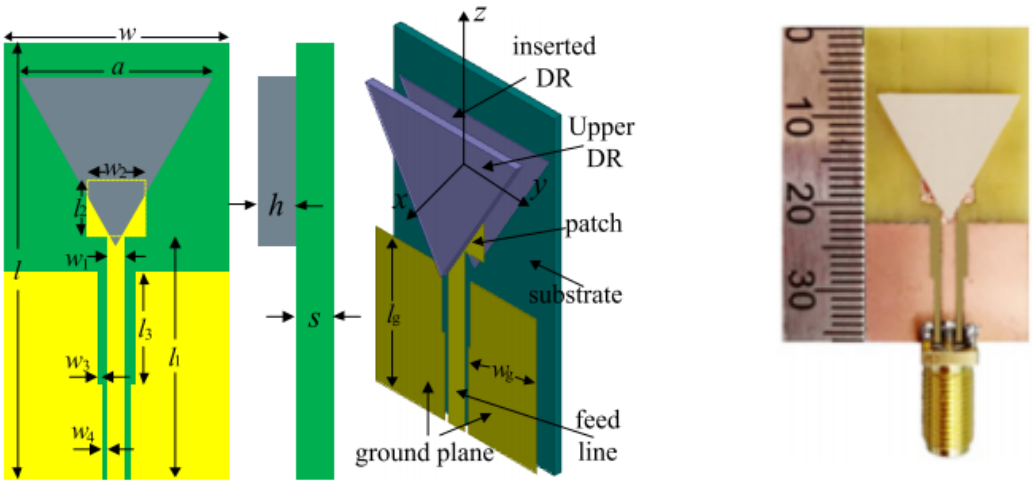

(a) (b)

Figure 2.20: (a) Geometry of the prototype UWB omnidirectional low-profile discrete embedded antenna (b) The fabricated antenna top view [15]

2.2 Overview According to Array Antenna

The most important characteristics of 5G antennas are a high gain, steady radiation pattern, and a broader frequency band. These special cations cannot be met by a single component hence a multi-element antenna (array antenna) is designed by most researchers for 5G applications.

An 8 x 8 planar array fed by Dolph Chebyshev distribution method is represented in [16]. (see figure2.21, figure2.22) 64- R-DRAs installed on top of the substrate type Arlon DiClad 880, each element excited by slot aperture coupling etched on the ground layer above the substrate, which was current to the slot from series-parallel hybrid feeding network printed on the bottom surface of the substrate. The total design achieved 2.1% impedance bandwidth at centre frequency 26 GHz, with again 20 dB for HPBW equal 74^o.

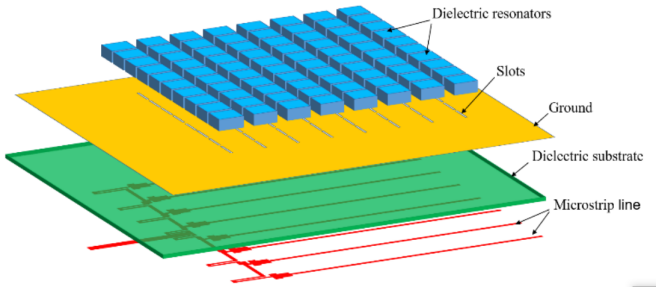

Figure 2.21: A 8 × 8 planar array simulated by series-parallel hybrid feeding network [16].

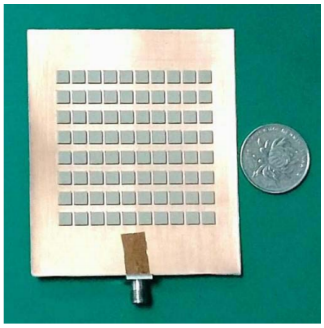

Figure 2.22: Photograph of prototype design [16].

When studying any design array antenna very important to look at side lobe level (SLL) so that the proposed design attained SLL was 25.3 dB and 29.4 dB in both E- and H-plane. Meanwhile, the first null of the proposed array pattern was much deeper, suitable for a directional broadside.

A CP has several benefits more than LP, as mentioned early such as flexibility in the orientation between TX and RX, mutiny to multi bath losses, and reduction of mismatch polarization. So, CP high gain (4 x 4) planar array antenna was represented in [17] as shown in figure2.23 (b). A 16- elements magnetic electric (EM) dipole as radiator fed by microstrip ridge gap waveguide (MRGW) without

connecting by strip line to the individual antenna can cause production dissipation that leads to spurious radiation. A substrate RO3003 deposit on top of pins and printed on the upper surface of the radiators and bottom the ground with slot was engraved in the Centre layer (figure2.23 (a)).

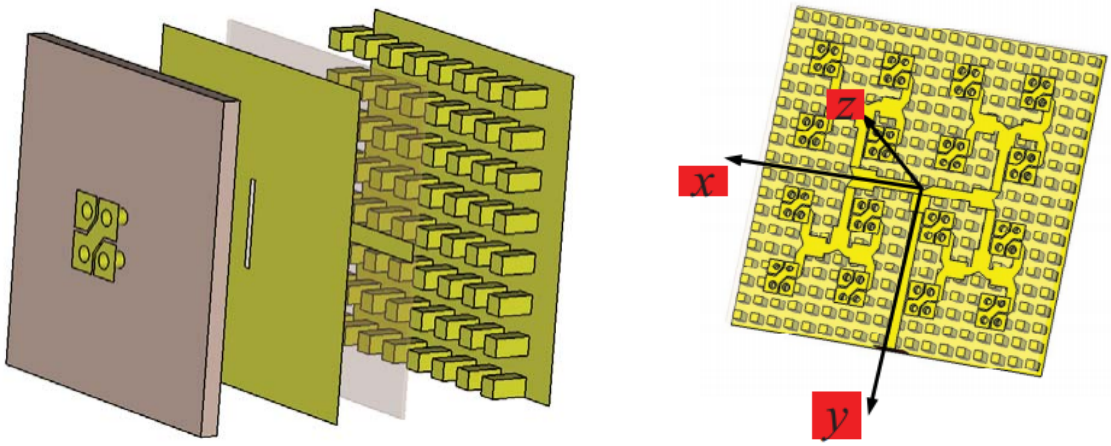

(a) (b)

Figure 2.23: (a) The structure of single element (b) The prototype array design [17].

Enhancement of the isolation was obtained by an air gap created between the ground and MRGW. A proposed design obtained wide bandwidth from 53.5 66 GHz at center frequency 60 GHz with AR 18.3% (52.4-68 GHz).

For increasing the coverage area, a beam-steering technique utilized in the array, as in the next research. A phased planar array 64- elements stacked patch antenna was represented in [18] (figure2.24(a)). The structure achieved rang scanning ± 50 and ± 25 in both H- and E- plane, respectively. A single antenna was stacked patch was excited by coaxial probe fed, which attained 14% bandwidth (28 - 32) GHz. Total gain of 22.5 dB on the centre frequency 28 GHz. To keep on impedance antenna during beam steering operation, multi dummy elements added around elements array this clear in figure.2.24 (b) .

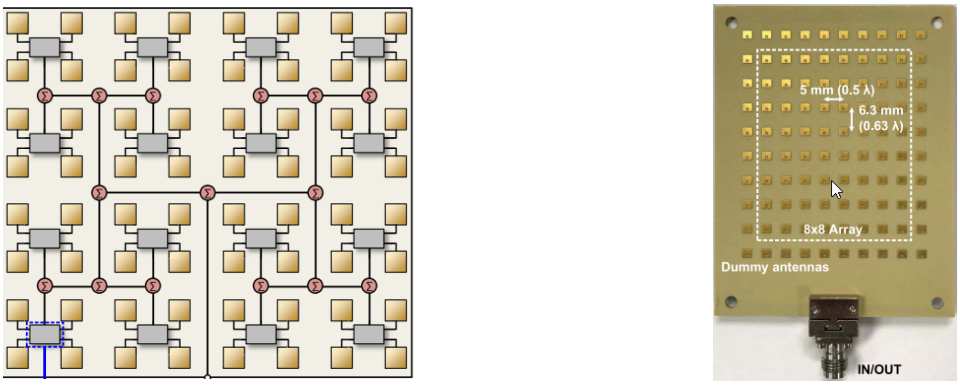

(a) (b)

Figure 2.24: (a) The schematic 8x8 patch array antenna (b) Photograph of prototype array design [18].

An R-DRA 3 x 3 planar array was proposed in [19], the center frequency is 28 GHz. figure2.25 (b) explained a nine elements array antenna, 6 - elements excited with six ports while the rest 3-elements was utilized as a parasitic component, which led to enhancing impedance bandwidth 18.9% (26.3 - 31.6)GHz with respectively the gain (13.7 dB). The array consisted of R-DRAs with special feeding single antenna figure?? (a) to achieved high band width 23.2% at resonant frequency 28 GHz

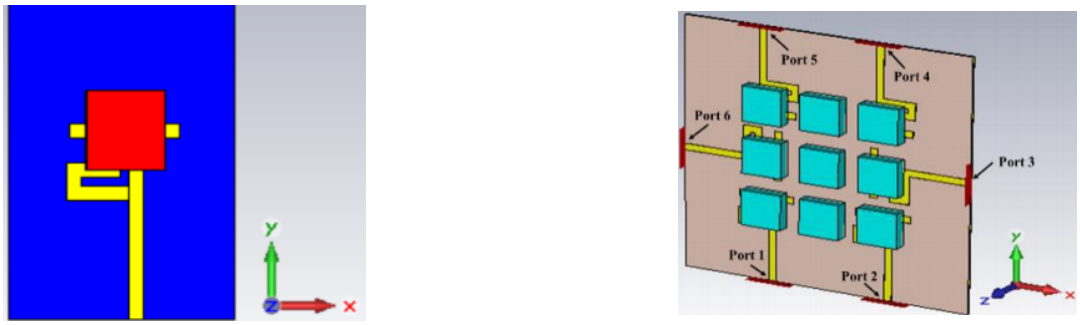

(a) (b)

Figure 2.25: Geometry shape of prototype antenna (a) Indivitual R-DRA antenna with the feeding (b) The proposed planar array [19] .

It is noteworthy, the geometry shape of a prototype antenna (figure 2.25 (b)) was structured with mounted R-DRAs, feeds, and parasitic components on the same top face of the substrate made by RT/Duroid 5880 with an ε_r of 2.2, so that many modes simulated in the same time.

A planar switchable 3 x 8 array was investigated in [20]. The complete array

consisted of a three-slot subarray, each sub-array was structured from a substrate with a low dielectric constant ($\varepsilon_r = 2.2$) and printed on one side a metal plate which the slots etched on the plate fed by the coaxial probe as shown in figure2.26.

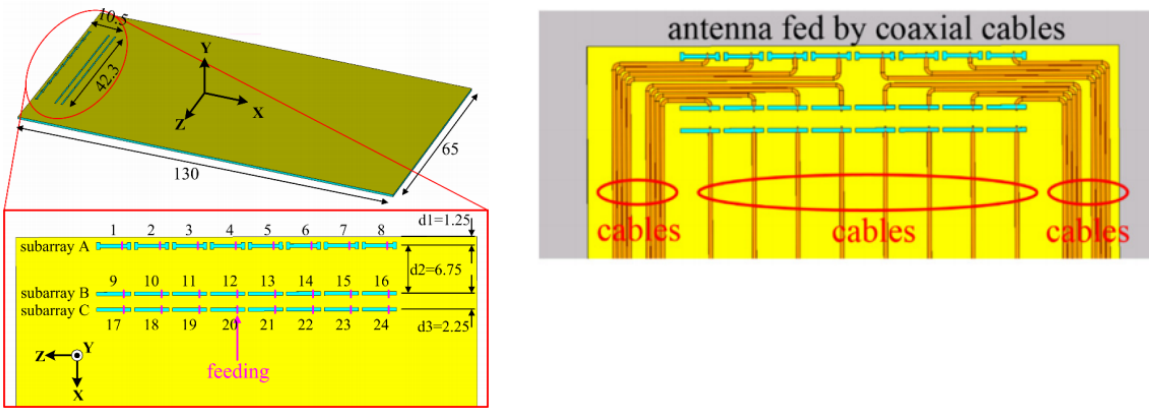

(a) (b)

Figure 2.26: (a) The total structure array (b) The slots with coaxial feeds [20].

The array realized a wide scanning range (more than ∓ 20) for each subarray because of impact surface waves which help to scalable the scan angle. A three sub-array operated as an alternative mean any sub-array operate other sub-arrays will be terminated. The proposed design suitable for mobile applications at mm-waves. Moreover, the edges of the slots in sub-array A modified to obtain the required frequency (28 GHz). Multibeam multi directions scanning was generated by a three sub-array (A, B, and C) with total gain 8 dB and impedance bandwidth 2 GHz.

A grid array antenna was presented in paper [21]. The prosed array consisted of 20 brick cells and printed on a substrate by Roger RT/Duroid 5880 ($\varepsilon_r = 2.2$), which was formed by length and width since length operated as transmission line while the width like a radiator, all cells fed by coaxial cable. Fractional bandwidth was realized 5.4% from 28.37 GHz to 28.85 and total gain 16.5 with HBPW = 25^o. The antenna is compared with a Microstrip Patch Array utilizing the same substrate and dimensions. figure2.27 illustrated the total structure.

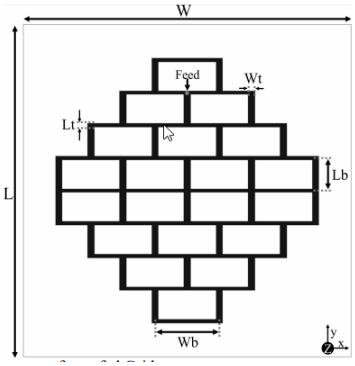

Figure 2.27: The geometry shape of grid array antenna [21].

Polarization diversity is one approach to improve the data rate without utilizing extra resources (frequency or time slot). By delivering two orthogonal polarized data streams at the same frequency and same time slot (horizontal and vertical),in [22] a 2x64 dual-beam dual-polarized 5G TRX phased antenna array was characterized at 28-32 GHz. figure 2.28 (a) encompassed the whole structure of the array consisting of a stacked patch antenna that excited by dual feeds coaxial probe to generate V- and H-polarization. Each beam in the proposed design attained the same scanning rang in both H- and E-plane with 13.7% from 28 to 32 GHz at center frequency 29 Ghz.

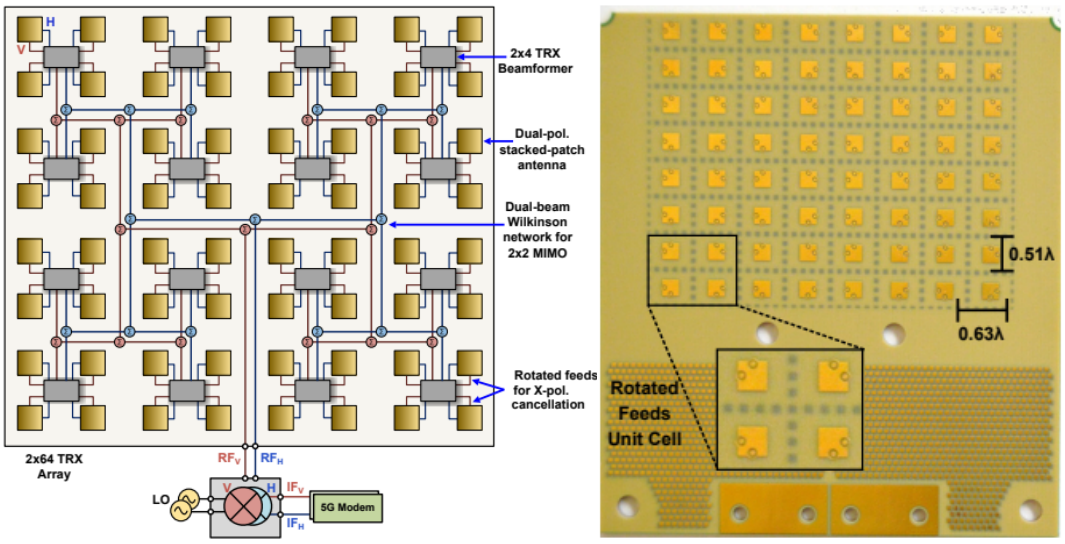

(a) (b)

Figure 2.28: (a) The geometry shape of a 2 x 64 - element phased array antenna (b) Photograph of prototype design [22].

In some times, the antenna must occur in different frequency bands, each with a bandwidth greater than 15% [23], to cover the 5G mm-wave bands. Addi-

tionally, the dual-polarized antenna may transmit and receive in both directions, reducing polarization adaptation effects.

In [23] A dual-band dual-polarization, a 1 x 4 patch array antenna with a compact size and operated in the 26 GHz and 39 GHz frequency bands, was proposed (see figure2.29). In general, two substrates with different materials (Rogers RT4350 and Rogers RO4450F for upper and lower substrate respectively) each one had patch antenna special geometry shape simulated by coaxial fed to attained dual bandwidth 14.6% (24.6 - 28.4)GHz excited by bottom patch and 19.4% (36.2 - 43.8) by top patch. The mentioned antenna suitable for mobile 5G applications and provide the fine gain in both frequency bands (11.9 dB at 28 GHz, 12.1 dB at 39 GHz) with a scanning range from 0 to 40^o by the top and 30^o by bottom.

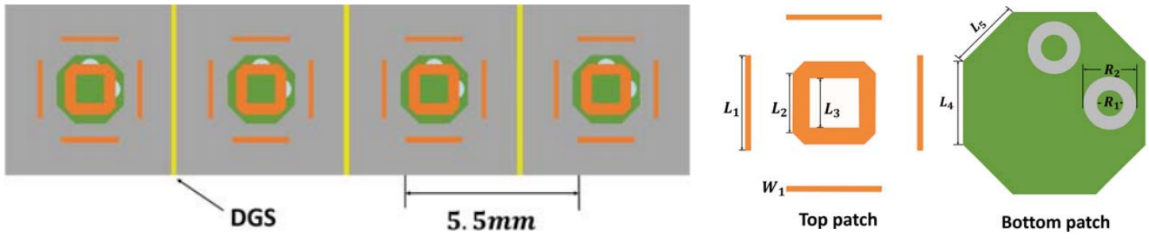

(a) (b)

Figure 2.29: (a) The geometry shape of a 1 x 4 patch array antenna (b) The single antenna of prototype array design [23] .

Multibeam, an 8 x 8 patch array antenna, was presented in [24]. The array consisted of eight sub-arrays arranged vertically with 8 - ports since each eight-element subarray fed from the first antenna and the current follow to remained seven antennas as serially illustrated in figure2.30 (a, b).). This configuration is beneficial for beam steering in a horizontal direction, which attained several steering angles.

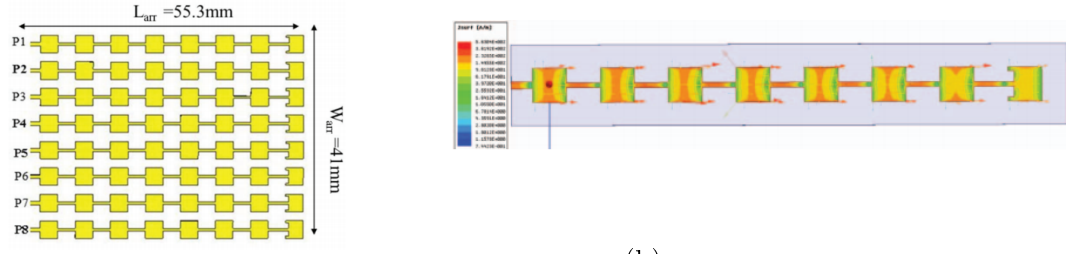

(a) (b)

Figure 2.30: (a) The geometry shape of a 8 x 8 patch array antenna. (b) 8-element Series-fed Patch Array [24].

It is worth noticing the side lobe level (SLL) parameter acceptable under - 15 dB as a threshold for any array design. In [25], a 2 x 3 patch array antenna was proposed. Firstly, all ports excited will equal amplitude and phase, and SLL was - 7.1 dB, but when selected, various amplitude SLL improved to -19.3 dB at the same design.

figure2.31 illustrates the geometry shape proposed design, which reduced the number of ports by depending on successive fed of a single element. Moreover, 2% impedance bandwidth attained from 27.64 to 28.34 and a total gain of 13.8 in the broadside when $\phi = \theta = 0$ at operating frequency 28 GHz.

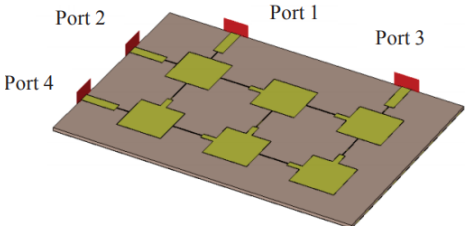

Figure 2.31: An 2 x 3 with 4-port patch array [25].

Lower mutual coupling levels between elements array required in 5G application because of the short wavelength of millimetre wave. A CDRA consisted of 1 x 4 PAA represented in paper [26]. Total array design formed from two layers (see figure.2.32 (a)), on the bottom face of the substrate of Rogers 5870 material with ε_r of 2.33, microstrip feeds line printed (figure2.32 (b)) and CDRA's which selected from Rogers 3010 having ε_r of 10.2 putting in the above face on the substrate as in figure2.32 (c). All DRA's excited by rectangular slots etched under C-DRA directly. For reduces mutual coupling between elements,

thin layers' metal instead vertical between CDRA's as explained in figure2.32 (d).

A three-quarter wavelength transformer with a 35-ohm impedance was used to deliver the same amount of power from the 50-ohm feed line to each CDRA array. The proposed design was achieved beam steering angle 45^o at operating frequency 7.5 GHz with a gain equal to 10 dB.

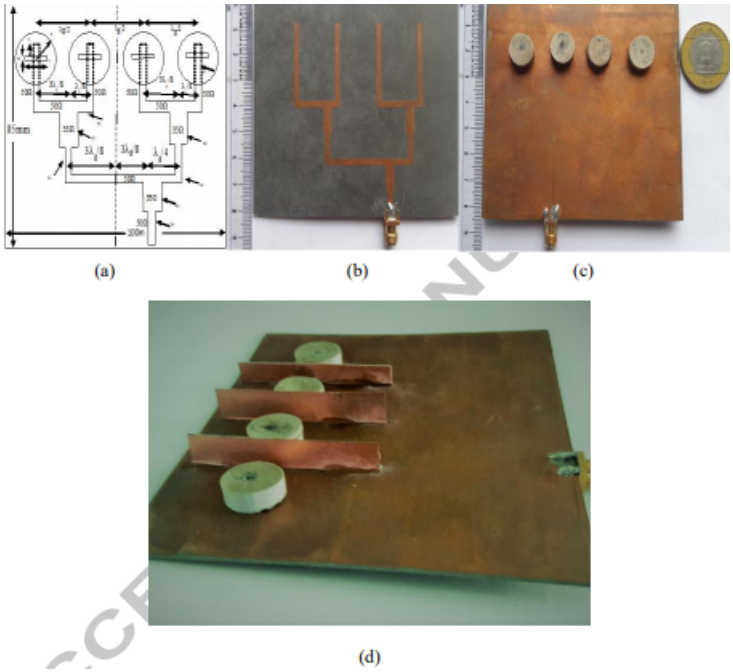

Figure 2.32: a) Schematic diagram of static phased array using shifted feed point, (b) Feed network of array prototype, (c) top view of antenna array (d) side view of antenna array with insertion of thin metallic layer [26].

CHAPTER THREE

Antenna Theory

3.1 Cylindrical Dielectric Resonator Antenna

Cylindrical dielectric resonators were used in circuit applications for many years [61]. Its high Q-factor and small design make it perfect for use in filters and oscillators, particularly in microstrip technology, where resonant waveguide cavities are not very practical. A large volume of literature is dedicated to the field configuration, resonant frequency, and coupling behaviour of the cylindrical dielectric resonator for circuit applications [62]-[63]. More recently, the radiation properties of the cylindrical dielectric resonator have been exploited, beginning with the first systematic analysis to investigate the radiation characteristics of the probe-fed cylindrical DRA [64].

The cylindrical DRA is defined by the height h, radius a, and the dielectric constant ε_r as seen in figure3.1. The cylindrical shape gives one degree of freedom more than the hemispheric form; it is the aspect ratio (a/h) that defines the k_{oa} and the Q-factor for a given dielectric constant. Thus, a high, thin cylindrical DRA can be produced to resonate at the same frequency as a large, thin DRA. However, the Q-factors for these two resonators would be distinct. This gives the designer a degree of precision that is not possible with the hemispheric DRA, which has only a single resonant frequency and one Q-factor for a given radius and a dielectric constant per mode (i.e., no degrees of freedom) [62].

For a cylindrical DRA, the designer should select the most appropriate aspect ratio to better realize the optimal frequency and bandwidth. All of the characteristics mentioned in figure3.1 (such as; a, h, θ, ε_r, and so on) as well as the mode of propagation affects the resonant frequency and radiating Q-factor of a DRA. figure3.2 displays the isolated dielectric cylindrical resonator a mode is characterized as the electromagnetic field pattern displayed within the DRA because of shape and boundary conditions of the component [62].

Cylindrical resonator modes can be classified into three major types: $TE\,(TE\,to\,z)$, $TM\,(TM\,to\,z)$, and hybrid mode. The fields for the TE and TM modes are axisymmetric and thus have no azimuthal difference. But on the other hand, the fields of hybrid modes are azimuthally depending. Hybrid modes can be further split into two groups: HE and EH [65]. For HE modes, the H_z component is comparatively small compared to the E_z component. The other field components for HE modes can then be obtained from the information of the E component only. The opposite is true of the EH modes [27].

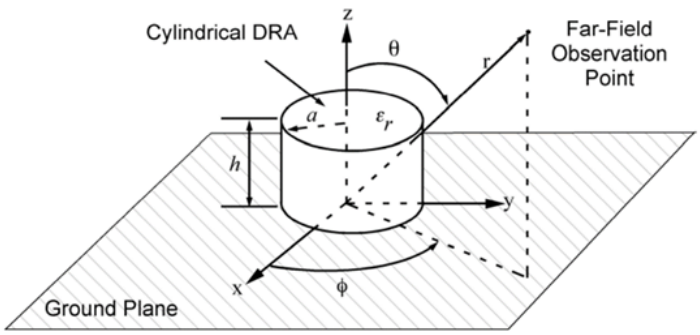

Figure 3.1: The geometry of the cylindrical DRA [27].

To denote the azimuthal, radial, and z-directional field variation within the resonator, the mode indices are applied as subscriptions to each mode family. Modes TE, TM, HE and EH are known as $TE_{0mp+\delta}$, $TM_{0mp+\delta}$,$HE_{nmp+\delta}$, and $EH_{nmp+\delta}$, respectively.

The first subscript, n indicates the number of full-period azimuthal field fluctuations, and the second index m whereas specifies how many radial variants there are. The number of half-wavelength fluctuations in the axial direction is

denoted by the subscript δ, which varies from zero to one, nearing one for high dielectric constant values .

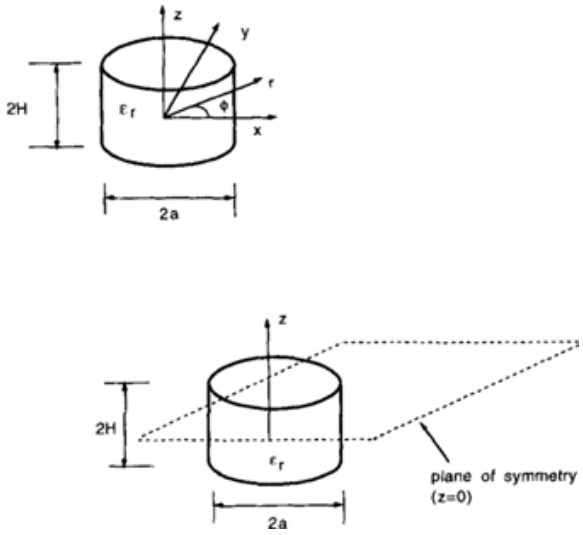

Figure 3.2: The isolated dielectric cylindrical resonator [28].

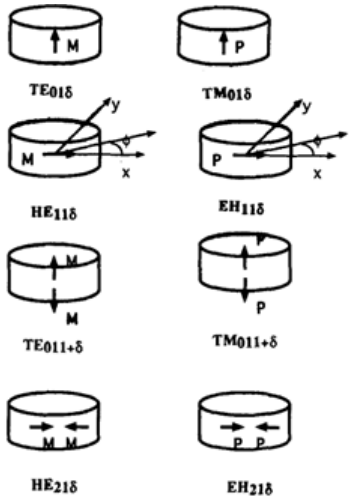

Figure 3.3: Nature of radiation of various types of an isolated cylindrical DR. M denotes a magnetic dipole, and P denotes an electrical dipole [28].

3.2 Radiation Characteristics of Various Modes

A attractive characteristic of isolated DR antennas is that, in general, the various DR modes radiate like electrical and magnetic multi-poles, such as dipoles, quadrupoles, octupoles, etc. The radiation pattern of the normal form of the DR antenna can be predicted very accurately without any detailed calculations. For eg, it is well recognized that the $TE_{01\delta}$ mode of an isolated cylindrical resonator

radiates along its axis like a magnetic dipole, as seen in figure 3.3. The $TE_{011+\delta}$ radiates as an axial magnetic quadruple [64].

Similarly, the modes $TM_{01\delta}$ and $TM_{011\delta}$ radiate like an axial electrical dipole and a quadrupole, respectively. The above-mentioned structure of the TE and TM radiated fields is independent of the dielectric constant of the resonator material [66]. It is also shown from the above discussion that the index denoting the field difference in the Z-direction within the resonator can be very useful for estimating the far-field trend in the elevation plane.

The field distribution of cylindrical DR hybrid modes has been analyzed in-depth by Kobayashi et al. [67],[65] . Kobayashi's results demonstrate that the lowest order of $HE_{11\delta}$, mode radiates like a magnetic dipole directed along the transverse (horizontal) direction as seen in figure 3.3, where it is assumed that the dielectric constant of the resonator material is strong ($\varepsilon r \geq 10$). This seems to be in line with the findings of far-field calculation based on rigorous theory [68]. These findings confirm that the far fields of the $HE_{11\delta}$ mode are similar to that of the magnetic dipole and are almost independent of the value of the Er and the aspect ratio (h/a) of the resonator.

Since the hybrid modes degenerate, there is a multi-pole corresponding to each degenerate hybrid mode. For eg, in the $HE_{11\delta}$ mode, where the Ez part varies as $\cos\phi$ inside the resonator, the radiating magnetic dipole corresponding to this mode is oriented along the radial direction of $\phi = \pi/2$, as this dipole would radiate a limit along the direction of $\phi = 0$. Mode $HE_{21\delta}$ radiates in the transverse direction like a magnetic quadrupole, as seen in figure 3.3. On the other hand, the modes $EH_{11\delta}$ and $EH_{21\delta}$ radiate like an electrical dipole and an electrical quadruple, respectively, aligned along the transverse direction.

It is important here to address some of the findings of Van Bladel's asymptotic theory [28],[69], which are very relevant. According to this principle, the modes of the arbitrary dielectric resonator are of the "unconfined" sort. The dominant

concept that leads to the radiation in non-confined modes is the term magnetic dipole.

It is also assumed that the dominant non-confined mode of an arbitrary high-permissive dielectric resonator would radiate like a magnetic dipole. This is also a rather surprising finding. The $TE_{01\delta}$ and $HE_{11\delta}$ modes, which are the lowest non-confined modes of the cylindrical resonator, radiate like the magnetic dipoles described above. The lowest order of the spherical and rectangular DR modes are also considered to radiate like a magnetic dipole. For higher-order modes, the first or first few leading terms that relate to radiation can disappear depending on the field configuration of the higher-order mode.

In that case, the dominant term that leads to radiation is "some" a higher-order multi-polar term. From the asymptotic principle, it can be predicted that various modes of a sufficiently high-permissive dielectric resonator radiate like dipole or higher-order multi-pole terms. Besides, Van Bladel concluded that in addition to non-confined modes, the axisymmetric resonator form embraces "confined" modes. For confined modes, the prevalent term that refers to radiation is the term electrical dipole; for these modes, the term magnetic dipole is always zero. Mode $TM_{01\delta}$ is the dominant confined mode of an isolated cylindrical resonator and is considered to radiate like an electrical dipole.

Figure 3.2 shows the cylindrical resonator. If the dielectric constant of the resonator is very high, the scale of the resonator would be very small relative to the wavelength. In that case, the various modes radiate as corresponding point multi-poles, and their directivity becomes the same as that of the corresponding multi-pole. (For example, modes that radiate as electrical or magnetic dipoles have a directivity of approximately 1.7 dB. The dielectric constant of the resonator may have a moderate value, in which case the size of the resonator cannot be ignored concerning the wavelength, particularly in higher-order modes.

In any case, the mode's directivity will vary from that of the corresponding

multi-pole stage. This effect would also be minimal for modes that radiate like a dipole (it is understood that the gain of a point dipole is not so different from that of a half-wave-long dipole) but can be significant for modes that radiate like higher-order multi-poles. It should be noted here that if the resonator is mounted on a wide ground plane, its directivity increases by 3 dB relative to that of an isolated resonator because the power is radiated only in half-space.

3.3 Resonant Frequencies of Isolated Cylindrical DR

The calculation of the resonant frequency of isolated dielectric resonators involves the use of systematic numerical methods (e.g., refs. [70] - [71]). Numerical processes are, however, of little use to designers due to their sophistication. One is interested in calculating the value of the normalized wavenumber $k_o a$ for the specified value of the ε_r and aspect ratio (h/a) of the resonator, where $k_o a$ ($k_o = 2\pi f_o/c$) denotes the free-space wavenumber corresponding to the resonant frequency f_o, and c is the velocity of light in free space. If the value of ε_r is very high ($\varepsilon r \geq 100$), the value of the normalized wavenumber can differ with ε_r [69], as [71] :

$$k_o a \propto \frac{1}{\sqrt{\varepsilon_r}} \tag{3.1}$$

For the specified aspect ratio (h/a) of the resonator. For high values of ε_r, one, thus the value of the normalized wavenumber must be determined as a function of the aspect ratio (h/a) of the resonator for a single value of ε_r only. The resonant frequency will then be calculated using Eq.3.1 for other values of ε_r. However, in the case of DR antennas, the ε_r of the material used does not be very large, in which case the formula of Eq.3.1 does not hold precisely. Therefore, strictly speaking, if the value of ε_r is not very high, calculations are expected for each different value of ε_r. By reviewing the outcomes of the robust methods available

in the literature [70] for the different values of ε_r, it was found that the following analytical relationship could be used as a strong approximation to explain the dependency of the normalized wavenumber as a function of ε_r, also for the mild values of ε_r, [71] :

$$k_o a \propto \frac{1}{\sqrt{\varepsilon_r + X}} \tag{3.2}$$

where X is determined empirically by evaluating numerical results from different numerical methods. It has a small value (of the order of unity) and is thought to be dependent only on the mode. It should be noted that for a broad value of ε_r, $X \lll \varepsilon_r$ and Eq.3.2 is reduced to Eq.3.1. In the literature, there are a few numerical values of $k_o a$ for discrete values of ε_r and h/a computed using rigors methods for various modes. Closed-form expressions for various modes were obtained using these results, as discussed below. Each expression is also providing the set of aspect ratios in which it is applicable. The accuracy of the various expressions for various ε_r quantities is discussed in the following section.

$HE_{11}\delta$ Mode: For quantities of $\varepsilon_r = 38$ and 20, expressions for the normalized wavenumber $k_o a$ are available in the literature [68], [72]. These expressions are considered to be very reliable because they are based on the numerical results of a strict procedure [73]. Based on these findings, a reasonable value of X for this mode was calculated to be nearly 2. For a value of $\varepsilon_r = 38$, the expression given in ref. [68] for the resonant wavenumber of the $HE_{11}\delta$ mode is [73] :

$$k_{oa_{(\varepsilon r=38)}} = 0.27 + 0.36\left(\frac{a}{2h}\right) + 0.02\left(\frac{a}{2h}\right)^2 \tag{3.3}$$

We get the following general formula by using Eqs.(3.2) and(3.3) and substituting the value of X = 2

$$k_o a = \frac{2\pi f_o a}{c} = \frac{6.325}{\sqrt{\varepsilon_r + 2}}\left[0.27 + 0.36\left(\frac{a}{2h}\right) + 0.02\left(\frac{a}{2h}\right)^2\right] \tag{3.4}$$

where c is the velocity of light in free space. The above expression is valid in the range of $0.4 \leq a/h \leq 6$.

$TE_{01}\delta$ Mode:[74] has given reliable data for the resonant frequency of the $TE_{01}\delta$ mode for discrete values of aspect ratio and true for any value of $\varepsilon_r(\varepsilon_r \geq 25)$. The following formula was extracted from these observations [74].

$$k_o a = \frac{2.327}{\sqrt{\varepsilon_r + 1}} \left[0.1 + 0.2123 \left(\frac{a}{h}\right) - 0.00898 \left(\frac{a}{h}\right)^2\right] \tag{3.5}$$

The above expression is valid in the range $0.33 \leq a/h \leq 5$.

$TE_{011} + \delta$ Mode: [74] also provided accurate results for the resonant frequency of the $TE_{011} + \delta$ mode. Using these findings, the normalized wavenumber of the $TE_{011} + \delta$ mode was calculated as follows [74]:

$$k_o a = \frac{2.208}{\sqrt{X + 1}} \left[0.1 + 0.7013 \left(\frac{a}{h}\right) - 0.002713 \left(\frac{a}{h}\right)^2\right] \tag{3.6}$$

The above expression is valid in the range $0.33 \leq a/h \leq 5$.

$TM_{01}\delta$ Mode: If the quality of ε_r is very large ($\varepsilon_r > 100$), the "magnetic wall" method (MWM) shows the true value of resonant frequency for the $TM_{01}\delta$ mode [66]. A relation of the kind given by Eq.3.2 can be used for lower values of ε_r. By comparing the numerical results available in the literature [70], the value of X, in this case, was found to be nearly 2. Consequently, the resonant wavenumber can be expressed as follows [66]:

$$k_o a = \frac{\sqrt{3.83^2 + \left(\frac{\pi a}{2h}\right)}}{\sqrt{X + 1}} \tag{3.7}$$

The above expression is valid in the range $0.33 \leq a/h \leq 5$.

3.4 Bandwidth of Cylindrical DRs

An antenna's impedance bandwidth is known as the frequency range over which the antenna's input VSWR is less than a specified value S. The total unloaded Q - factor (Q_u) of a resonant antenna, which is fully matched to a transmission line at its "resonant frequency," is connected to its impedance bandwidth by the relation [28]:

$$BW = \frac{S-1}{Q_u\sqrt{S}} \tag{3.8}$$

The total unloaded Q-factor Q_u is related to the radiation Q-factor (Q_{rad}) for a DR antenna with small dielectric and conductor loss compared to its radiated power by the following relationship,

$$Q_u \simeq Q_{rad}$$

$TE_{01}\delta$ Mode: The literature [74] contains correct results for the radiation Q - factor of the $TE_{01}\delta$ mode for discrete values of aspect ratio and true for any value of ε_r ($\varepsilon_r > 25$). following formula for the radiation Q-factor of the $TE_{01}\delta$ mode [74] :

$$Q_{rad} = 0.078192(\varepsilon_r)^{1.27}\left[1.0 + 17.31(\left(\frac{h}{a}\right) - 21.57\left(\frac{h}{a}\right)^2 + 10.86\left(\frac{h}{a}\right)^3 - 1.98\left(\frac{h}{a}\right)^4\right] \tag{3.9}$$

The above equation is valid in the range $0.5 < a/h < 5$. There are also the remaining three modes ($HE_{11}\delta, TM_{01}\delta, and\ TE_{011}\delta$) which were discussed in detail in the researches [27],[28].

3.5 Arrays

Typically, a solitary component's radiation pattern is relatively enormous, and

every component gives low upsides of directivity (gain). To satisfy the needs of significant distance correspondence, antennas with directive qualities (extremely high gains) are required in numerous applications. This must be acquired by expanding the antenna's electrical size. Extending the dimensions of single components often results in more directive characteristics. Another technique for growing the antenna's measurements without really expanding the size of the individual segments is to shape a gathering of transmitting components in an electrical and mathematical course of action [29].

This latest antenna, made up of several components, is known as an array. In the majority of instances, the elements of an array are the same. This is not always mandatory, but it is often more efficient, smoother, and more practical. An array's elements can take any shape (wires, apertures, etc.) [29].

The vector inclusion of the fields radiated by the individual elements determines the array's total area. This means that the current in each unit is the same as the isolated element's current (neglecting coupling). This is not always the case, because it is dependent on the isolation of the elements. To provide very directive patterns, the fields from the array's components must intervene constructive way (add) in the required direction and destructively (cancel each other) in the space available [29].

In theory, this is possible, but in fact, it is just approached. Many factors control an array of similar elements which can be used to form the overall pattern of the antenna. They are as the total array's geometrical design (linear, circular, rectangular, square, and so forth), the relative movement of the elements, the amplitude and the phase for excitation of an individual element, and the relative pattern of the individual components [29].

A variety of antenna arrays are often used for personal, industrial, and military purposes, with various elements such as dipoles, loops, apertures, micro-strips, horns, reflectors, and so on. The shortest and most realistic array is created by

aligning the elements in a straight line. A two-element collection would be considered first to ease the presentation and provide a clearer physical understanding of the techniques. After that, we'll look at an N-element sequence. The first subject would be two-dimensional analysis. Three-dimensional methods will be implemented in the later sections.

3.5.1 Array With Two Elements

Assume the antenna in question is an arrangement of two infinitesimal horizontal dipoles arranged along the z-axis, as seen in figure3.4. In the y-z plane, the overall field radiated by the two elements is equivalent to the total of the two, implying no coupling between the elements [29].

$$E_t = E_1 + E_2 \tag{3.10}$$

Since E_1, E_2 are field radiated for antenna1 and antenna2 respectively

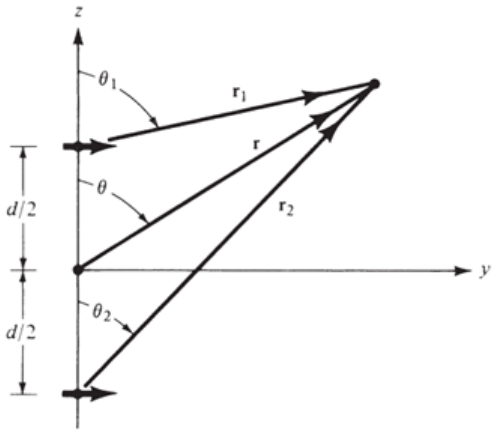

Figure 3.4: Two infinitesimal dipoles [29]

The radiators' magnitude excitation is similar. Assuming far-field measurements and using figure3.5 as a guide [29],

$$\left.\begin{array}{l} \theta_1 \simeq \theta_2 \simeq \theta \\ r_1 \simeq r - \frac{d}{2}\cos\theta \\ r_2 \simeq r + \frac{d}{2}\cos\theta \end{array}\right\} \text{for phase variations}$$

$r_1 \simeq r_2 \simeq r$ for amplitude variation

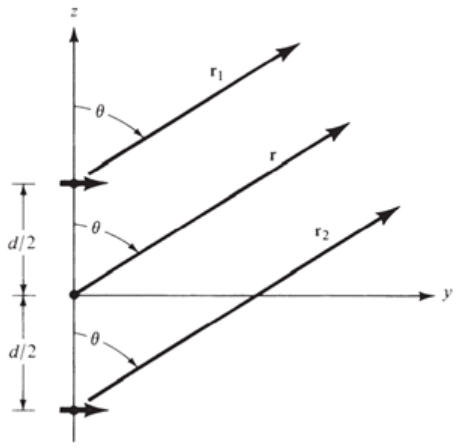

Figure 3.5: Far-field observation, a two-element array with its geometry oriented around the z-axis [29].

3.5.2 Array With N-Elements

The total field of the array is equivalent to the field of a single unit centred at the origin multiplied by a factor known as the array factor. The array factor for a two-element array with constant amplitude [29] is :

$$AF = 2\cos\left[\frac{1}{2}\left(kd\cos\theta + \alpha\right)\right] \tag{3.11}$$

Where α is the phase excitation variation between the components and can be written as in the normalized form :

$$(AF)_n = \cos\left[\frac{1}{2}\left(kd\cos\theta + \alpha\right)\right] \tag{3.12}$$

The array factor is determined by the array's geometry and excitation process. The characteristics of the array factor and the overall area of the array can be managed by adjusting the separation d and/or the step between the components. The far-zone field of a uniform two-component array of comparative components is equivalent to the result of a solitary component's field at a picked reference point (generally the inception) and the array factor of that array. That is to say,

$$E_{(total)} = \left[E_{(single\,element\,at\,reference\,point)}\right] \mathbf{x} \left[array\ factor\right] [29] \tag{3.13}$$

For arrays of similar elements, this is applied to pattern multiplication, and it is analogous to the pattern multiplication of (total field = (element factor) x (space factor) for continuous sources. It is also true for arrays of any number of identical elements that do not have similar magnitudes, periods, or distances between them, even though it has only been demonstrated with an array of two elements, both of identical magnitude.

There is an array factor for each array. In general, the array component depends on the number of components, their geometrical structure, relative magnitudes, relative phases, and spacing. If the components have the same amplitudes, phases, and spacing, the array factor would be easier. Since the array component is independent of the directional characteristics of the radiating elements, it can be expressed by substituting isotropic (point) sources for the individual elements. After obtaining the array factor using the point-source array, the complete area of the real array is obtained using Eq.3.12 . The amplitude, phase, and position of each point-source are supposed to be the same as the corresponding factor it is replacing. The designer must not only choose the correct radiating components, but also the geometry (coordination) and excitation of the individual elements to synthesize the complete pattern of an array [29].

Now we've covered element arraying and seen how it operates for a two-element array, let's extend the approach to include N elements. Let us presume that all of the elements in figure3.6(a) have the same amplitudes, except that each following element has a α progressive phase lead current excitation relative to the preceding one (α represents the phase through which the current in each element follows the current in the preceding element).

By treating the components as point sources, the array component can be calculated. The general field can be shaped by duplicating the array factor of the

isotropic sources by the field of a solitary component if the individual components are not isotropic sources. This is the Eq. 3.12 pattern multiplication law, which only works for arrays of identical elements [29].

$$AF = \sum_{n=1}^{N} e^{j(n-1)\psi} \quad \textbf{where} \quad \psi = kd\cos\theta + \alpha \tag{3.14}$$

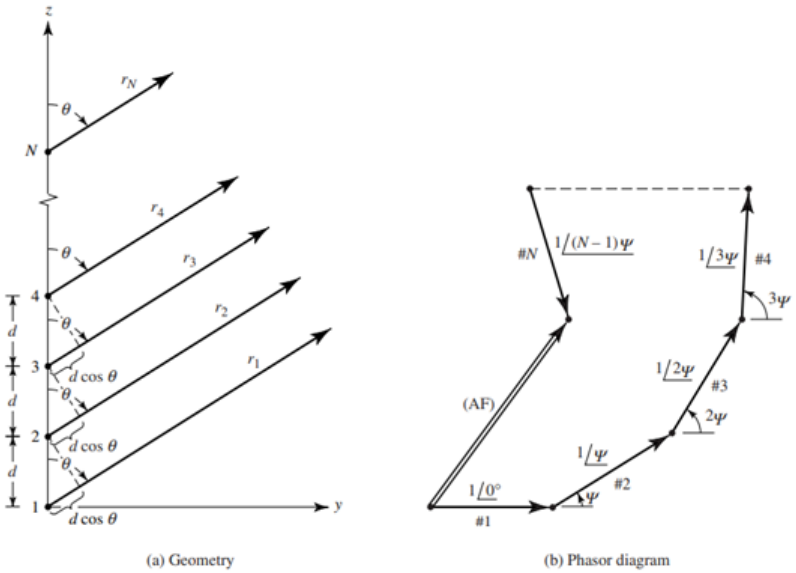

Figure 3.6: Far-field geometry and phaser diagram of an N-element sequence of isotropic origins around [29].

The total array factor for the uniform array can be expressed by the vector number of N phasers, each unit amplitude and progressive phase ψ relative to the previous one since it is a summation of exponentials. The phasor diagram in figure 3.6 graphically illustrates this. The amplitude and phase of the AF in uniform arrays can be managed by properly choosing the relative phase ψ between all the elements.

CHAPTER FOUR

Configuration of proposed single Antenna Designs.

4.1 Introduction

In this chapter, stacked cylindrical DRA with different dielectric constants used for each layer and the SC-DRA is excited by orthogonal dual MSLs based on two substrates . What distinguishes this design is that it is high purity CP compared to the previous type mentioned in chapter two. And Another proposed antenna design that works with millimeter frequencies, is characterized by high isolation between ports and a polarization ratio (AR) close to zero, this antenna is CDRA loaded patch antenna installed on one substrate and excited by dual U-slots.

4.2 The dimensions of cylindrical dielectric resonator

The method paragraph [27] explains how the preceding graphs should be utilize to design a C-DRA based on a required impedance BW and frequency resonated. The $HE_{11}\delta$ mode will be choice according to the proposed designs in this thesis, since it is necessary to calculate the DRA height (h), radius (a), and dielectric constant ε_r in purpose of satisfy these parameters, first step calculate the Q-factor (It is approximately defined as the ratio of the initial energy stored

in the resonator to the energy lost in one radian of the cycle of oscillation) by knowing the B.W which determined as Eq.4.1 when f_{max}, f_{min} are be equal to 30 GHz and 26 GHz respectively with center frequency f_o = 28 GHz [27]:

$$BW = \frac{f_{max} - f_{min}}{f_o} = \frac{30 - 26}{28} = 0.14\ \% \tag{4.1}$$

After knowing BW, Q-factor can determine as below:

$$BW = \frac{s - 1}{\sqrt{s}Q} \tag{4.2}$$

$$Q = 0.01007(\varepsilon_r)^{1.3}\frac{a}{H}\{1 + 100\exp^{-2.05\ [0.5\ a/h - 0.0125\ (a/h)^2]}\} \tag{4.3}$$

where s is the highest value acceptable voltage standing wave ratio (VSWR) which between (1-2), however, in worst case choice it is be 2 and by using Eq5.2 can get Q = 5. Now, to determine the ε_r, the required Q-factor value is plot upon the Q-factor graph for the $HE_{11}\delta$ mode with respective ration a/h (which given in Eq4.3) by using Matlab program , as shown in figure 4.1. Any value above Q = 5 will be ignored in this figure, indicating an area where the combination of a/h and ε_r will not reach the minimum needed bandwidth.

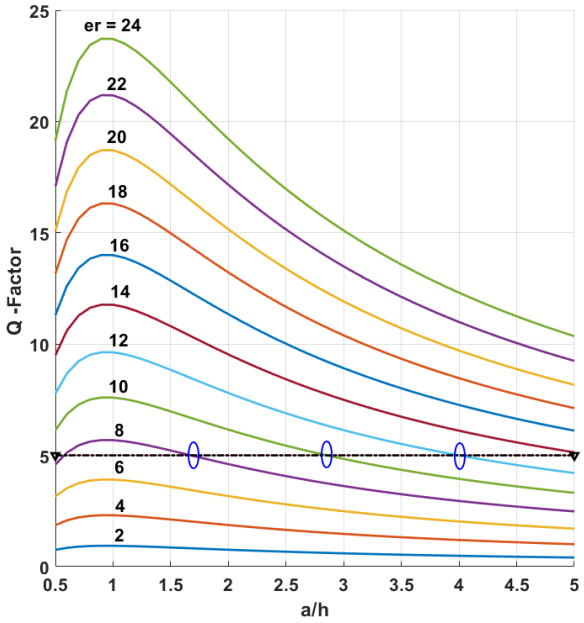

Figure 4.1: Acceptable ε_r values for a 14% fractional bandwidth.

On the other hand, solutions are limited to the area under the discrete line Q = 5 (the small circles mean the cross horizontal line with indeed Q-factor carves). Consequent, a DRA with approximately $\varepsilon \leqslant 12$ will match the bandwidth needs regardless of the a/h ratio used, whereas there will be a good range of a/h values that will meet the bandwidth requirement for $8 < \varepsilon_r \leqslant 12$. This enables the designer to rapidly decide which dielectric constant values for the DRA can be used. Next, $k_o a$ should be determined from Eq4.4 which mean wave-number is a standard quantity that depends only on the resonant frequency (28 GHz in this work) and determines the phase change per meter of the wave [27].

$$k_o a = \frac{6.324}{\sqrt{\varepsilon_r + 2}} \left[0.27 + 0.36 \left(\frac{a}{2H} \right) + 0.02 \left(\frac{a}{2H} \right)^2 \right] \tag{4.4}$$

The Eq4.4 is then shown for a series of values for h_{cm} on the $(k_o a)$ versus (a/h) graph for the HE_{11} mode, as shown in figure4.2.

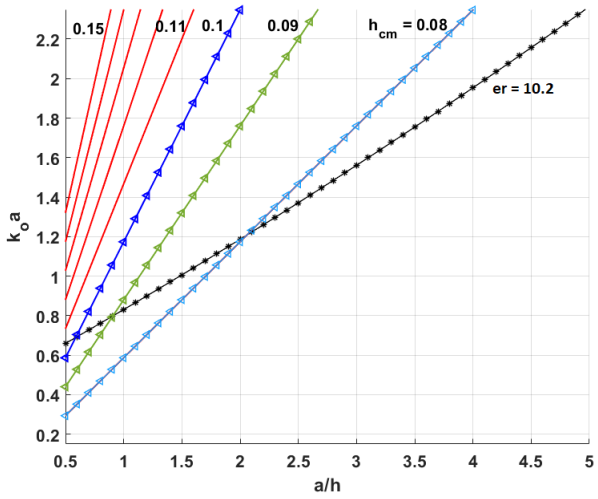

Figure 4.2: C-DRA designs at 28 GHz for $\varepsilon_r = 10.2$.

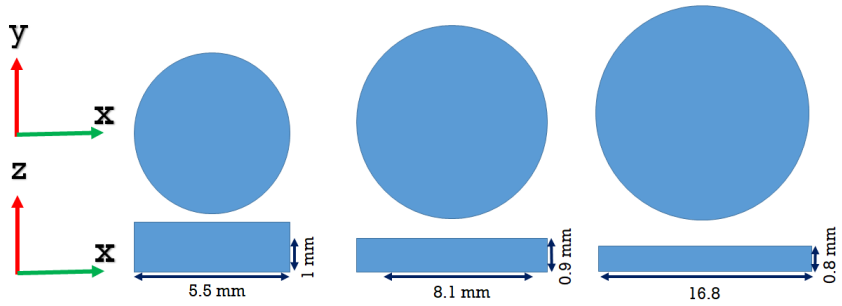

Figure 4.3: The dimensions of the 28-GHz cylindrical DRAs with $\varepsilon_r = 10.2$.

In figure4.3, the three DRAs are plotted. The designer has more flexibility in choosing the DRA design that is best suited to the application. Table 4.1 show the compersion between the suggested and optimal dimensions.

Table 4.1: Final DRA Parameters.

Design Parameter	Initial	Final 1st prototype	Final 2nd prototype
Element Height	1 mm	2.2 mm	2.85 mm
Element Radius	5.5 mm	4.14 mm	2.4 mm

4.3 Stacked Cylindrical DRA Prototype

A stacked C-DRA is mean several DR layers arrange each one above each other vertically or put each one beside or inside other, this technique help to enhance BW or G with slightly increased antenna size. Also other beneficial,

easy of control over the improvement of a specific parameter as well as keeping original antenna shape as shown in 4.4.

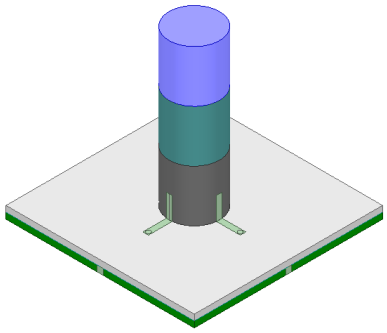

Figure 4.4: The proposed SC-DRA

At 28 GHz, a SC-DRA with dual feeding lines has been constructed and tested. The dual feeds line is intended to excite the DR with multiple relative permittivity, resulting in a high impedance bandwidth operation. A Rogers TMM 10i (tm)1 substrate Rogers RO3010 (tm) ($\varepsilon_r = 10.2$ and $tan\delta = 0.0035$) was used to manufacture the suggested single CDRA. To improve the gain and achieve the needed gain performance, the optimized single element with SC-DRA method was utilised. The gain, impedance bandwidth, and radiation pattern are all simulated. The proposed antenna has a reflection coefficient response ranging from 26.2 to 30 GHz, covering the intended frequency spectrum.

figure4.5 showed the initial prototype design is consisted of C-DRA made by Rogers RO3010 (tm) ($\varepsilon_r = 10.2$ and $tan\delta = 0.0035$) and mounted above the substrate which fabricated from A Rogers TMM 10i (tm)($\varepsilon_r = 9.8$ and $tan\delta = 0.002$), DR excited by orthogonal dual feeds to generate CP with 3-dB axial ratio. MSLs from copper are glued to the C-DRA wall vertically with lumped port for each individual MSL, led to best matching with input ports when the length of vertical feed (V1 and V2) is 0.98 mm after optimized length this excitation method which inspired by [75], but don't like it in this work because MSL in proposed design does not pass between cylindrical and substrate as like [75], since this made air gap underneath cylindrical which lead to superior radiation effect on the antenna efficiency [76]. Finally, a metal layer ground with the same length and width as the substrate is installed directly beneath the substrate as

shown in figure4.5 (c).

Referring to Table 4.1, we found a difference between the values that were calculated from the paragraph method and the values used in the design, and this reason is attributed to choosing the most appropriate dimensions to achieve the best coupling between C-DRA and MSL feeds. Also, feed width and feed length of MSL determined by Microstrip Line Calculator website.

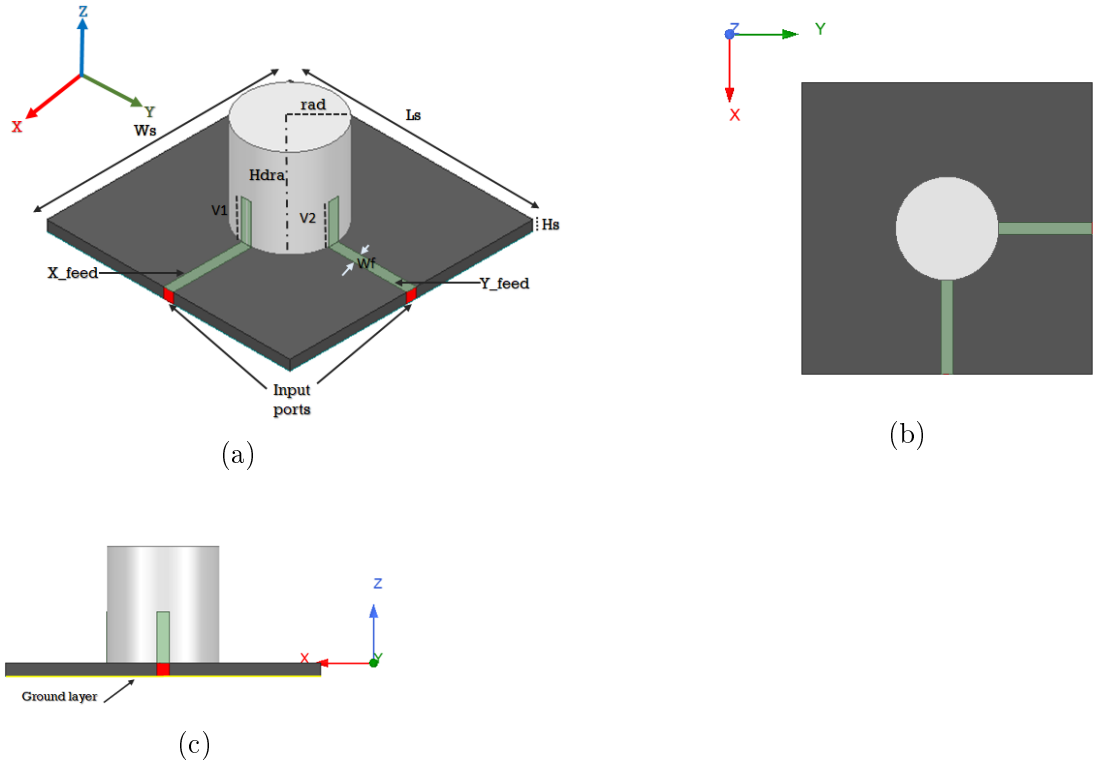

Figure 4.5: Geometry shape proposed C-DRA and all dimensions are mentioned in the table 1(a) 3D view (b) top view (c) side view.

Referring to figure 4.5, the last thing a copper layer work as ground install up or down the substrate depending on type the application. So S-parameter in figure.4.6 will be presented without any modification in the network feeding or the radiator part (C-DRA).

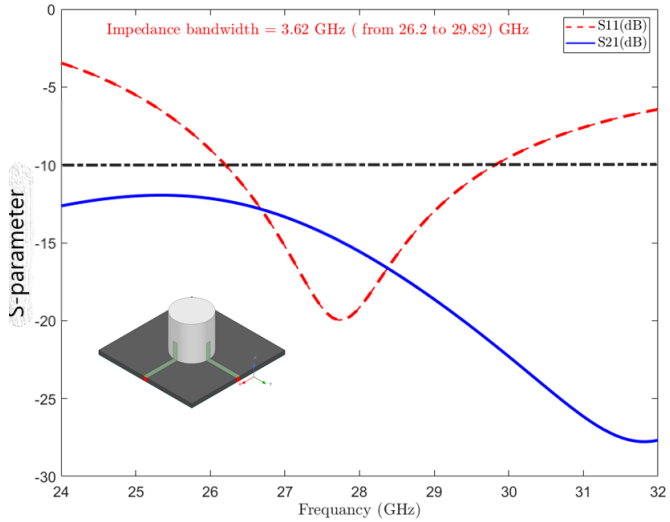

Figure 4.6: The reflection coefficient of traditional CP C-DRA dual feeds.

Initial prototype design attained -10 dB impedance bandwidth of 12.92% (26.2 - 29.82)GHz at resonant frequency 28 GHz. CP is excited by the orthogonal dual MSLs as explained in Fig.4.5, these MSLs are indicated in the magnitude with different phase 90^o between 1st port and 2nd port, which features 3-dB AR bandwidths of 28.57% upon total band (24 - 32)GHz as such in Fig.4.7 (a). The proposed antenna achieved a gain 5.75 dB at operated frequency 28 GHz as shown in Fig.4.7 (b).

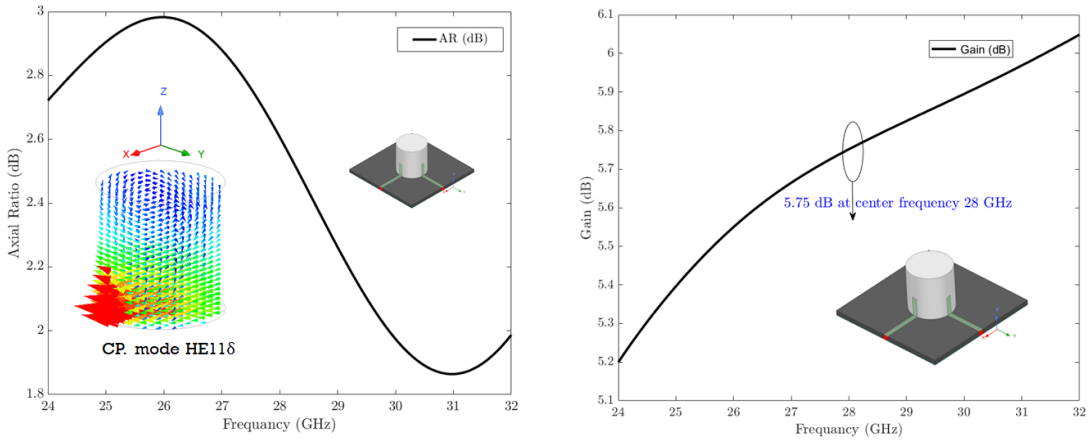

(a) (b)

Figure 4.7: (a) Axial ratio 3-dB which generate by merge $HE_{x11}\delta$ with $HE_{y11}\delta$ mode and CP is occur . (b) Total Gain at center frequency 28 GHz.

figure.4.8 (a) and figure 4.8 (b) show the radiation pattern of the antenna at the center frequencies, 28 GHz in two different planes(the x-z plane when $\phi = 0^o$ and the y-z plane when $\phi = 90^o$.

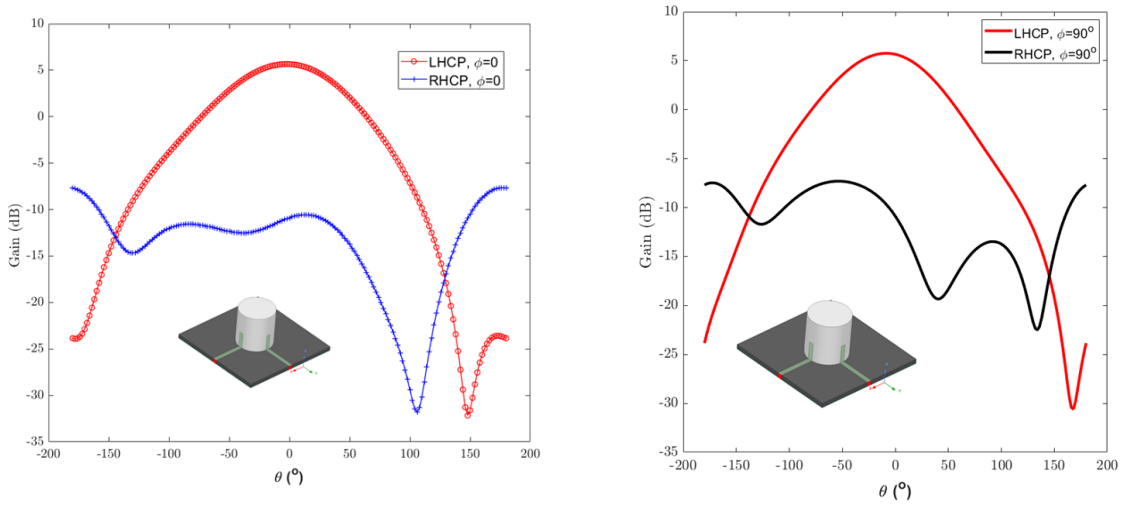

(a) (b)

Figure 4.8: (a) LHCP and RHCP at the x-z plane . (b) LHCP and RHCP at the y-z plane

4.3.1 Feeding network and via.

Following that, the MSL excited C-DRA was printed over the substrate, which had an effect on antenna efficiency by simulating superior radiation, as stated in [76], so to avoid this effectiveness, part of the MSL network feed engraving at the bottom of another substrate of the same size and material, which is arranged as a sandwich beneath the original substrate, as explained in figure.4.9.The lower parts of the MSL are linked to the upper parts of the MSL on a metal cylindrical structure (via).To test the efficiency of final network feeding, the diameter and height of via are checked and are optimal at 0.18 mm and 0.508 mm respectively.

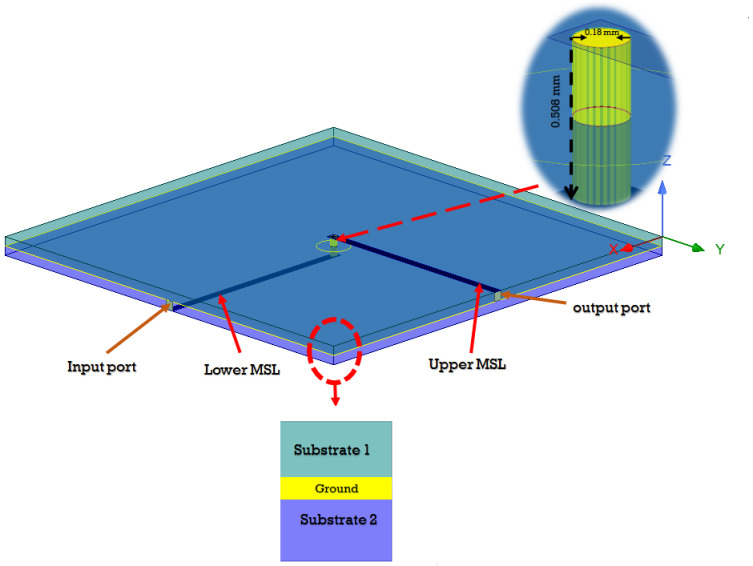

Figure 4.9: Structure shape of final network feeding after added lower substrate and Via without C-DRA

Via was used in the feeding network composition to limit the effect of undesired radiation from printed feeding lines on the port, as illustrated by [77]. When you don't want your board to be cluttered with wires, you can connect to the ground with via (drilled cylindrical holes filled with conducting metal), which serve the same purpose when creating multi-layer boards as draw in figure4.9. By reading the futures figure 4.10 S11 curve mean the power will be passing from each port to other which be S11 $\simeq$ 0 dB, consonantly, all currents transfer through via without disturbance by choice properly dimensions of copper cylindrical.

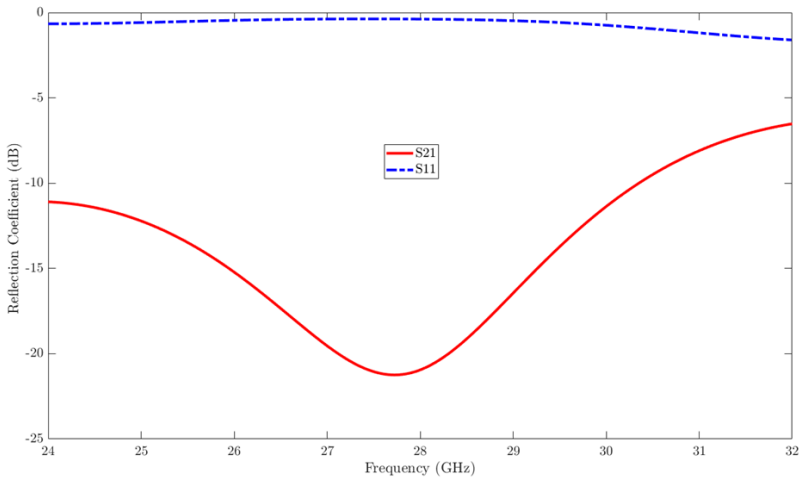

Figure 4.10: The reflection coefficient of the network feeding with via.

4.3.2 Generation of orthogonal modes in C-DRA.

figure 4.5 depicts the entire technique for generating orthogonal modes in cylindrical DR. As illustrated in figure4.11 (a), the fundamental mode $HE_{x11}\delta$ is initially generated by inserting a vertical MSL on the y-axis (V2= 0.98 mm) at the cylindrical wall. The $HE_{y11}\delta$ on the y-axis can be formed by putting MTL horizontally on the X-axis (V1= 0.98mm) as shown in figure4.11 (b).

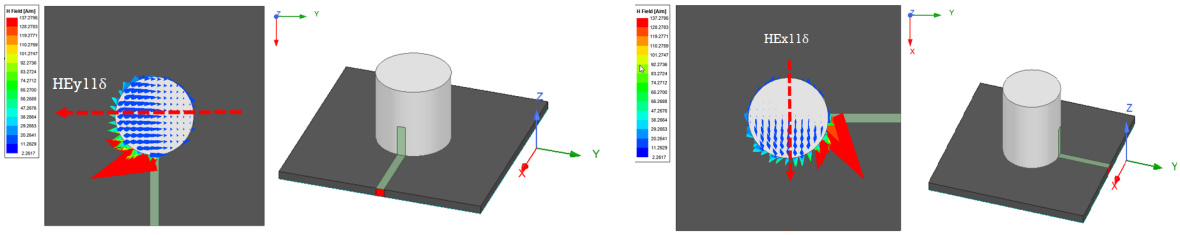

(a) (b)

Figure 4.11: (a) Describe the $HE_{x11}\delta$ generate mode on the Y-axis: simulated electric field distribution at 28 GHz on the left, proposed methodology for designing proposed MSL feed on the right. (b) Describe the $HE_{y11}\delta$ generate mode on the X-axis: simulated electric field distribution at 28 GHz on the left, proposed methodology for designing proposed MSL feed on the right

4.3.3 Modifying radiation pattern by using Stacked DRs technique.

A dual polarizations dual ports stacked C-DRA (SC-DRA) is presented in this section, three C-DRs putting each one on other vertically which laid on a substrate and excited by orthogonal MSLs for generated CP as shown on figure4.12.

The chassis SC-DRA involved three dielectric constant and arrange from upper to lower layer according to ε_r which used. The top layer had been $\varepsilon_r = 6.8$ is made by **Be-O** ($tan\delta = 0$), afterwards, 2nd layer which structured from **marble** ($\varepsilon_r = 8.3$ *and* $tan\delta = 0$). The lower and 3rd layer is selected from **Rogers RO3010 (tm)** ($\varepsilon_r = 10.2$ and $tan\delta = 0.0035$). It is noteworthy, substrates size,

substrates material, and feeds width are remaining as before insert SC-DRA. All dimensions in Tab 4.2.

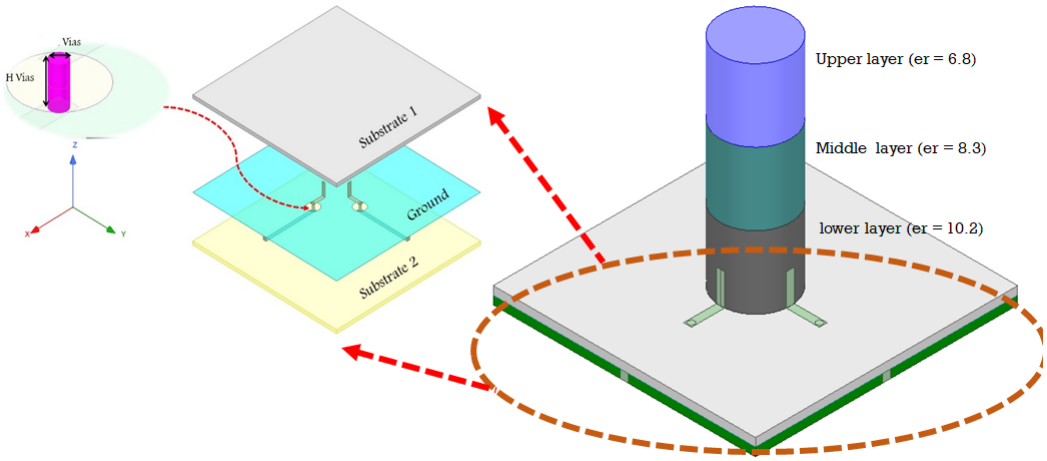

Figure 4.12: Total optimized prototype Stacked Cylindrical Dielectric Resonator design with the network feeding dual MSLs and vias inset through substrates

Table 4.2: Designs parameter of SC-DRA antenna

Element Names	Parameter	Dimensions
Substrate length=width	$L_s = W_s$	$6mm$
Substrate height	H_s	$0.254mm$
Cylindrical DRA radius	rad	$1.07mm$
Cylindrical DRA height	H_{dra}	$2.2mm$
Vertical feed height	$V_1 = V_2$	$0.98mm$
Feed width	W_{feed}	$0.24mm$
Feed length	$X_{feed} = Y_{feed}$	$1.93mm$

Looking at the geometry shape in figure4.12, multi stacked cylindrical with dielectric constant belongs to each layer in radiator which enhanced the gain by 2 dB (from 5.75 to 7.55) dB at operated frequency 28 GHz (figure4.13)

Furthermore,the matching increased from - 24.89 dB. In figure 4.14, the impedance slightly affected and also the axial ratio in figure4.15 had been improved . The insertion losses (S21) improve from - 15.29 dB to -17.30 dB (figure4.14.

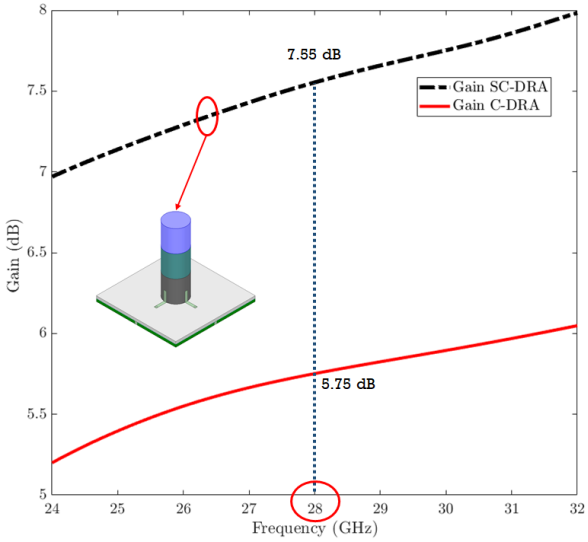

Figure 4.13: Total gain SC-DRA comparison C-DRA

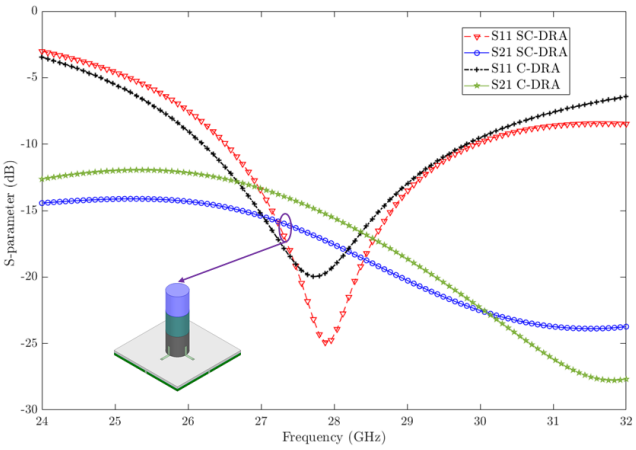

Figure 4.14: The reflection coefficient of SC-DRA comparison C-DRA.

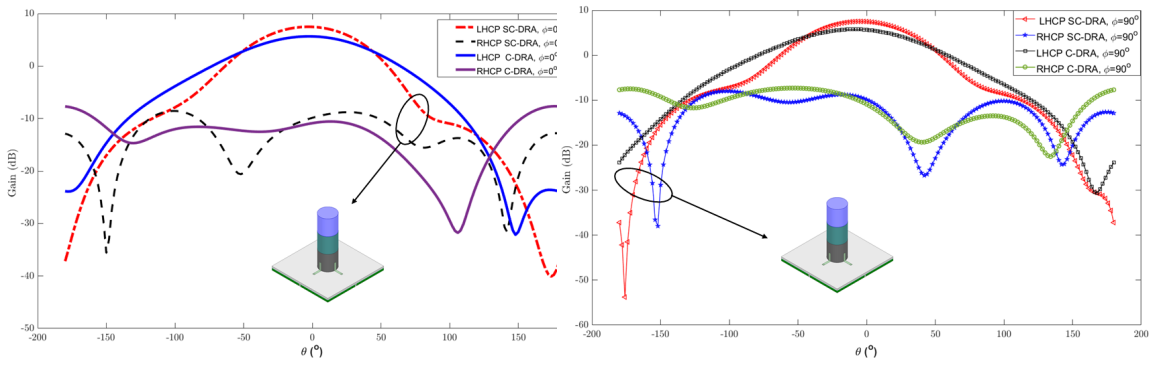

(a) (b)

Figure 4.15: (a) Gain LHCP, RHCP SC-DRA at the x-z plane compared Gain LHCP, RHCP C-DRA in x-z plane. (b) Gain LHCP, RHCP SC-DRA at the y-z plane compared Gain LHCP, RHCP C-DRA in y-z plane.

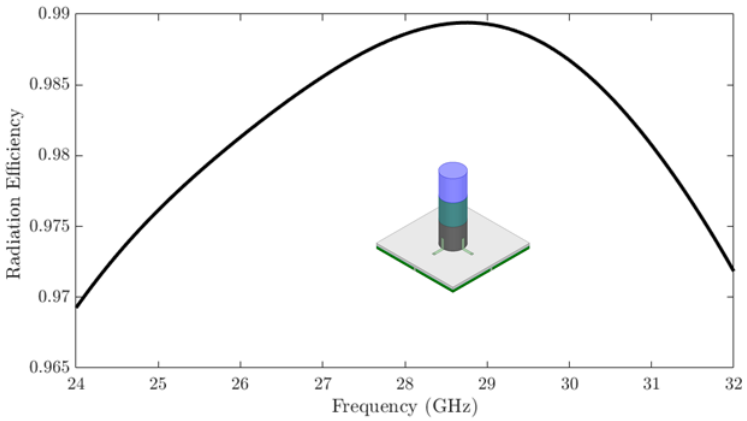

Figure 4.16: The Radiation Efficiency of final SC-DRA

The proposed design is achieved fine co-polarization with lowest value of cross-polarization on both x-z plane ($\phi = 0^o$) and y-z plane ($\phi = 90^o$) since explained in figure 4.15 (a,b).

Another significant criterion is radiation efficiency. In the prototype 1st design, a high radiation efficiency antenna was attained 98% as appear in figure4.16.

4.3.4 Fields distribution inside radiator SC-DRA

For explain analysis and fields distribution inside SC-DRA, foremost, recalling figure4.12 with change the numerate of cylindrical layers according to dielectric constant as following : the upper layer ($\varepsilon_r = 6.8$) will be 3rd layer, the middle layer ($\varepsilon_r = 8.3$) will be 2nd layer, and the lower layer ($\varepsilon_r = 10.2$) will be 1st layer. As is know to all, utilization dual orthogonal feeds is give purity CP by create different excitation phased 90^o to get the time delay between the ports feeds. Moreover, multi layer multi dielectric constant help to generated other modes will be added to the original mode which lead to enhance the total gain. By using **Eignemodes** option analysis in the program HFSS2020R2, eight modes will be studied as pictorial analysis. The mode $HE_{y11}\delta$ will be simulate by MSL on X-axis, after ward, the mode $HE_{x11}\delta$ is be excite in 1st and 3rd layer as shown in figure4.17 (a) , figure4.17 (b) respectively.

Constantly, the circular mode $HE_{11}\delta$ will be contracted and contributes to

the total radiation in 1st and 3rd layer (figure4.17 (c) , it's worth notice 2nd layer is represent the vanishing area of modes in 1st layer and construction area of modes in 3rd layer this cleared in figure4.17 (i), so no mode will be contribute in 2nd layer. The $HE_{y21}\delta$, $HE_{x21}\delta$ modes is simulates (figure4.17 (d),(e))and give the circular $HE_{21}\delta$ mode which is be weak relatively and vanished at 3rd layer without is be contributes with the radiation pattern, see figure 4.17 (f).

The mode $EH_{11}\delta$ is excited inside total cylindrical,since the current focused in the center radiator (figure 4.17 (g)) which radiate as **horizontal electric dipole**, while mean, the mode $EH_{21}\delta$ is generated at 2nd and 3rd layer (figure 4.17 (h))which had been radiation pattern such as **horizontal electric quadrupole**, both modes ($EH_{11}\delta$ and $EH_{21}\delta$) will be contributes in total radiation and which merged with the original mode $HE_{11}\delta$ which emit as **horizontal magnetic dipole**, as result the three important modes ($EH_{11}\delta$, $EH_{21}\delta$, and $HE_{11}\delta$) co-operate to improve the total gain. The high order modes ($EH_{11}\delta$, $EH_{21}\delta$) are excited in higher band frequency lead to slightly shifting towards the center frequency 28 GHz.

A comparison Table4.3 between the previous works and the first design, based on some parameters studied in this work.

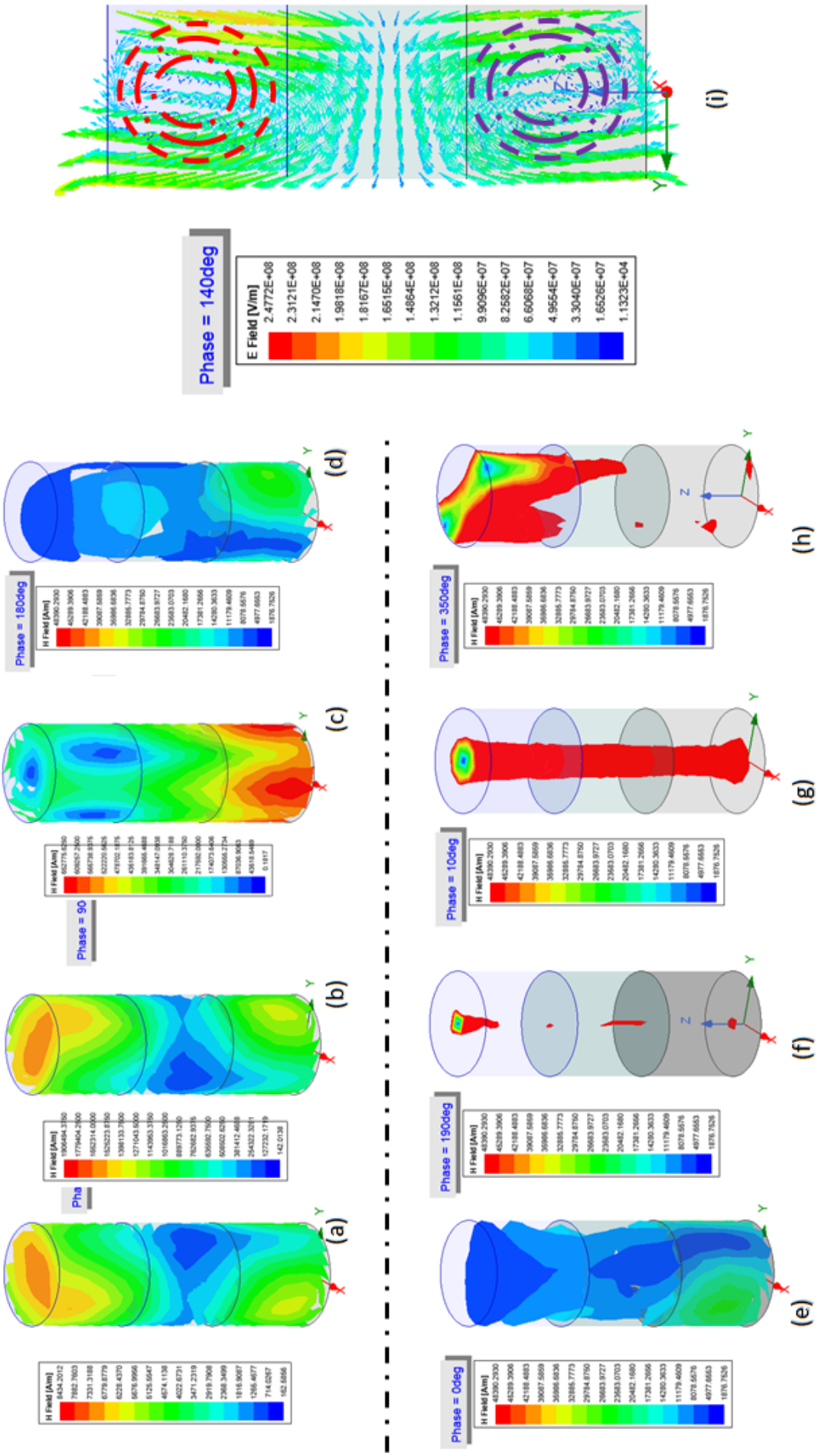

Figure 4.17: The field distribution inside SC-DRA

Table 4.3: Comparison of the 1st design with a previous S-DR's works.

Researcher	[3]	[4]	[5]	[6]	[7]	[8]	[9]	[10]	1st work
Radiator geometry shape	R-DRA	R-DRA	R-DRA	C-DRA	R-DRA	R-DRA	R-DRA	C-DRA	C-DRA
Profile (λ)	0.52	0.14	0.69	NA	0.1	0.09	0.37	0.4	0.56
Feed mechanism	Slot	Coaxial	Coaxial	Coaxial	Slot	Coaxial	Micro-Strip	Micro-Strip	Micro-Strip
Operating frequency(**GHz**)	26	60, 81	9.82	7.5	4	27.5	28, 38	28	28
Bandwidth (%)	17.3%	19%, 20%	29%	NA	54%	148.5%	(21.4, 14.2, 16.5)%	22.5%	25%
Gain (**dB**)	9.28	5.1, 6.3	9.8	8.68	9.2	7.14	7.6	10.93	7
Polarization (Lp/Cp)	LP	CP	LP	LP	LP	L P	LP	CP	CP

4.4 Cylindrical Dielectric Resonator embedded Patch Antenna prototype.

A cylindrical-dielectric resonator antenna (C-DRA) loaded by a circular patch is presented in this section for emerging wide-band wireless communications. The proposed antenna is fed by two orthogonal aperture-coupled feeding slots in order to generate polarization diversity pattern. The shape and location of the slots were optimized to realize the highest operating bandwidth and highest isolation between the two feeds. To achieve high polarization purity a crossed dumbbell-shaped slots were etched on the circular patch.

Simulation results show that the proposed antenna realizes 2 GHz of impedance bandwidth centred at 27.6 GHz with isolation between the two feeding ports better than 25 dB over the operating bandwidth, which indicates a pure diverse polarization that can be realized by such antenna. The proposed antenna is seen as an excellent candidate for the emerging 5G wireless communication system and Ka-band satellite communication. Figure4.18 is presents total structure of prototype C-DRA loaded patch antenna.

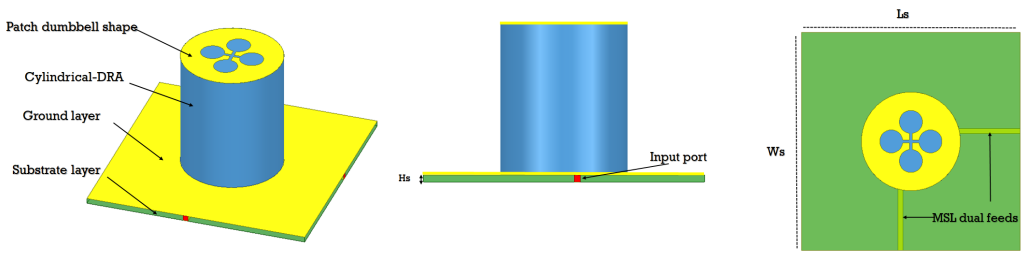

Figure 4.18: Goemetry shape proposed C-DRA loaded patch antenna (a) 3D view . (b) Side view (c) Top view

4.4.1 Cylindrical Dielectric resonator U-slot coupling single feed.

Initially, CDRA excited by U-slot coupling which fed by single MSL printed beneath the substrate, U-shaped slot was presented [78]. Furthermore, using U-slot instead of rectangular shape slot lead to reduction back-lobe in the antenna

[7] and decrease the total slot size with considered to the diameter CDRA.

At first, the position of the slot was in the center of CDRA, for getting good coupling among DR and MSL feed, the slot's position was moved to positive x-axis by depending on parametric sweep, so the slot shifted by (0.658 mm) from the point center, figure4.19 expressed this structure.

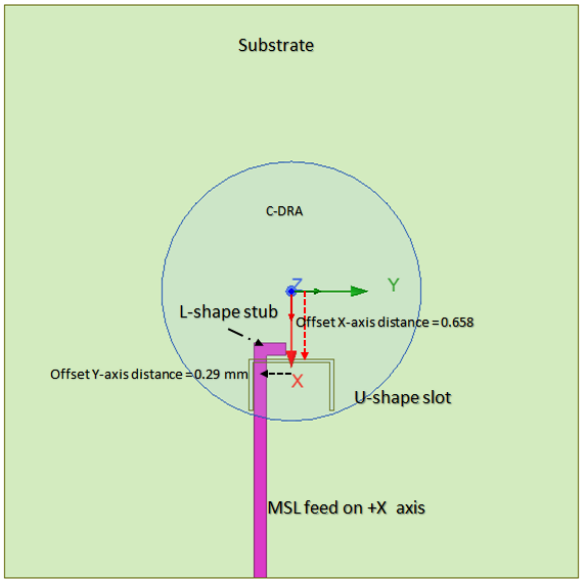

Figure 4.19: U- shape slot width offset distance

Additionally, By putting stubs at the end of the MSL, you may regulate the impedance matching which call the open-circuit micro-strip lines. It's worth mentioned, the stub improve the coupling and increase from impedance bandwidth, since L-shape stub idea which shown in figure4.19 was inspired by [79].

Furthermore, the MSL position also was shifted (+y axis or -y axis) according to U-slot, since best offset distance attained good matching on 0.29 mm in negative y-axis (figure4.19).

The S-parameter for this the primitive structure shown in figure4.20, since BW is 4.75% (29.15 - 27.82)GHz at operated frequency 28 GHz and G is be 5.58 dB.

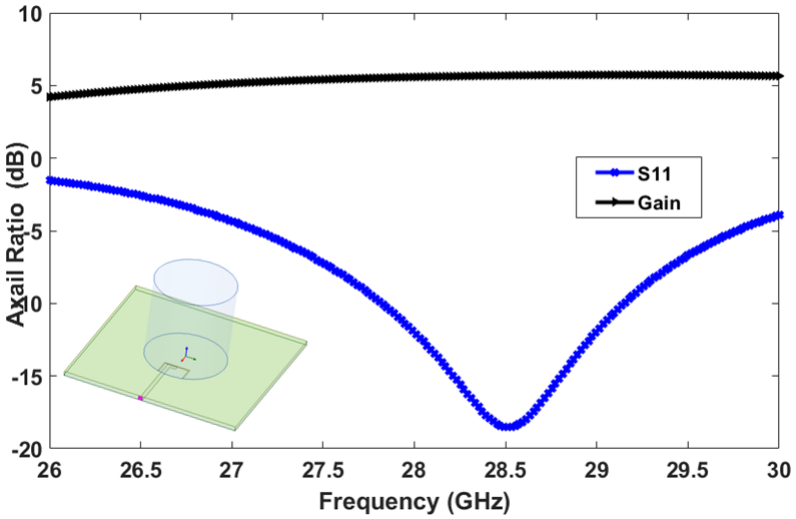

Figure 4.20: Reflection Coefficient and Gain of C-DRA single U-shape slot one MSL feed .

4.4.2 Generate to Circular Polarization in C-DRA embedded Patch.

As mentioned earlier in prototype design 1, since same technique was utilised in this prototype design, the CP obtained by two orthogonal U-shape slots with dual MSL feeds and a port for each MSL feed which explained in figure4.22.

Moreover, to enhance the insertion loss (S21) (as will see in results chapter 5) two feeding ports with S21, two metal pieces used to improve the isolation by suppression the electromagnetic radiations which is be emitted by MSL stubs. In figure4.21, the two copper rectangular involved among MSL stubs.

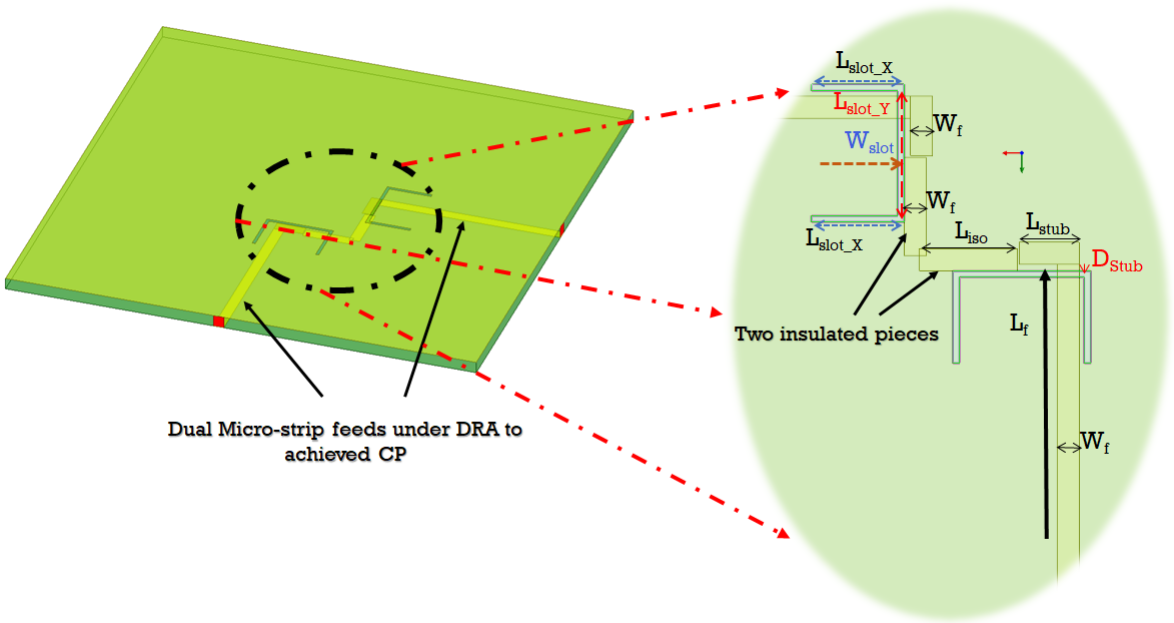

Figure 4.21: Proposed feeding network

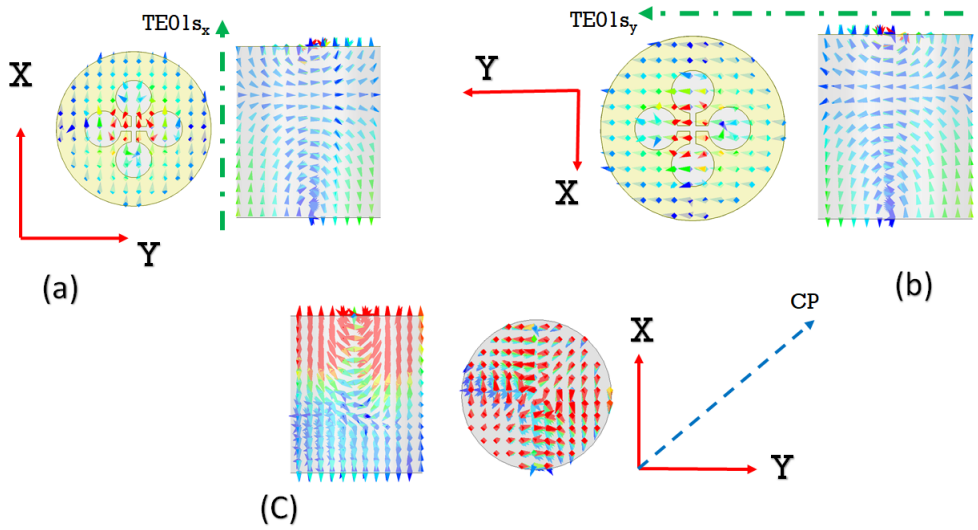

Figure 4.22: Simulated electric field at 28 GHz. (a) $TE_{01}\delta X$. (b) $TE_{01}\delta Y$. (c) Both polarization.

The proposed antenna was designed and optimized as shown in figure4.22 (a) illustrates the generation of $TE_{01}\delta$ mode on x-axis when x-polarized port is excited and Y-polarized port is terminated. Similarly, figure4.22 (b) illustrates the generation of $TE_{01}\delta X$ mode on y-axis when y-polarized port is excited and x-polarized is terminated. On the other hand, to generate a circularly polarized radiation both ports are excited with same amplitude and 90^o phase difference as shown in figure4.22 (c).

4.4.3 Modifying radiation pattern by using CDRA embedded patch antenna method.

The presented antenna consists of a CDRA loaded with a circular patch antenna to increase the operating frequency bandwidth and to enhance the gain of the DRA. The antenna is fed with two orthogonal aperture-coupled slots that have been used to isolate the active beam-steering circuit from the radiating antenna and to avoid the spurious radiation. Furthermore, two crossed dumbbell-shaped slots are etched on the circular patch in order to enhance the polarization purity and the isolation between the two orthogonal feeds. The CDRA is made of Rogers RT/duroid 6010/6010LM (tm) (ε_r= 10.2 and $tan\delta$ = 0.0023). This C-DRA is loaded with a circular patch on the top as shown in figure4.23

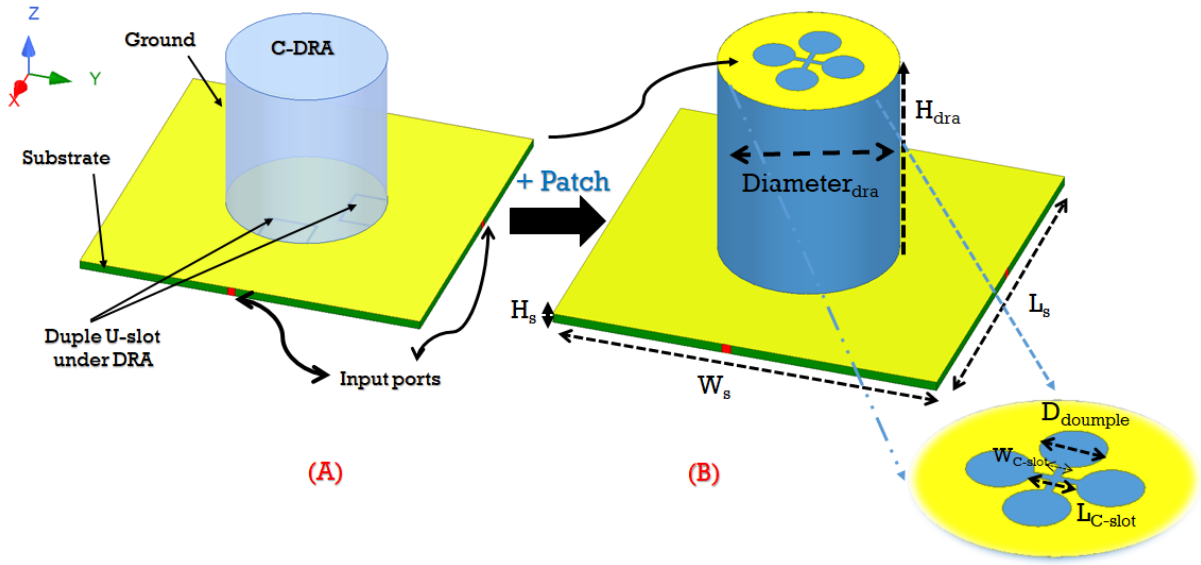

Figure 4.23: a) CDRA without patch. b) CDRA loaded by patch.

The proposed radiator is mounted on a metallic ground layer where two orthogonal and identical U-slots are etched on the ground to provide two orthogonal excitation, so polarization diversity can be generated from the proposed antenna; these slots are located below the CDRA to achieve high coupling and reduce the spurious radiation. The feeding substrate is used similar to that used for the CDRA. The rare side of the proposed antenna consists of two orthogonal MSLs. The feeding network is demonstrated in figure4.21. The optimized design parameters of the proposed antenna are listed in table 4.4.

Table 4.4: Design parameters of CDRA-P

Parameter	$L_s = W_s$	W_{slot}	H_s	D_{stub}
Dimensions (mm)	5.3	0.035	0.13	0.035
Parameter	$Diemeter_{dra}$	H_{dra}	$D_{doumple}$	L_{stub}
Dimensions (mm)	2.4	2.85	0.56	0.325
Parameter	$W_{C_{slot}}$	$L_{S_{slot}}$	L_{slot_X}	L_{iso}
Dimensions (mm)	0.075	0.95	0.75	0.535
Parameter	L_{slot_Y}	L_f	W_f	
Dimensions	0.47	2.05	0.12	

The CDRA loaded with a circular patch antenna to increase BW and to enhance the G of the DRA as was presented in figure4.23(a). As can be seen from figure4.25, the proposed antenna achieved BW (S11) of 2 GHz centred at 27.6 compared with the BW of the C-DRA without patch that achieved an BW of 1.4 GHz.

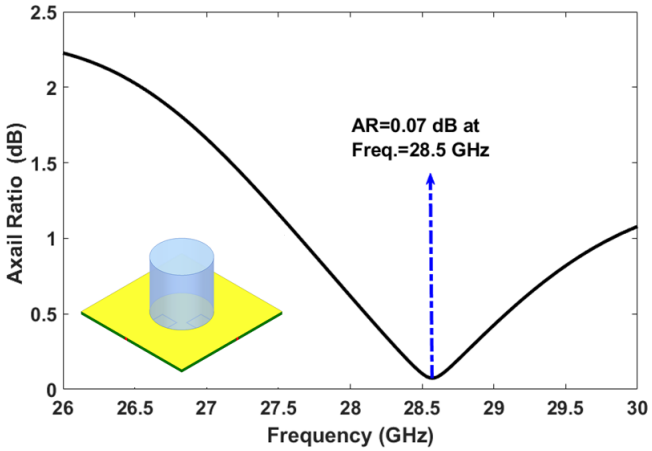

Figure 4.24: Axial Ration of C-DRA without patch antenna .

Moreover, the presented antenna shows better isolation level between the two feeding ports with S21 better than 25 dB over (figure4.26)the operating frequency bandwidth; as a result, a pure polarization diversity can be realized from such antenna (figure4.24). Additionally, almost flat gain was attained with high circularly polarized performance ($AR \simeq 0dB$) over the operating frequency bandwidth when it is excited with similar amplitude and 90^o phase difference at the feeding ports as shown in figure4.25. Moreover, figure4.27 explain the antenna give good Co and Cross polarization before and after add metal disk to DR.

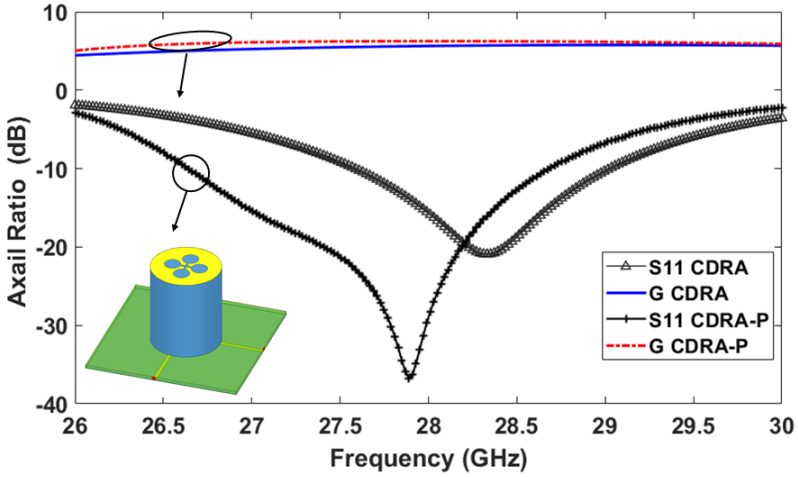

Figure 4.25: Simulated gain and S11 vs frequency. G:gain, CDRA-P: C-DRA loaded patch antenna.

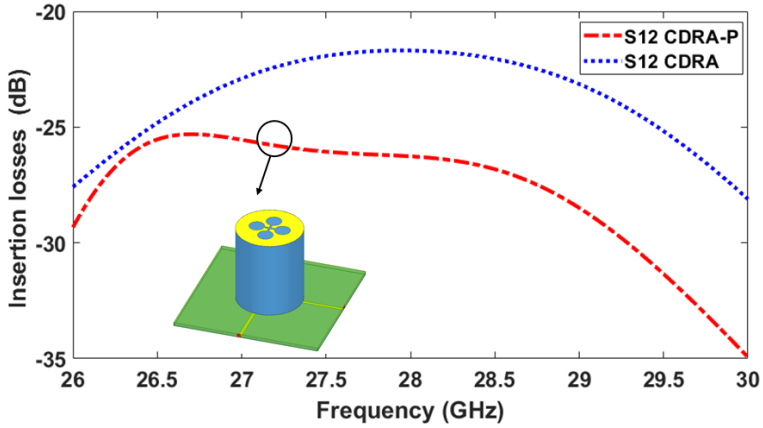

Figure 4.26: The S12 C-DRA with patch and C-DRA without patch. CDRA-P: C-DRA loaded patch antenna

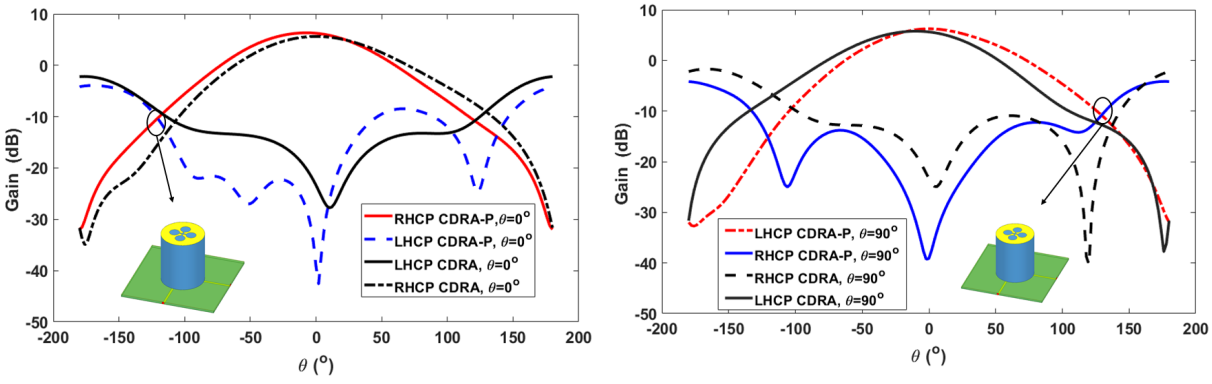

(a) (b)

Figure 4.27: (a) Gain LHCP, RHCP CDRA-P at the x-z plane compared Gain LHCP, RHCP C-DRA in x-z plane. (b) Gain LHCP, RHCP CDRA-P at the y-z plane compared Gain LHCP, RHCP C-DRA in y-z plane. CDRA-P: CDRA loaded patch antenna

Also the proposed antenna attained work efficiency up to 96% as shown in figure4.28.

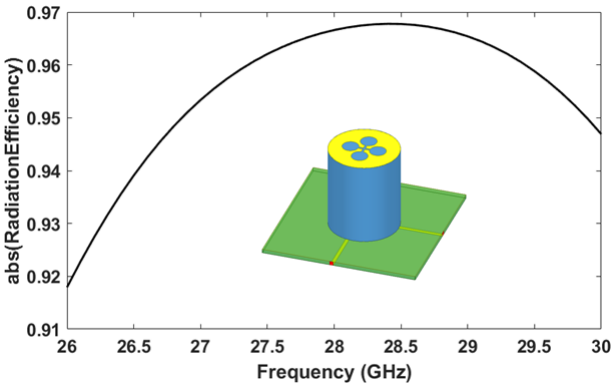

Figure 4.28: The reflection coefficient of CDRA-P.

4.4.4 Electric field distributions in C-DRA loaded patch antenna.

In order to understand the antenna mechanism, the 2nd prototype design with metal disk, which is based on (finite integration method). Referring to the simulation results of the reflection coefficients are shown in figure4.25. It is observed that the resonant frequency of the $TE_{01}\delta$ mode shifts to a lower frequency as when CDRA embedded patch copper. In the CDRA without metallic patch case, the quarter wavelength along z-direction is almost identical to the height (L) of the antenna as shown in figure4.29 (a).

When the metal cap is placed on the CDRA , the electric field tangent to the wall of the CDRA will vanish and focus inside the cylinder towards the z axis, on the other hand, the rest of the field components will gradually vanish and merge inside the center of the cylinder causing an increase in the field from the z axis lead to an increase in the wavenumber generated on the boresight while keeping the size of the DR unchanged, the response is directed towards the low frequency of the frequencies range as shown in figure4.29 (b).

The reason for shifting the peak of the reflection coefficient towards low frequencies (figure4.25) is the result of a decrease in the wavenumber towards the y

axis and an increase in their intensity at the z-axis at the metal patch.

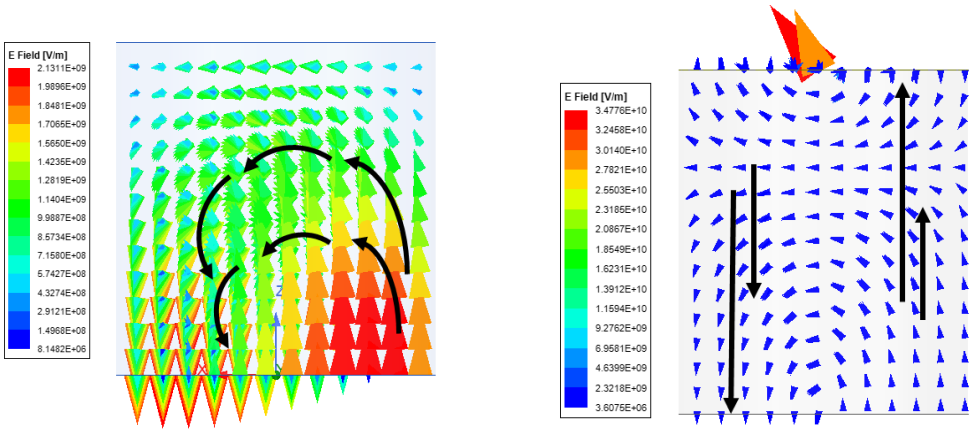

(a) (b)

Figure 4.29: Simulated E-field distribution Vs metallic patch (a) without patch, (b) with patch. CDRA-P: CDRA loaded patch antenna

Table 4.5: Comparison of the proposed design in this thesis with a previous DR loaded patch antenna works.

Researcher	[60]	[11]	[12]	[13]	[14]	[15]	2nd work
Shape	C-DRA	C-DRA	R-DRA	C-DRA	C-DRA	T-DRA	C-DRA
Profile(λ)	0.1	0.26	0.14	0.12	0.0001	0.012	0.26
Feeding	Slot	CPW	Coaxial	CPW	CPW	CPW	Slot
Freq.(GHz)	9.27	28	5.5	5.2	60	4.25	28
B.W (%)	16.5%	40%, 20%	52%	12%	10%, 20%	112%	7.28%
Gain (**dB**)	4.65	7.1	11.5	1.3	7.83	3.3	6.25
(Lp/Cp)	LP	LP	LP	CP	LP	LP	CP

4.5 Comparison between both prototypes .

In this section, comparison SC-DRA with CDRA-P for selection the optimised antenna which is be consisted the array antenna. According to antenna parameters such as low-profile, the diameter of C-DRA, gain, bandwidth, the isolation between two ports and so on. which are explained more in Table4.6 bellow:

Table 4.6: A comparison table between the two designs

Parameter	1st (SC-DRA)	2nd (CDRA-P)
H_{dra}	6.6 mm	2.85 mm
$Diameter_{dra}$	2.14 mm	2.4 mm
Feeding mechanism	directed MSL	U-shape slot
Bandwidth (GHz)	12.92%	7.28%
Axial Ratio (dB)	3.1	0.07
Gain (dB)	7	6.25
The insertion losses S_{21} (dB)	-17	-25
Radiation Efficiency	98%	96%

So according to the results above with consider to moderate design, 2nd prototype will be chosen to formed array antenna.

CHAPTER FIVE

Cylindrical Dielectric Resonator Array Antenna Design.

5.1 Introduction

In this chapter studying the effect of changing a number of elements on the performance of the antenna, as well as obtaining results after simulating the designs which include S-parameter, gain , directivity, current distribution and the bandwidth, radiation pattern.

According to results which will be discussion in Table4.6 in next chapter, C-DRA embedded patch prototype is be selected to form 8x8 array design.

5.1.1 A 4X4 Array Design

A 16 element array was created before attempting to design a large DRA array. Due to its reduced physical dimensions, the smaller array would be easier to simulate in HFSS. The primary purpose to presented simulation of the 4x4 array was to investigate mutual coupling effects. A half-wavelength element spacing would create the best beam pattern, according to classic array theory. At 28 GHz the spacing is 5.3 mm between adjust two element .

Figure5.1 show the 16-element planar array. As mentioned in [26], metal plate added vertically would reduce the mutual coupling between array elements. As illustrate in figure5.2 the insertion thin layers of vertical metal structures between

the CDRA-P elements to further decrease the mutual coupling and hence SLL (side lobe level).

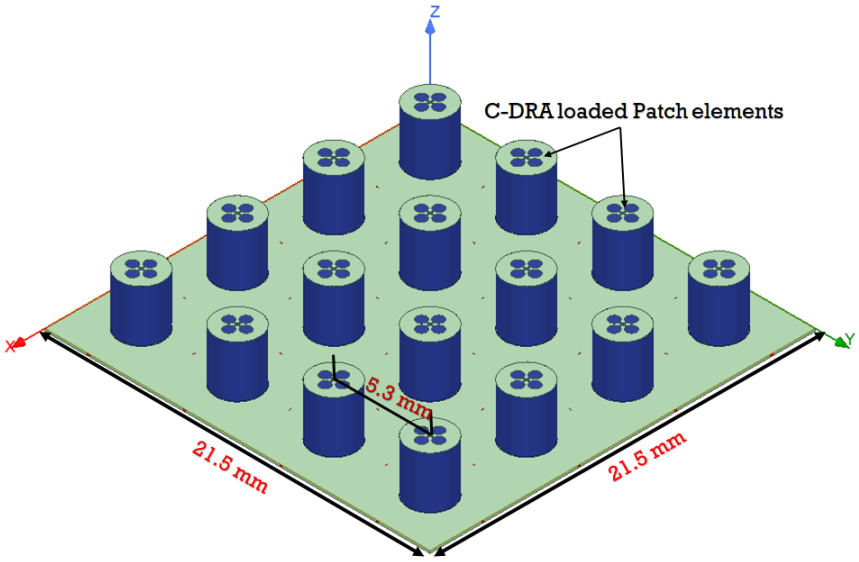

Figure 5.1: 4x4 CDR-P Array. since CDRA-P: C-DRA embedded patch antenna.

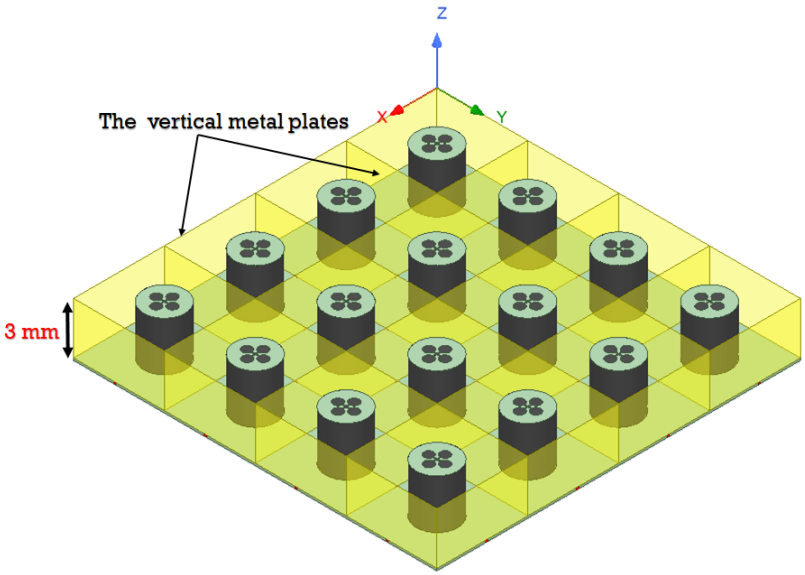

Figure 5.2: 4x4 CDR-P Array with metal plate .

Referring to figure5.1, 16-element array without inserted the thin layer since figure5.3 the reflection coefficient shows two lower peaks, which is caused by the phenomenon mutual coupling among array elements. This phenomenon causes divergence of the merged modes resulting from the patch and DR. Consequently, the highest bottom beam caused by C-DRA mode (-21 dB at frequency 28.8 GHz) and other beam by patch which is be -15 at frequency 27 GHz.

Also figure5.3 shows impedance bandwidth $\geq 2\ GHz$ and isolation level between the two feeding ports with S21 which is be 25 dB over the operating frequency bandwidth.

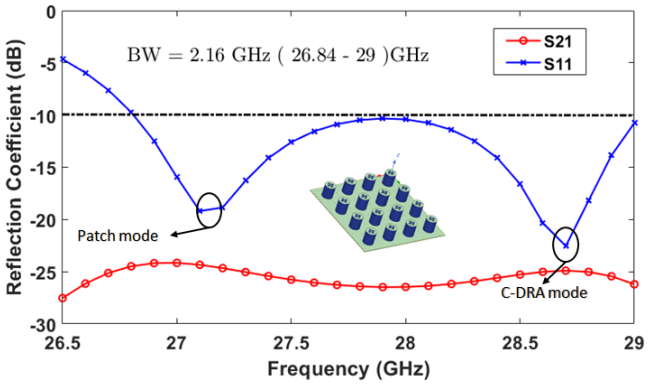

Figure 5.3: The reflection coefficient of 4x4 array CDRA-P.

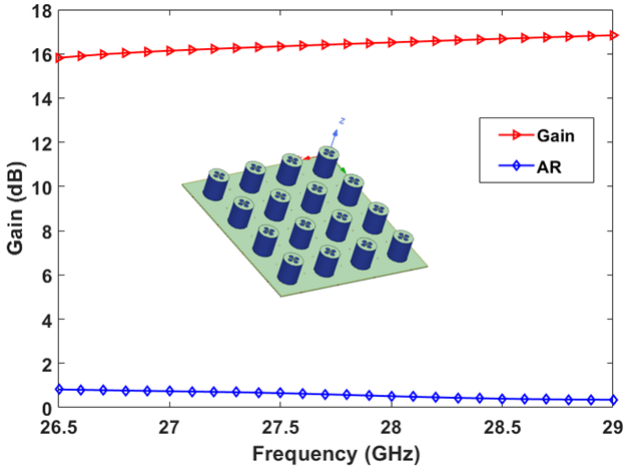

Figure 5.4: The Gain and Axial Ratio of 16 array CDRA-P.

Figure5.4 it's AR $\leq$ 0.52 dB for all bandwidth frequency which mean high purity circular polarization. Moreover, this figure shown flat gain $\geq$ 16 dB for all frequency band. Furthermore, Co- and cross polarization illustrated in figure5.5 to study the performance before and after insert thin layers among array elements.

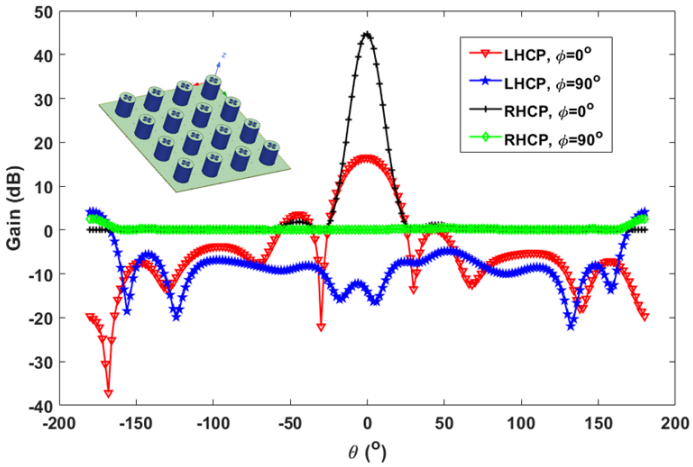

Figure 5.5: Co-polarization and Cross polarization of 16-elements before inset the thin layer which plot in both x-z plane($\phi = 0^o$) and y-z plane ($\phi = 90^o$).

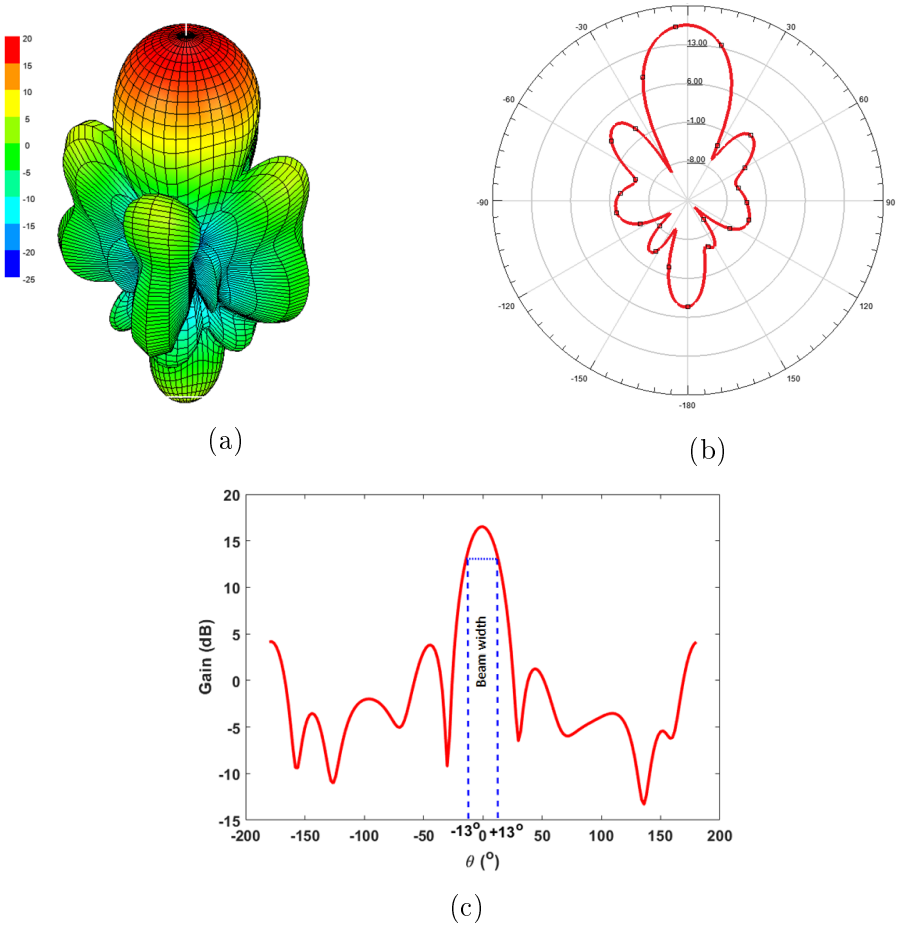

Figure 5.6: (a)3D view . (b) 2D view. (c) Beam width for total radiation 4x4 CDRA-P array.

Figure5.6 shown the radiation pattern of 16-element array CDRA-P without any addition, since it is appeared fine beamwidth ($\pm 13^o$) and the back radiation $\leqslant -11dB$.

5.1.2 A 4x4 CDRA-P array antenna after inserted thin metal plates.

The figure5.2 which explains the structure for 16 -array antenna with metal plates. These layers act like insulators as they work to curb emissions from neighboring elements and thus reduce the phenomenon of mutual coupling. Reducing the mutual helps to converge the combined modes from each other, as shown in the figure5.7.

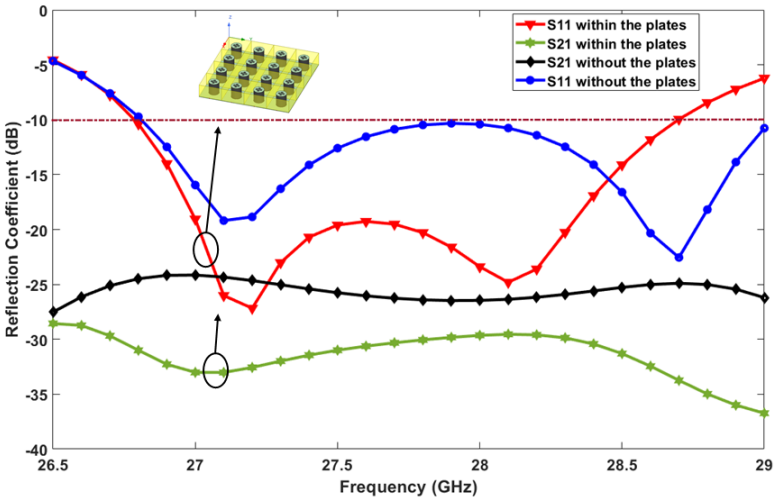

Figure 5.7: S-parameter of CDRA-P with copper plates.

Moreover, S21 is be enhanced ≤ -30dB after added the metal layer. The total gain increase by 0.52 dB when inserted the plate as shown in figure5.8 (a) , furthermore, the side lobe level has become more clear and distinct than the previous case, and this helps to avoid the problems of multiple paths, as well as the back radiation is also reduced as shown in the figure5.8 (b)

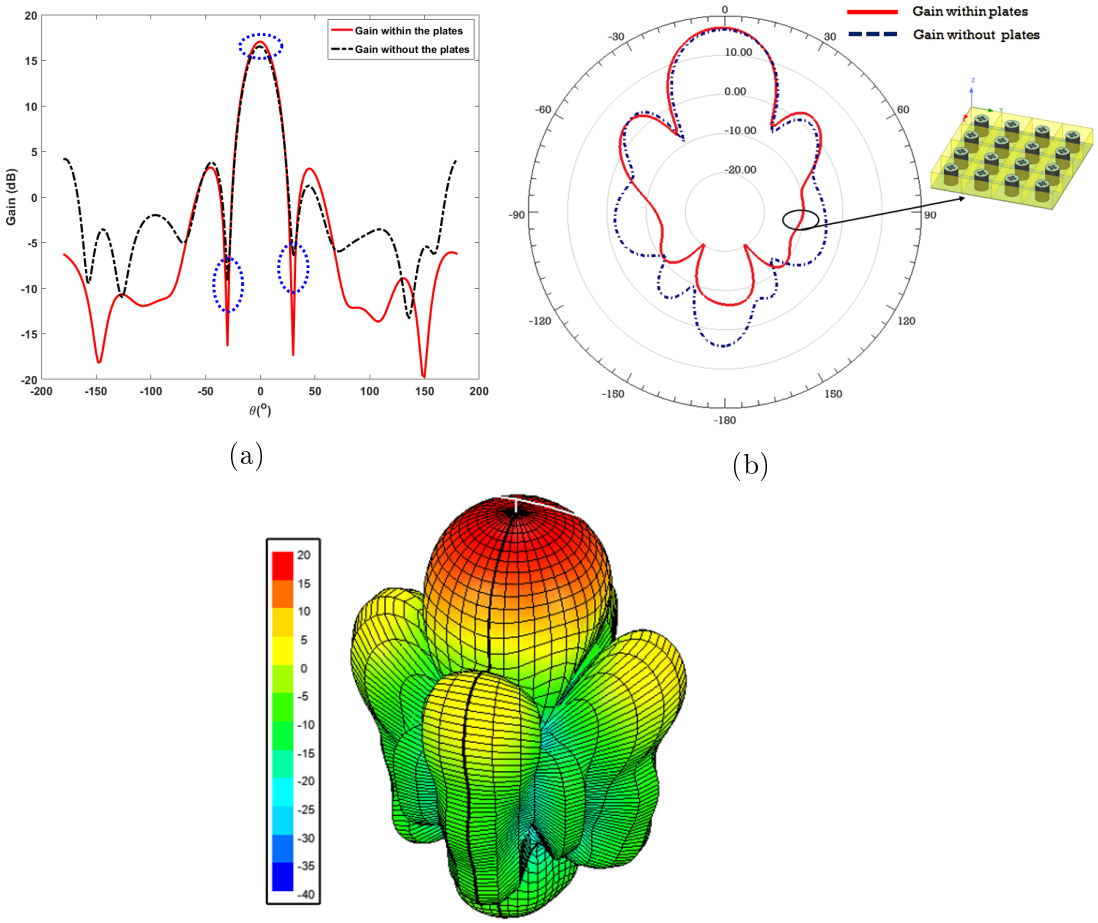

Figure 5.8: (a)3D view . (b) 2D view. (c) Radiation Pattern of 4x4 array with plates.

The figure5.9 explains the change in the gain after adding the metal spacers when measuring the gain with frequency, as well as the change in the AR While maintaining the polarization ratio at the acceptable limit of 3-dB.

Follow the previous results, the co- and cross polarization in x-z and y-z plane also check since figure5.10 (a) , (b) illustrated these reading and compared than Co- and X-polarization before inserted copper sheet.

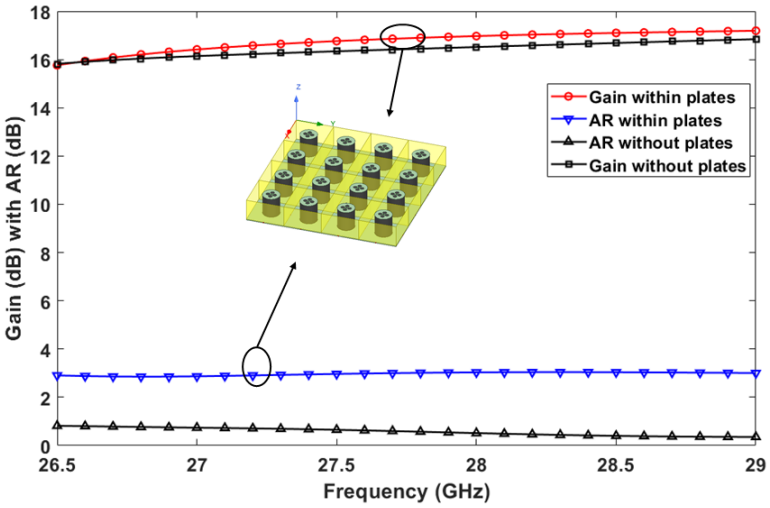

Figure 5.9: Gain and AR VS frequency before and after added the copper sheet plates

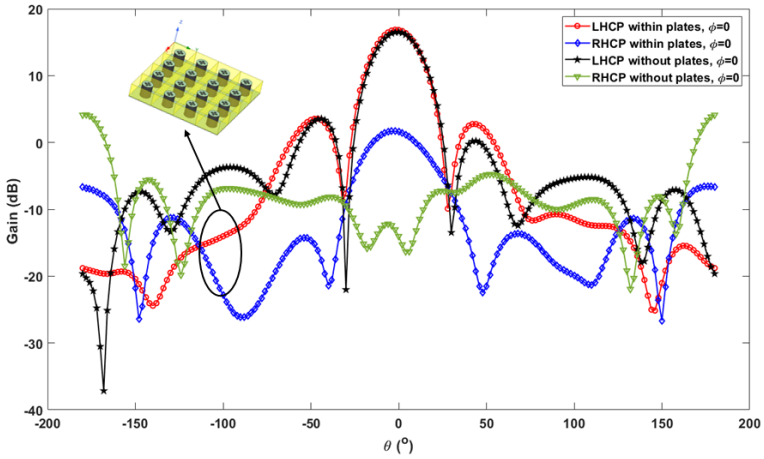

(a)

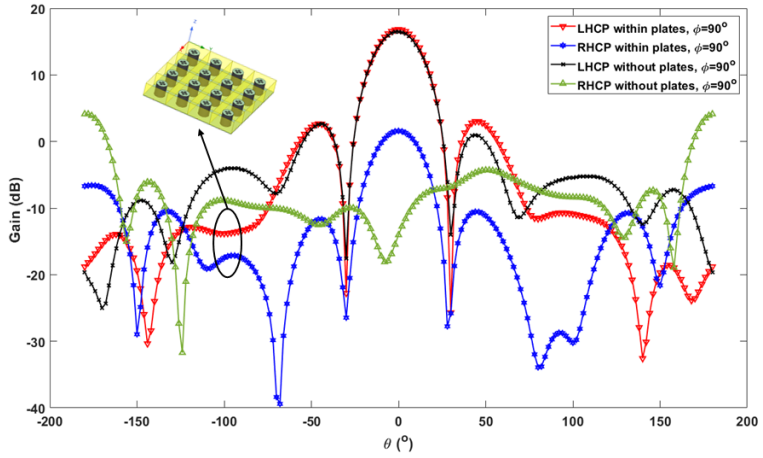

(b)

Figure 5.10: (a)x-z plane when $\phi = 0$, LHCP mean Co-polarization and RHCP X-polarization . (b) y-z plane when $\phi = 90^o$, LHCP mean Co-polarization and RHCP X-polarization.

5.1.3 A 8x8 Array Design

A 64- element planar array suitable for phased shifter array will studies in this section.The array is consist of one substrate layer made from Rogers RT/-duroid 6010/6010LM (tm) ($\varepsilon_r = 10.2$ and $tan\delta = 0.0023$), second layer of copper as ground which is installed above the substrate. All elements array which excited by U-shaped slot printed on the ground. Moreover, thin layers of vertical copper structures are injected between elements array at x- and y- axis with height 3 mm.

The purpose of scalable size of the array antenna from 4x4 to 8x8 is to increase the scanning range used for the beamforming angle. By depending on Eq.5.1 and 5.2 since the planar array 8x8 which be attained rang scanning ±60 which be explained more in results chapter [29].

$$\alpha_x = -k\ d_x\ \sin\theta_o \cos\phi_o \tag{5.1}$$

$$\alpha_y = -k\ d_y\ \sin\theta_o \sin\phi_o \tag{5.2}$$

Figure5.11 showed total planar array 8x8, which has a length and width of 42.4 mm and 42.4 mm, respectively. The height proposed array is 3 mm while the height of single element equal 2.4 mm this means the different 0.6 mm is caused by insertion copper plates in array to reduction the mutual coupling and back radiation.

The planar array of 64-Cylindrical Dielectric Resonator loaded patch Antennas had been suitable for beam steering capability which is designed, investigated and validated experimentally. In order to achieve a specific progressive phase distribution, the phase coupled to each array element is controlled by changing the phase at the feeding ports which produce the progressive phase.

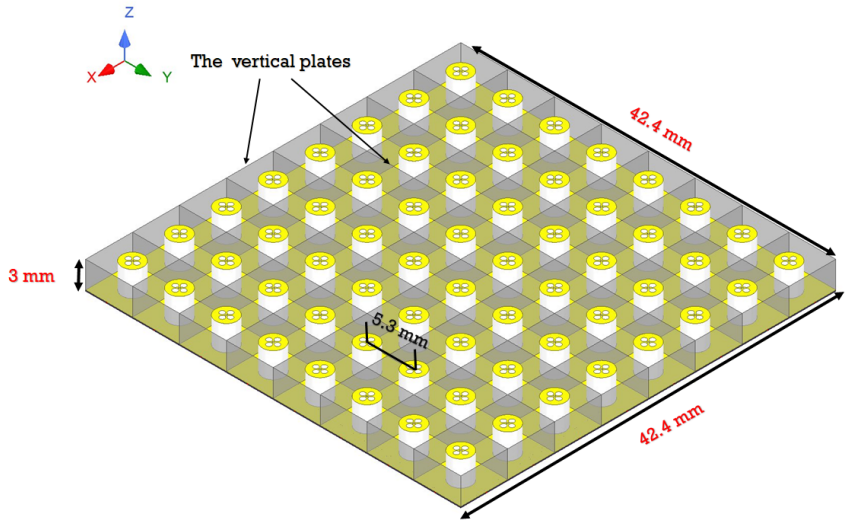

Figure 5.11: An 8x8 CDRA-P .

Moreover to reduce the mutual coupling between array elements sheet made of metal inserted vertically in the array (figure5.11).

Figure5.12 shown S-parameter of the proposed 64-elements planar array, since attained impedance bandwidth $\simeq$ 2 GHz (26.78 - 28.65) at resonant frequency 28.2 GHz. Furthermore, the isolation among two ports is be ≤ -27 dB for all frequencies band.

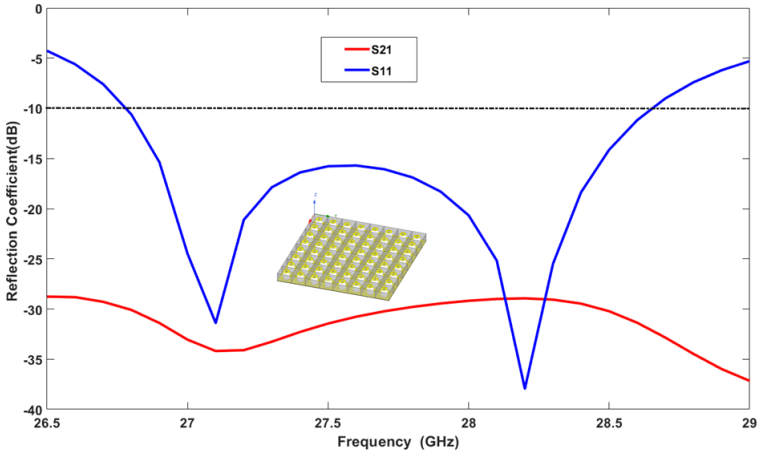

Figure 5.12: S-parameter of 8x8 planar array with S21 curve.

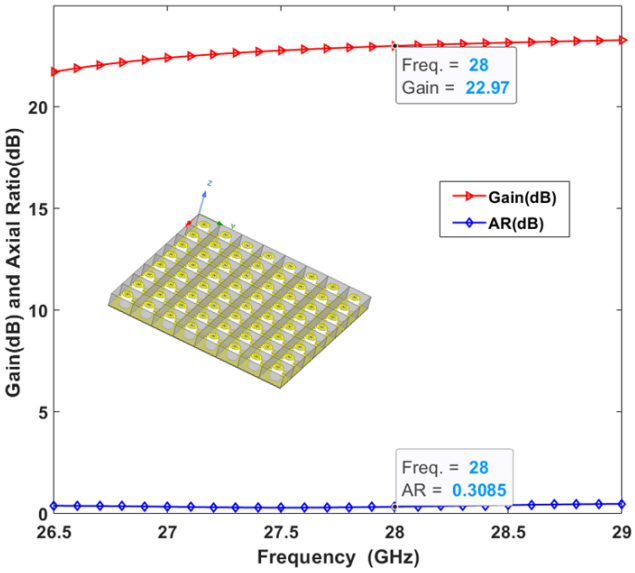

Figure 5.13: Gain and axial ratio vs frequency of 8x8 planar array.

The final structure of the proposed array antenna yields a total gain of 22.97 dB as shown in figure5.13. Moreover, the circular polarization purity is less than 0.31 dB at all frequencies of the bandwidth (26.5 - 29)GHz which plot in figure5.13.

The array antenna design's planar geometric shape was chosen to achieve a consistent radiation pattern in both the E- and H-planes, as shown in figure5.14. That is, the quantity of co-polarization and cross-polarization measured in the E-plane ($\phi = 0^o$) will be nearly identical to that measured in the H-plane ($\phi = 90^o$), with a tiny difference. This supports the notion that the design is ideal for a phased array antenna, which provides a large scanning angle in four directions, as we'll see later in this chapter.

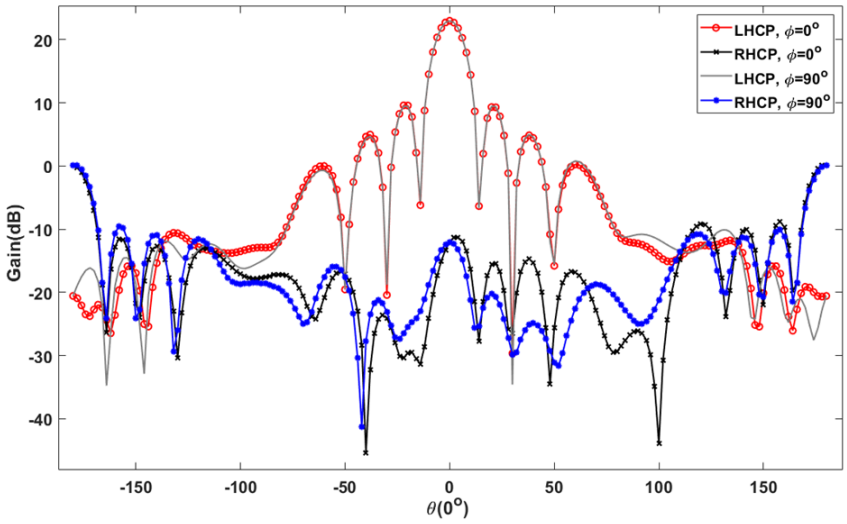

Figure 5.14: Gain (LH and RH) vs Theta 0^o of 8x8 planar array.

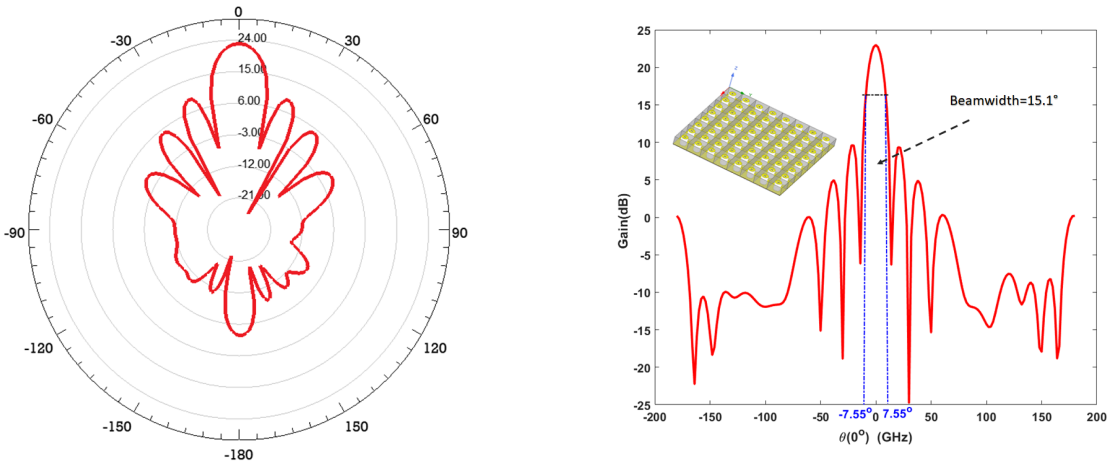

(a) (b)

Figure 5.15: (a)Radiation pattern . (b) Total beamwidth.

In figure5.15 (a), radiation pattern was present which display acceptable SLL $<$ 10 dB. Moreover, back radiation shown less than -2 dB. At the intersection of gain and theta angle in figure5.15 (b), the total beamwidth be 15.1^o (± 7.55) in the broadside direction when $\phi = \theta = 0^o$. figure5.16 shown final radiation pattern gain which be radiate by proposed antenna.

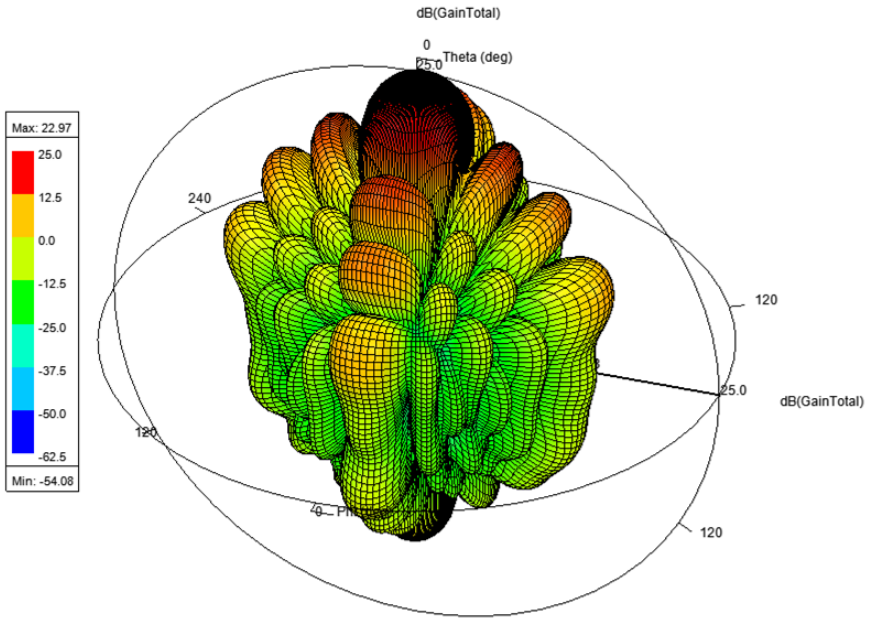

Figure 5.16: 3D polar gain.

5.1.4 Possible scanning angles in the final installation of the array antenna.

To scan a moving target, the array beam must be steered away from the bore point. ψ must be zero to steer the peak in the direction of $\theta = 0^o$, as in Eq5.1. Hence to steer the beam at θ^o for any direction, $d = \lambda/2$ with $\psi = 0$, $\beta = 2\pi/\lambda$. we get:

$$\alpha = (\mathbf{2}\pi/\lambda)\ \mathbf{x}\ \lambda/\mathbf{2}\ \mathbf{x}\ \sin\mathbf{45^o}\ \cos\mathbf{0^o} = \mathbf{127^o}$$

For example, to steer the peak at 45^o, the needed progressive phase difference between the excitation should be 127^o when $\phi = 0$.

In the proposed design, the position of the beam had four locations, each location with four angles to scan. For more explain, every time for scanning, will be called beam1, beam 2, beam3, and beam4 that very clear in figure5.17. Actually, figure5.17 (a) the required beam (beam1) will be moving from the scanning range theta equal 0^o to -60^o on E-field ($\phi = 0$) which can be obtained by changing the progressive phase on the excitation ports (0^o to (-173^o)) and so on. For beam2 in figure5.17 (b) same mechanical but in the opposite direction. In beam3 and

beam4 as shown in figure5.18 (a) same procedure applies but in H-plane mean $\phi = 90^o$. The Table5.1 had angle values for scanning operation.

Table 5.1: Scanning angles for beam steering of a 64-element planar array

Beam's Num.	E / H – plane	α	θ
Beam1	E – plane	$\alpha 1 = -173^o$	$\theta 1 = -15^o$
Beam1	E – plane	$\alpha 2 = -155^o$	$\theta 2 = -30^o$
Beam1	E – plane	$\alpha 3 = -127^o$	$\theta 3 = -45^o$
Beam1	E – plane	$\alpha 4 = -90^o$	$\theta 4 = -60^o$
Beam2	E – plane	$\alpha 1 = 173^o$	$\theta 1 = 15^o$
Beam2	E – plane	$\alpha 2 = 155^o$	$\theta 2 = 30^o$
Beam2	E – plane	$\alpha 3 = 127^o$	$\theta 3 = 45^o$
Beam2	E – plane	$\alpha 4 = 90^o$	$\theta 4 = 60^o$
Beam3	H – plane	$\alpha 1 = -173^o$	$\theta 1 = -15^o$
Beam3	H – plane	$\alpha 2 = -155^o$	$\theta 2 = -30^o$
Beam3	H – plane	$\alpha 3 = -127^o$	$\theta 3 = -45^o$
Beam3	H – plane	$\alpha 4 = -90^o$	$\theta 4 = -60^o$
Beam4	H – plane	$\alpha 1 = 173^o$	$\theta 1 = 15^o$
Beam4	H – plane	$\alpha 2 = 155^o$	$\theta 2 = 30^o$
Beam4	H – plane	$\alpha 3 = 127^o$	$\theta 3 = 45^o$
Beam4	H – plane	$\alpha 4 = 90^o$	$\theta 4 = 60^o$

Since θ is means the required direction and α is progressive phase difference between the antennas.

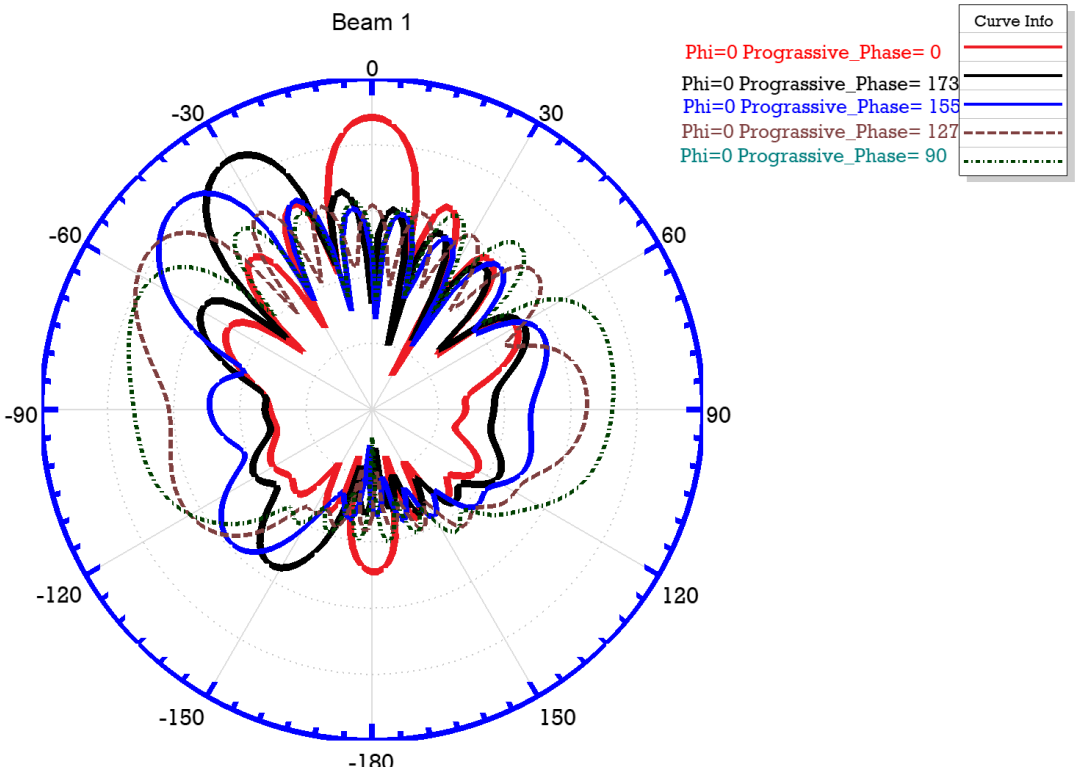

(a)

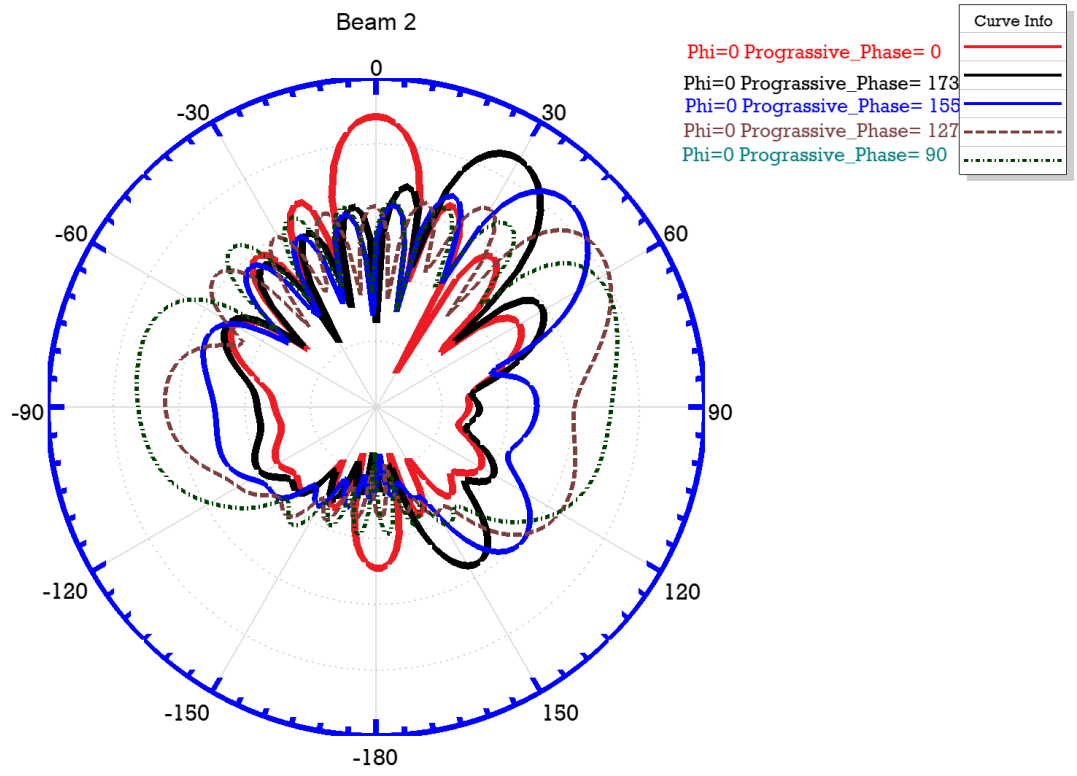

(b)

Figure 5.17: The direction of beam with each possible scanning

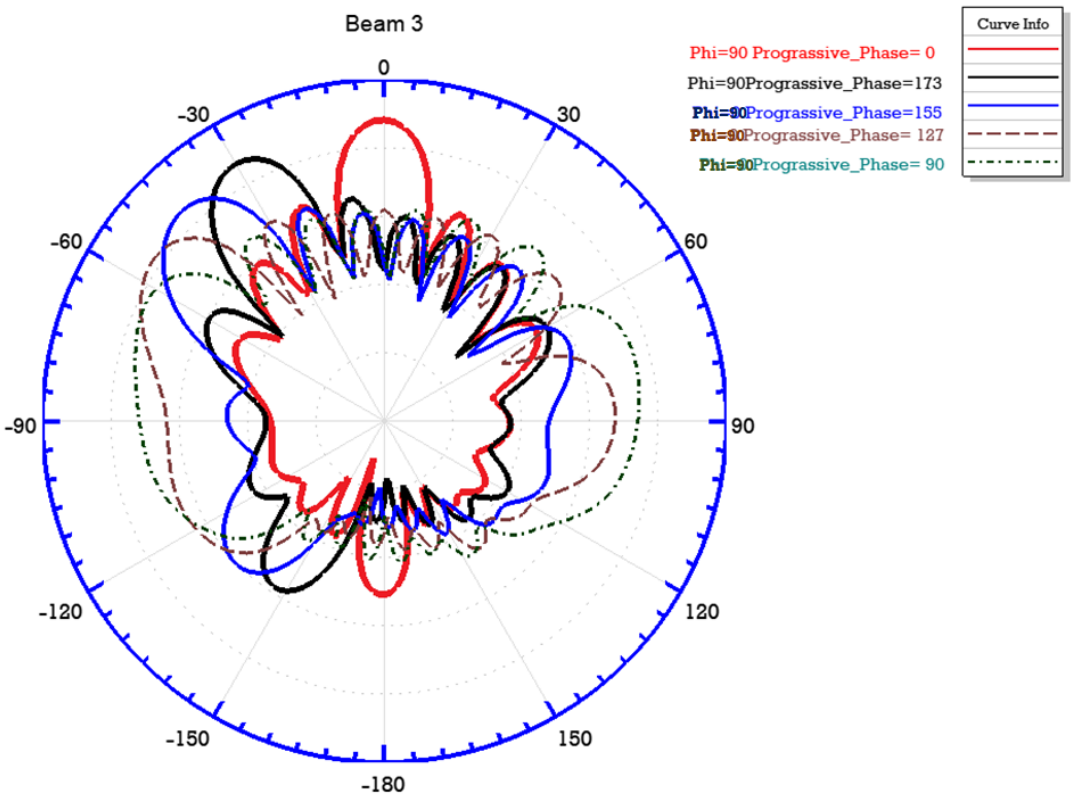

(a)

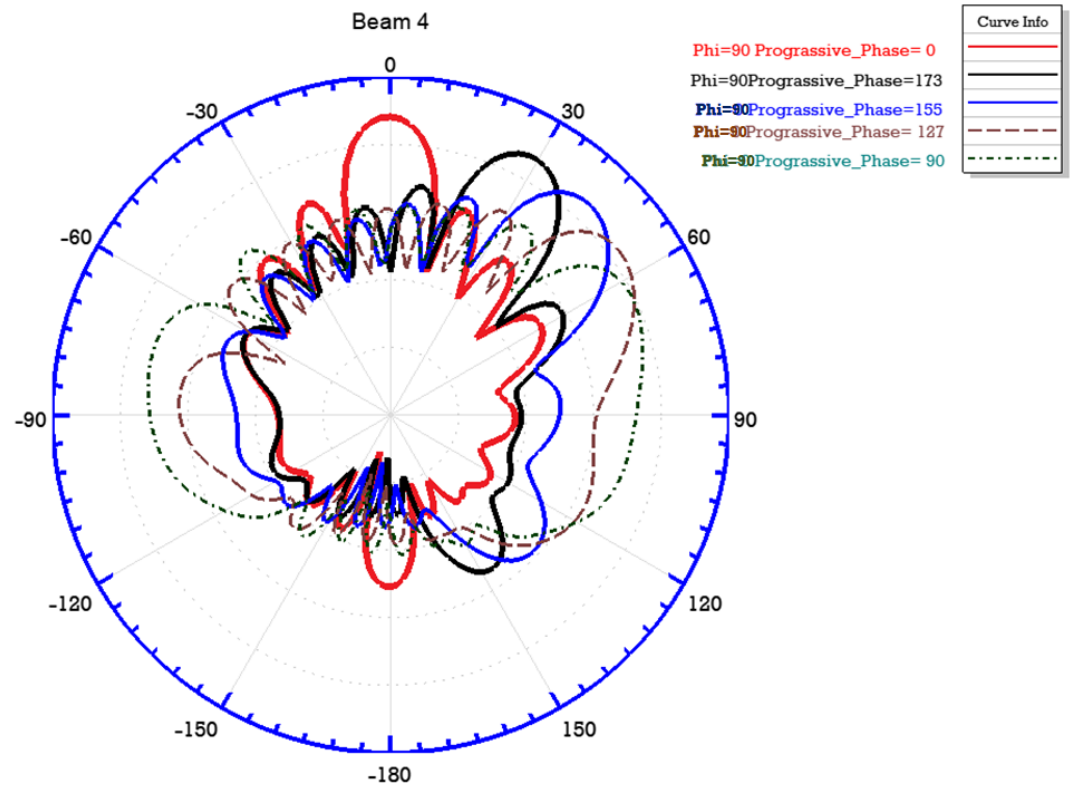

(b)

Figure 5.18: The direction of beam with each possible scanning

The Table5.2 shown comparison between the results in this thesis with other work since type of radiator, impedance bandwidth, gain, frequency operated, quality of elements, and rang scanning, are considerable.

Table 5.2: Comparison of the proposed design in this thesis with a previous DR loaded patch antenna works.

Paper	Radiator	f(GHz)	B.W(%)	G(dB)	Qyt	Rang scanning
[16]	R-DRA	26	20.8%	20	64	NA
[17]	ME dipole	60	14%	20.3	16	NA
[18]	Patch	28	18.9%	22.5	64	$\pm 50/H \pm 25/E$
[19]	R-DRA	28	18.9%	13.7	9	NA
[20]	Slot	28	5.41%	8	24	$\pm(20-128)/H \pm 70/E$
[21]	Brick cell	28	13.7%	16.5	20	NA
[22]	Patch	29	19.4%	25	12	$\pm 50/H \pm 25/E$
[23]	Patch	28	1.78%	11.9	4	$\pm(42, 38)/E$
[24]	Patch	28	1.78%	12.1	64	$\pm(55-7.5)/E$
[25]	Patch	28	2%	24	8	$\pm(15-5)E$
[26]	C-DRA	7.5	6.6%	13.8	4	$\pm 45/E$
3rd work	C-DRA	28	8.92%	22.97	64	$\pm(0-60)/E, \pm(0-60)/H$

CHAPTER SIX

Conclusions and future work

6.1 Introduction

The most important goals of this work, will be mentioned also the conclusion that is drawn from each design. After that highlight the recommendations that are most relevant.

6.2 Conclusion

The radiation pattern of the cylindrical dielectric resonator antenna (C-DRA) exhibited various resonant modes dependent on the magnitude of the dielectric constant (ε_r). To manage the excited mode, certain parameters can be modified, such as the diameter and height of the cylinder, the value of ε_r, and the excitation mechanism. It's worth noting that the total electric in an array is determined by the radiation of a single element, so it's necessary to improve parameters like bandwidth, isolation between ports at dual feeds antennas, and the diameter of the space between two adjust antennas in the array ($\leq \lambda_o/4$).

Many methods were used to improve the performance of the antenna while maintaining the antenna size without increasing. This is commensurate with the characteristics of the antenna used in the 5G applications.

The vertically stacked DR method is one of the ways to improve the total antenna radiation in a way that contributes to increasing the gain and bandwidth.

In this work, several cylinders with different values permittivity were used, which helped to increase the total gain of the antenna, as well as adding improvements to the bandwidth while maintaining the compact size for antenna. Moreover, one of the important techniques in antenna development is DRA loaded patch technique, induction a metal disk is placed over a cylinder of the DR and stimulated by a U-shaped slot and fed from two perpendicular ports to generate circular polarization. All the results regarding bandwidth, gain, polarization purity, current distribution inside the cylinder, and the effect of additions on antenna performance, as well as the modes generated by each antenna, there were be discussed and plotted.

In addition to what was previously mentioned, the composition of the array antennas is largely based on the geometric shape of the arrangement of the elements within the array and also determines the direction and magnitude of the beam's movement. The planar shape of the array is most appropriate geometric structure to make the beam steering more free to change the rang scanning of the beam.

6.3 Recommendations for future work

The feeding network plays a key role in reducing the manufacturing cost of the antenna, although the use of two feed lines gives a pure circular polarization, but it increases the complexity of the overall antenna installation.

The design of a cooperate network for the array antenna that feeds all the elements from one port is one of the things that are taken into consideration in the study and manufacture of the array antenna, in most cases, the formation of a feed for the antenna consists of several elements, including the amplifier and phased shifter that generates the delay time by creating a phase difference between the elements. Therefore, in this work, the formation of the joint feeding network is an integrated project in terms of choosing the type and composition of the element.

Also, the proposed antenna array can work with dual polarization (vertical or horizontal polarization) by using diode to make the antenna is reconfigurable, since this modifying increase capacity and number of users and which very suitable for 5G communication mobile system.

6.4 List of Publications

1. High Impedance Bandwidth Cylindrical Dielectric Resonator Antenna Stacking layers excitation by dual feeds with Via technique working at 28 GHz millimeter waves.

2. "Dual-Fed C-DRA Loaded by Modified Circular Patch Antenna", has been accepted for presentation at the 2021 IEEE International Symposium on Antennas and Propagation and USNC-URSI Radio Science Meeting at Marina Bay Sands in Singapore, on 4-10 December 2021.

3. "Steered Rectangular 64 – Elements Array of a Cylindrical Dielectric Resonator loaded Patch Antenna" has been submission to Al-Furat Al-Awsat Technical University.

Bibliography

[1] S. Kumar, A. S. Dixit, R. R. Malekar, H. D. Raut, L. K. Shevada, Fifth generation antennas: a comprehensive review of design and performance enhancement techniques, *IEEE Access 8 (2020) 163568–163593*.

[2] S. Keyrouz, D. Caratelli, Dielectric resonator antennas: basic concepts, design guidelines, and recent developments at millimeter-wave frequencies, *International Journal of Antennas and Propagation 2016 (2016)*.

[3] I. Ali, M. H. Jamaluddin, M. Kamarudin, A. Gaya, R. Selvaraju, Wideband and high gain dielectric resonator antenna for 5g applications, *Bulletin of Electrical Engineering and Informatics 8 (3) (2019) 1047–1052*.

[4] T.-Y. Lin, Y.-C. Chang, C. Hsieh, D.-C. Chang, Design of dual-band dual-polarization millimeter-wave stacked dielectric resonator antenna, in: *2018 20th International Conference on Electronic Materials and Packaging (EMAP), IEEE, 2018, pp. 1–2*.

[5] K. Aggarwal, R. Kumari, S. Das, et al., A rectangular—stacked dra and its mode analysis, in: *2017 International Conference on Communication and Signal Processing (ICCSP), IEEE, 2017, pp. 1514–1517*.

[6] T.-W. Kim, S.-O. Pak, Enhanced gain and miniaturisation method of stacked dielectric resonator antenna using metallic cap, *IET Microwaves, Antennas & Propagation 13 (8) (2019) 1198–1201*.

[7] W.-J. Sun, W.-W. Yang, P. Chu, J.-X. Chen, A wideband stacked dielectric resonator antenna for 5g applications, *International Journal of RF and Microwave Computer-Aided Engineering 29 (10) (2019) e21897*.

[8] A. Al-Azza, N. A. Malalla, F. J. Harackiewicz, K. Han, Stacked conical-cylindrical hybrid dielectric resonator antenna for improved ultrawide bandwidth, *Progress In Electromagnetics Research Letters 79 (2018) 79–86*.

[9] M. Anab Khattak, M. I. Khattak, S. M. Owais, A. Ali Khattak, A. Sultan, Design and analysis of millimeter wave dielectric resonator antenna for 5g wireless communication systems, *Progress In Electromagnetics Research 98 (2020) 239–255*.

[10] M. I. Fadzli, M. I. Sulaiman, Q. Pei, S. Kamal, M. F. Ain, Circularly polarized cylindrical dielectric resonator antenna for 5g applications, in: *AIP Conference Proceedings, Vol. 2233, AIP Publishing LLC, 2020, p. 030002*.

[11] J. Kowalewski, J. Eisenbeis, A. Jauch, J. Mayer, M. Kretschmann, T. Zwick, A mmw broadband dual-polarized dielectric resonator antenna based on hybrid modes, *IEEE Antennas and Wireless Propagation Letters 19 (7) (2020) 1068–1072*.

[12] S. Fakhte, H. Oraizi, M. H. Vadjed-Samiei, A high gain dielectric resonator loaded patch antenna, *Progress In Electromagnetics Research 30 (2012) 147–158*.

[13] R. Kumar, M. Ameen, R. K. Chaudhary, Wideband circularly polarized half-split embedded cylindrical dra excited with slotted patch for wlan/wi-max applications, in: *2017 IEEE International Conference on Antenna Innovations & Modern Technologies for Ground, Aircraft and Satellite Applications (iAIM), IEEE, 2017, pp. 1–4*.

[14] M. Sallam, M. Serry, S. Sedky, A. Shamim, G. A. Vandenbosch, E. A. Soliman, On-chip micromachined dielectric resonator antennas loaded with parasitic circular/crescent patch for mm-wave applications, in: *2020 14th European Conference on Antennas and Propagation (EuCAP), IEEE, 2020, pp. 1–5*.

[15] Z. Song, H. Zheng, M. Wang, Y. Li, T. Song, E. Li, Y. Li, Equilateral triangular dielectric resonator and metal patch hybrid antenna for uwb application, *IEEE Access 7 (2019) 119060–119068*.

[16] W. Luo, L. Shi, W. Xu, W. Chen, Y. Yang, Y. Ren, High gain dielectric resonance antenna array for millimeter wave vehicular wireless communication, *Progress In Electromagnetics Research 108 (2021) 63–78*.

[17] A. T. Hassan, A. A. Kishk, Circularly polarized antenna array based on microstrip ridge gap waveguide at 60 ghz, in: *2020 14th European Conference on Antennas and Propagation (EuCAP), IEEE, 2020, pp. 1–4*.

[18] K. Kibaroglu, M. Sayginer, T. Phelps, G. M. Rebeiz, A 64-element 28-ghz phased-array transceiver with 52-dbm eirp and 8–12-gb/s 5g link at 300 meters without any calibration, *IEEE Transactions on Microwave Theory and Techniques 66 (12) (2018) 5796–5811*.

[19] N. M. Nor, M. H. Jamaluddin, M. R. Kamarudin, S. Z. N. Z. Ambia, Design of planar dielectric resonator antenna array at 28 ghz, *Indonesian Journal of Electrical Engineering and Computer Science 5 (3) (2017) 622–627*.

[20] S. Zhang, X. Chen, I. Syrytsin, G. F. Pedersen, A planar switchable 3-d-coverage phased array antenna and its user effects for 28-ghz mobile terminal applications, *IEEE Transactions on Antennas and Propagation 65 (12) (2017) 6413–6421*.

[21] Z. Ahmed, P. McEvoy, M. J. Ammann, Comparison of grid array and microstrip patch array antennas at 28 ghz, in: 2018 IEEE MTT-S International Microwave Workshop Series on 5G Hardware and System Technologies (IMWS-5G), *IEEE, 2018, pp. 1–3*.

[22] A. Nafe, M. Sayginer, K. Kibaroglu, G. M. Rebeiz, 2x64 dual-polarized dual-beam single-aperture 28 ghz phased array with high cross-polarization rejection for 5g polarization mimo, in: *2019 IEEE MTT-S International Microwave Symposium (IMS), IEEE, 2019, pp. 484–487*.

[23] Y. He, M. Rao, Y. Liu, G. Jing, M. Xi, L. Zhao, 28/39-ghz dual-band dual-polarized millimeter wave stacked patch antenna array for 5g applications, in: *2020 International Workshop on Antenna Technology (iWAT), IEEE, 2020, pp. 1–4*.

[24] M. K. Ishfaq, T. Abd Rahman, Y. Yamada, K. Sakakibara, 8× 8 phased series fed patch antenna array at 28 ghz for 5g mobile base station antennas, in: *2017 IEEE-APS Topical Conference on Antennas and Propagation in Wireless Communications (APWC), IEEE, 2017, pp. 160–162*.

[25] M. A. Nassar, H. Y. Soliman, A. Ghoneim, S. Abuelenin, Beam steering antenna arrays for 28-ghz applications (2017).

[26] N. K. Mishra, S. Das, D. K. Vishwakarma, Beam steered linear array of cylindrical dielectric resonator antenna, *AEU-International Journal of Electronics and Communications 98 (2019) 106–113*.

[27] A. Petosa, Dielectric resonator antenna handbook, Artech, 2007.

[28] R. K. Mongia, P. Bhartia, Dielectric resonator antennas—a review and general design relations for resonant frequency and bandwidth, *International Journal of Microwave and Millimeter-Wave Computer-Aided Engineering 4 (3) (1994) 230–247*.

[29] C. A. Balanis, Antenna theory: analysis and design, John wiley & sons, 2015.

[30] W. D. de Mattos, P. R. Gondim, M-health solutions using 5g networks and m2m communications, IT Professional 18 (3) (2016) 24–29.

[31] N. Bayat-Makou, K. Wu, A. A. Kishk, Single-layer substrate-integrated broadside leaky long-slot array antennas with embedded reflectors for 5g systems, *IEEE Transactions on Antennas And Propagation 67 (12) (2019) 7331–7339*.

[32] H. Liu, W. Yang, A. Zhang, S. Zhu, Z. Wang, T. Huang, A miniaturized gain-enhanced antipodal vivaldi antenna and its array for 5g communication applications, *IEEE Access 6 (2018) 76282–76288*.

[33] A. S. Dixit, S. Kumar, A miniaturized antipodal vivaldi antenna for 5g communication applications, in: *2020 7th International Conference on Signal Processing and Integrated Networks (SPIN), IEEE, 2020, pp. 800–803*.

[34] R. Khan, A. A. Al-Hadi, P. J. Soh, Recent advancements in user effect mitigation for mobile terminal antennas: A review, *IEEE Transactions on Electromagnetic Compatibility 61 (1) (2018) 279–287*.

[35] N. Behdad, M. Al-Joumayly, M. Salehi, A low-profile third-order bandpass frequency selective surface, *IEEE Transactions on Antennas and Propagation 57 (2) (2009) 460–466*.

[36] L. Zhao, Z.-M. Chen, J. Wang, A wideband dual-polarized omnidirectional antenna for 5g/wlan, *IEEE Access 7 (2019) 14266–14272*.

[37] B. A. Esmail, H. A. Majid, S. H. Dahlan, Z. Zainal abidin, M. Himdi, R. Dewan, M. K. Rahim, A. Y. Ashyap, Reconfigurable metamaterial structure for 5g beam tilting antenna applications, Waves in Random and Complex Media (2020) 1–14.

[38] S. Hussain, S.-W. Qu, W.-L. Zhou, P. Zhang, S. Yang, Design and fabrication of wideband dual-polarized dipole array for 5g wireless systems, *IEEE Access 8 (2020) 65155–65163*.

[39] Z. Li, Y. Sun, M. Yang, Z. Wu, P. Tang, A broadband dual-polarized magneto-electric dipole antenna for 2g/3g/lte/wimax applications, Progress In Electromagnetics Research 73 (2017) 127–136.

[40] J. Yin, Q. Wu, C. Yu, H. Wang, W. Hong, Broadband endfire magnetoelectric dipole antenna array using sicl feeding network for 5g millimeter-wave applications, *IEEE Transactions on Antennas and Propagation 67 (7) (2019) 4895–4900*.

[41] M. S. Sharawi, M. Ikram, A. Shamim, A two concentric slot loop based connected array mimo antenna system for 4g/5g terminals, *IEEE Transactions on antennas and propagation 65 (12) (2017) 6679–6686*.

[42] N. K. Darimireddy, R. R. Reddy, A. M. Prasad, A miniaturized hexagonal-triangular fractal antenna for wide-band applications [antenna applications corner], *IEEE Antennas and Propagation Magazine 60 (2) (2018) 104–110*.

[43] A. S. Dixit, S. Kumar, A survey of performance enhancement techniques of antipodal vivaldi antenna, *IEEE Access 8 (2020) 45774–45796*.

[44] D. Q. Liu, H. J. Luo, M. Zhang, H. L. Wen, B. Wang, J. Wang, An extremely low-profile wideband mimo antenna for 5g smartphones, *IEEE Transactions on Antennas and Propagation 67 (9) (2019) 5772–5780*.

[45] J. Deng, J. Li, L. Zhao, L. Guo, A dual-band inverted-f mimo antenna with enhanced isolation for wlan applications, *IEEE Antennas and Wireless Propagation Letters 16 (2017) 2270–2273*.

[46] H. T. Chattha, 4-port 2-element mimo antenna for 5g portable applications, *IEEE Access 7 (2019) 96516–96520*.

[47] D. Q. Liu, M. Zhang, H. J. Luo, H. L. Wen, J. Wang, Dual-band platform-free pifa for 5g mimo application of mobile devices, *IEEE Transactions on Antennas and Propagation 66 (11) (2018) 6328–6333*.

[48] K. Luk, K. Leung, Dielectric resonator antennas research studies press limited, Hertforodshire, England, UK (2002).

[49] S. K. K. Dash, T. Khan, A. De, Dielectric resonator antennas: An application oriented survey, *International Journal of RF and Microwave Computer-Aided Engineering 27 (3) (2017) e21069*.

[50] G. D'Amato, G. Avitabile, G. Coviello, C. Talarico, Dds-pll phase shifter architectures for phased arrays: Theory and techniques, *IEEE Access 7 (2019) 19461–19470*.

[51] J. Ashmore, Design and analysis of a dielectric resonator antenna array and its feed network (2011).

[52] R. J. Mailloux, Phased array antenna handbook, Artech house, 2017.

[53] N. M. Nor, M. H. Jamaluddin, M. R. Kamarudin, M. Khalily, Rectangular dielectric resonator antenna array for 28 ghz applications, *Progress In Electromagnetics Research 63 (2016) 53–61*.

[54] I. Ali, M. H. Jamaluddin, A. Gaya, H. A. Rahim, A dielectric resonator antenna with enhanced gain and bandwidth for 5g applications, Sensors 20 (3) (2020) 675.

[55] N. Ojaroudi Parchin, H. J. Basherlou, R. A. Abd-Alhameed, Uwb microstrip-fed slot antenna with improved bandwidth and dual notched bands using protruded parasitic strips, *Progress In Electromagnetics Research 101 (2020) 261–273*.

[56] Y. Fan, M. H. Ghayesh, T.-F. Lu, Enhanced nonlinear energy harvesting using combined primary and parametric resonances: Experiments with theoretical verifications, *Energy Conversion and Management 221 (2020) 113061*.

[57] S. Trinh-Van, Y. Yang, K.-Y. Lee, K. C. Hwang, Single-fed circularly polarized dielectric resonator antenna with an enhanced axial ratio bandwidth and enhanced gain, *IEEE Access 8 (2020) 41045–41052*.

[58] C. Máximo-Gutiérrez, J. Hinojosa, F. L. Martínez-Viviente, A. Alvarez-Melcon, Design of high-performance microstrip and coplanar low-pass filters based on electromagnetic bandgap (ebg) structures, *AEU-International Journal of Electronics and Communications 123 (2020) 153311*.

[59] P. F. Hu, Y. M. Pan, K. W. Leung, X. Y. Zhang, Wide-/dual-band omnidirectional filtering dielectric resonator antennas, *IEEE Transactions on Antennas and Propagation 66 (5) (2018) 2622–2627*.

[60] T.-W. Kim, R. S. Aziz, S.-O. Park, Design of patch loaded with metallic posts inside dielectric resonator antenna, *IET Microwaves, Antennas & Propagation 11 (10) (2017) 1483–1487*.

[61] J. K. Plourde, C.-L. Ren, Application of dielectric resonators in microwave components, *IEEE Transactions on Microwave Theory and Techniques 29 (8) (1981) 754–770*.

[62] K. Chow, On the solution and field pattern of cylindrical dielectric resonators (correspondence), *IEEE Transactions on Microwave Theory and Techniques 14 (9) (1966) 439–439*.

[63] H.-C. Chang, K. A. Zaki, Unloaded q's of axially asymmetric modes of dielectric resonators, *IEEE transactions on magnetics 25 (4) (1989) 2938–2940*.

[64] S. Long, M. McAllister, L. Shen, The resonant cylindrical dielectric cavity antenna, *IEEE Transactions on Antennas and Propagation 31 (3) (1983) 406–412*.

[65] Y. Kobayashi, S. Tanaka, Resonant modes of a dielectric rod resonator short-circuited at both ends by parallel conducting plates, *IEEE Transactions on Microwave Theory and Techniques 28 (10) (1980) 1077–1085*.

[66] M. Verplanken, J. V. Bladel, The electric-dipole resonances of ring resonators of very high permittivity (short papers), *IEEE Transactions on Microwave Theory and Techniques 24 (2) (1976) 108–112*.

[67] Y. Kobayashi, M. Miura, Optimum design of shielded dielectric rod and ring resonators for obtaining the best mode separation, in: 1984 IEEE MTT-S International Microwave Symposium Digest, *IEEE, 1984, pp. 184–186*.

[68] A. A. Kishk, A. Glisson, D. Kajfez, Computed resonant frequency and far fields of isolated dielectric discs, in: Proceedings of IEEE Antennas and Propagation Society International Symposium, *IEEE, 1993, pp. 408–411*.

[69] J. Van Bladel, On the resonances of a dielectric resonator of very high permittivity, *IEEE Transactions on Microwave Theory and Techniques 23 (2) (1975) 199–208*.

[70] M. Tsuji, H. Shigesawa, K. Takiyama, Analytical and experimental investigations on several resonant modes in open dielectric resonators, *IEEE transactions on microwave theory and techniques 32 (6) (1984) 628–633*.

[71] W. Zheng, Computation of complex resonance frequencies of isolated composite objects, *IEEE transactions on microwave theory and techniques 37 (6) (1989) 953–961*.

[72] A. Kishk, A. Ittipiboon, Y. Antar, M. Cuhaci, Dielectric resonator antennas fed by a slot in the ground plane of a microstripline, in: *1993 Eighth International Conference on Antennas and Propagation, IET, 1993, pp. 540–543*.

[73] A. W. Glisson, D. Kajfez, J. James, Evaluation of modes in dielectric resonators using a surface integral equation formulation, *IEEE transactions on microwave theory and techniques 31 (12) (1983) 1023–1029*.

[74] R. De Smedt, Correction due to a finite permittivity for a ring resonator in free space, *IEEE transactions on microwave theory and techniques 32 (10) (1984) 1288–1293*.

[75] R. Chowdhury, N. Mishra, M. M. Sani, R. K. Chaudhary, Analysis of a wideband circularly polarized cylindrical dielectric resonator antenna with broadside radiation coupled with simple microstrip feeding, *IEEE Access 5 (2017) 19478–19485*.

[76] R.-Y. Sun, R.-C. Han, Design of dual-polarized differential feed dielectric resonator antenna, in: 2015 IEEE MTT-S International Microwave Workshop Series on Advanced Materials and Processes for RF and THz Applications (IMWS-AMP), *IEEE, 2015, pp. 1–3*.

[77] A. Hardock, R. Rimolo-Donadio, H.-D. Brüns, C. Schuster, Application of vias as functional elements in microwave coupling structures, *IEEE transactions on microwave theory and techniques 61 (10) (2013) 3541–3550*.

[78] C. Mak, K. Luk, K. Lee, Proximity-coupled u-slot patch antenna, Electronics Letters 34 (8) (1998) 715–716.

[79] N. Felegari, J. Nourinia, C. Ghobadi, J. Pourahmadazar, Broadband cpw-fed circularly polarized square slot antenna with three inverted-l-shape grounded strips, *IEEE Antennas and Wireless Propagation Letters 10 (2011) 274–277*.